Dissertation

submitted to the

Combined Faculties for the Natural Sciences and for Mathematics

of the Ruperto-Carola University of Heidelberg, Germany

for the degree of

Doctor of Natural Sciences

presented by

M Pharm. Subhajit Ghosh

Kolkata, India

Oral-examination: 15.01.2015

Role of the focal adhesion protein zyxin in hypertension-induced cardiovascular remodelling

Referees: Prof. Dr. Markus Hecker

Prof. Dr. Thomas Wieland

CONTENTS

ABBREVIATIONS

°C	Degree celsius
ANGII	Angiotensin II
ANP	Atrial natriuretic peptide
AP-1	Activator protein -1
APS	Ammonium persulfate
AT_1R	Angiotensin receptor type 1
AV	Atrioventricular
BNP	Brain natriuretic peptide
bp	Base pairs
BSA	Bovine serum albumin
BSS	Balanced salt solution
BW	Body weight
$Ca(CH_3COO)_2(H_2O)$	Calcium acetate hydrate
$CaCl_2$	Calcium chloride
cAMP	Cyclic adenosine monophosphate
CCD	Charge-coupled device
Ccl12	Chemokine (C-C motif) ligand 12
cDNA	Complementary deoxyribonucleic acid
cGMP	Cyclic guanosine monophosphate
CO	Cardiac output
CO_2	Carbon dioxide
CTGF	Connective tissue growth factor
DABCO	1,4-diazabicyclo [2.2.2] octane
DAG	Diacyl glycerol
DAPI	4',6-diamidino-2-phenylindole

DMEM	Dulbecco's Modified Eagle Medium
DMSO	Dimethyl sulfoxide
DOCA	Deoxycorticosterone acetate
DTT	Dithiothreitol
EC	Endothelial cell
ECG	Electrocardiography
ECM	Extracellular matrix
EDTA	Ethylenediaminetetraacetic acid
EDV	End diastolic velocity
Egr-1	Early growth response protein-1
EGTA	Ethylene glycol tetraacetic acid
Eph	Epinephrine
ER	Endoplasmic reticulum
ET-1	Endothelin-1
ET_A-R	Endothelin receptor subtype A
F-actin	Filamentous actin
FAK	Focal adhesion kinase
FasL	Fas ligand
FCS	Fetal calf serum
g	Gravitational constant
GFP	Green fluorescent protein
GO	Gene ontology
GPCR	G-protein coupled receptor
GSEA	Gene set enrichment analysis
GSK	Glycogen synthase kinase
HDAC	Histone deacetylase
HEPES	4-(2-hydroxyethyl)-1-piperazineethanesulfonic acid

HUVECs	Human umbilical vein derived endothelial cells
HW	Heart weight
ICC	Immunocytochemistry
IF	Immunofluorescence
IGF-1	Insulin-like growth factor-1
IHC	Immunohistochemistry
IL10	Interleukin 10
IL1b	Interleukin 1β
IL-8	Interleukin 8
ILP	Invadosome like protrusion
Itga8	Integrin α_8
IP_3	Inositol trisphosphate
Itgb1	Integrin β_1
Itgb8	Integrin β_8
KCl	Potassium chloride
kDa	Kilodalton
KEGG	Kyoto encyclopedia of genes and genomes
KH_2PO_4	Potassium dihydrogen phosphate
KLF2	Krüppel-like factor 2
LB	Luria-Bertani
LIM	Lin11, Isl-1 &Mec-3
LOX	Lysyl oxidase
LPP	Lipoma preferred partner
MEF2	Myocyte enhancer factor 2
MLCK	Myosin light chain kinase
MLCP	Myosin light chain phosphatase
M-MLV	Moloney Murine Leukemia Virus

MMP	Matrix metalloproteinase
MRTF-A or B	Myocardin related transcription factor A or B
MT-MMP	Membrane type matrix metalloproteinase
Na_2HPO_4	Disodium hydrogen phosphate
Na_3VO_4	Sodium orthovanadate
NaCl	Sodium chloride
$NaHCO_3$	Sodium hydrogen carbonate
NaOH	Sodium hydroxide
NE	Norepinephrine
NES	Nuclear export signal
NFAT	Nuclear factor of activated T cells
NFκB	Nuclear factor kappa B
NO	Nitric oxide
Nrf2	nuclear factor erythroid 2 [NF-E2]-related factor 2
O_2	Oxygen
OAG	Oleyl-acetyl-glycerol
PBS	Phosphate buffered saline
PCNA	Proliferating cell nuclear antigen
pCO_2	Partial pressure of CO_2
PCR	Polymerase chain reaction
PDGF-B	Platelet derived growth factor subunit B
PECAM	Platelet endothelial cell adhesion molecule
PFA	Paraformaldehyde
PI_3	Phosphoinositide 3-kinase
PIM	Protease inhibitor mixture
PKC	Protein kinase C
PLC	Phospholipase C

pO_2	Partial pressure of O_2
PSV	Peak systolic velocity
PVDF	Polyvinylidene difluoride
RGS5	Regulator of G-protein signalling 5
RI	Resistivity index
ROCK	Rho-associated protein kinase
RPL32	60S ribosomal protein L32
rpm	Revolutions per minute
RT-PCR	Reverse transcription polymerase chain reaction
SA	Sino Atrial
SDS-PAGE	Sodium dodecyl sulphate-polyacrylamide gel electrophoresis
SEM	Standard error of the mean
SHR	Spontaneously hypertensive rat
siRNA	Small interfering ribonucleic acid
SMA	Smooth muscle actin
SMCs	Smooth muscle cells
SM-MHC	Smooth muscle myosin heavy chain
SOC	Store-operated channels
SRF	Serum response factor
STIM	Stromal interaction molecule
TAC	Transverse aortic constriction
TBE	Tris-borate-EDTA
TBS	Tris buffered saline
TEMED	Tetramethylethylenediamine
TG2	Transglutaminase 2
TGF-β	Transforming growth factor β
Tgfbr1	Transforming growth factor β receptor type 1

TIMP	Tissue inhibitors of matrix metalloproteinases
TNF-α	Tumour necrosis factor α
TRIP6	Thyroid receptor-interacting protein 6
TRPC	Transient receptor potential canonical channel
TUNEL	Terminal deoxynucleotidyl transferase dUTP nick end
V	Volts
w/v	weight per volume
WHO	World Health Organization
WT	Wild type
XeC	Xestospongin C
$Zn(CH_3COO)_2.2H_2O$	Zinc acetate dihydrate
$ZnCl_2$	Zinc chloride

Zusammenfassung

Bluthochdruck gehört zu den weltweit häufigsten Todesursachen und ist ein Hauptrisikofaktor für kardiovaskuläre Erkrankungen wie Herzinfarkt, Schlaganfall, Herzinsuffizienz und die diabetische Makroangiopathie. Obwohl diese Krankheit klinisch gut untersucht ist, ist relativ wenig über die zellulären Mechanismen zu Krankheitsbeginn bekannt. Bei Bluthochdruck bewirkt eine chronisch erhöhte Wandspannung in den Arterien eine vermehrte biomechanische Dehnung der glatten Gefäßmuskelzellen (GMZ). Dies führt zu charakteristischen Veränderungen der Genexpression, wodurch ein komplexer Gefäßwandumbauprozess initiiert wird. Dies wird maßgeblich durch eine Phänotypänderung der GMZ von einem kontraktilen zu einem aktivierten, synthetischen Zustand verursacht. Deshalb ist die durch veränderte hämodynamische Bedingungen hervorgerufene Mechanotransduktion in den GMZ ein entscheidender Schritt im Verlauf der durch Bluthochdruck induzierten maladaptiven Gefäßwandumbaus.

In diesem Zusammenhang haben wir und andere das Protein Zyxin aus den fokalen Kontaktpunkten als einen möglichen Mechanosensor identifiziert, der die Anpassungsreaktion vaskulärer Zellen an übermäßige mechanische Dehnung reguliert. Aufgrund dessen postulierten wir, dass Zyxin eine wichtige Rolle beim Bluthochdruck-induzierten kardiovaskulären Remodelling spielt. Die vorliegende Arbeit beschäftigte sich erstmals mit den funktionellen Konsequenzen eines Verlusts von Zyxin während pathologischer Umbauprozesse in Arterien und im Herzen von hypertensiven Mäusen. Eine *Microarray*-Analyse von gedehnten Zyxin-defizienten GMZ deckte eine dramatische Änderung in der Expression dehnungsabhängiger Gene auf. Ein Vergleich von GMZ aus Wildtyp und Zyxin-defizienten Mäusen zeigte in den Zyxin-defizienten GMZ einen wachstums- und migrationsfördernden sowie Apoptose-hemmenden Phänotyp bei gleichzeitig verringerter Kontraktilität. Dies konnte auf eine Aktivierung des Rho-A-MRTF-A Signalweges zurückgeführt werden, der in Zyxin-defizienten GMZ zumindest teilweise die dehnungsabhängige Genexpression induziert.

Experimentell induzierte Hypertonie führte besonders in älteren Zyxin-defizienten Tieren zu einem signifikant geringeren Anstieg des systolischen und diastolischen arteriellen Blutdrucks. Dies wurde auf strukturelle Veränderungen in den remodellierenden Arterien zurückgeführt. Diese Beobachtung ging einher mit einer verminderten Perfusionswiderstand der Femoralarterie, was wahrscheinlich auf einem Verlust der Integrität der extrazellulären Matrix in der Gefäßwand älterer Zyxin-defizienter Mäuse beruht. Des Weiteren führte eine hämodynamische Überlastung in Zyxin-defizienten Mäusen zu einer ausgeprägte kardialen interstitiellen Fibrose, Apoptose und schließlich zu kardialer Dysfunktion. Höchstwahrscheinlich war dies einer übersteigerten Expression Fibrose-fördernder Gene geschuldet, die insbesondere von kardialen Fibroblasten exprimiert werden. Schließlich konnte durch den Einsatz einer ratiometrischen Bestimmung temporaler Veränderungen der Calciumkonzentration in Endothelzellen der vermutete Zusammenhang zwischen einer TRPC3-Kanalaktivierung und der dehnungsabhängigen Translokation von Zyxin in den Kern vaskulärer Zellen bestätigt werden; dabei ging der TRPC3-Kanalaktivierung eine Aktivierung der β1-Isoform der Phospholipase C voraus, sodass der mutmaßlich beteiligte Mechanosensor ein G_q-Protein-gekoppelter Rezeptor sein muss.

Zusammenfassend weisen diese Ergebnisse auf eine bisher unentdeckte Rolle von Zyxin bei der Verhinderung des Bluthochdruck-induzierten kardiovaskulären Remodelling hin und unterstreichen die Bedeutung der Mechanotransduktion in der Pathophysiologie dieser weit verbreiteten kardiovaskulären Erkrankung.

SUMMARY

Hypertension is one of the leading causes of morbidity and mortality worldwide, serving as a major risk factor for cardiovascular events such as stroke, myocardial infarction and diabetes. Although clinically well studied, relatively little is known about the cellular mechanisms at the onset of this disease. A chronic increase in arterial wall tension in hypertension translates into elevated levels of biomechanical stretch experienced by vascular smooth muscle cells (SMCs). This leads to prominent changes in gene expression initiating a complex remodelling process driven by a shift in phenotype of otherwise contractile vascular SMCs to an activated, synthetic state. Therefore, mechanotransduction in vascular SMCs in response to altered hemodynamic forces is a crucial step in the progression of hypertension-induced maladaptive remodelling.

In this context, we and others have identified the focal adhesion protein zyxin as a putative mechanotransducer which regulates the cellular adaptation to exaggerated biomechanical stretch. As such, we hypothesized that zyxin might play an important role in hypertension-induced cardiovascular remodelling. This work addressed the functional consequences of loss of zyxin during pathological remodelling of arteries and the heart in hypertensive mice. Microarray analysis revealed a dramatic alteration of stretch-regulated gene expression in zyxin-null vascular SMCs. A comparison of vascular SMCs from wild type and zyxin-null mice revealed a growth-promoting, pro-migratory, anti-apoptotic and poorly contractile phenotype of zyxin-null vascular SMCs. This could be attributed to an activation of the RhoA-MRTF-A signalling axis partially driving stretch-induced gene expression in the zyxin-null SMCs.

Induction of experimental hypertension led to a significantly lower increase in systolic and diastolic arterial blood pressure in zyxin-null mice particularly in older animals, an outcome that could be attributed to structural changes in the remodelling arteries. This response was paralleled by a reduced resistivity in the femoral artery of these animals likely caused by a loss of extracellular matrix (ECM) integrity observed in older zyxin-null mice. Hemodynamic overload further induced pronounced cardiac interstitial fibrosis, apoptosis and resultant cardiac dysfunction in zyxin-null mice, owing to a major shift towards a pro-fibrotic gene expression pattern within the myocardium, most likely

derived from the cardiac fibroblasts. Lastly, using a ratiometric calcium imaging method, this study confirmed a TRPC3 channel-dependent stretch-induced zyxin activation in vascular cells that is mediated through activation of the β1 isoform of phospholipase C.

Collectively, these findings highlight a novel role of zyxin in hypertension-induced cardiovascular remodelling and underscore the importance of mechanotransduction in the pathophysiology of this highly prevalent cardiovascular disease.

1 INTRODUCTION

1.1 The cardiovascular system

The cardiovascular system consists of three major components namely blood, the heart and the blood vessels. This system serves to channel blood to different parts of the body and is intricately associated with all vital functions. The circulation of blood in the body requires a central pumping organ, namely the heart which generates the force to propel the blood to the tissues and individual cells. Additionally, for efficient directionality and distribution of blood flow, a complex network of blood vessels spanning the entire body is required.

1.1.1 The heart

The heart is a cone-shaped organ located near the midline of the thoracic cavity. It is protected by a layered membrane called the pericardium. The wall of the heart is built of three layers: an external layer (epicardium), the middle layer of cardiac muscle tissue termed the myocardium and the innermost endocardium. Built up of two superior chambers or atria and the two inferior chambers called ventricles, the mammalian heart is interconnected by valves which regulate the directionality of blood flow and prevent mixing of oxygenated and deoxygenated blood. The right atrium receives blood from three veins: the inferior and superior vena cava and the coronary sinus while the left atrium receives blood from four pulmonary veins. On the other hand, the right ventricle pumps blood into the pulmonary arteries whereas the left ventricle delivers it to the aorta and its branches.

The heart is a muscular organ composed of cardiac muscle fibres which connect to each other through intercalated discs. The discs further have desmosomes which hold the fibres together in addition to various gap junctions which allow connectivity between fibres. The pumping action of the heart is maintained by its rhythmic electrical activity which begins at the sinoatrial (SA) node located in the right atrial wall. The generated action potential is conducted to the atrioventricular (AV) node further to the bundle of His propagating to the apex of the heart. The Purkinje fibres finally conduct the action potential from the apex to the remainder of the ventricular myocardial wall. The contraction and relaxation of atria and ventricles are coordinated by the regional

generation of this action potential and its ordered propagation. The resultant cardiac cycle comprising a systole (contraction phase) and a diastole (relaxation phase) of the four chambers of the heart drives the flow of blood. Changes in electrical activity of the heart or deficits in cardiac contraction and relaxation are major causes of cardiovascular complications.

1.1.2 The blood vessels

The blood circulates in the body through a complex network of blood vessels which includes arteries, arterioles, capillaries, veins and venules. The diameter and structural composition of these vessels vary and are responsible for the large surface area of the vascular network. Both arteries and veins are composed of three layers. The innermost layer composed of a single layer of endothelial cells is the tunica interna. The middle layer known as the tunica media is composed of multiple layers of smooth muscle cells (SMCs) separated from the endothelial layer by the internal elastic lamina. The outermost layer is connective tissue which forms the Tunica adventitia which is separated from the medial layer by the external elastic lamina. Arteries which are exposed to high pressure have a thicker medial wall composed of several concentric layers of smooth muscle cells in comparison to veins. Similarly, the endothelial cell monolayer in capillaries is surrounded by pericytes while small arterioles and venules have one or two layers of SMCs.

The endothelial cells act as a barrier to transport of molecules from the luminal space into the vessel wall. In addition, they influence the transendothelial transport of inflammatory cells such as leucocytes by regulation of endothelial cell-cell junctions. They are also the predominant sensors of blood flow thereby releasing vasodilatory mediators such as nitric oxide (NO). Thus, they regulate vascular homeostasis and also contraction of the underlying SMCs by interacting with them. The main function of the vascular SMCs is contraction and regulation of vessel tone and helping the vessel wall to adapt to changes in blood pressure. The vascular SMCs are embedded in an extracellular matrix (ECM) which also regulates gene expression in these cells (outside-in signalling). Alternatively, composition of the ECM can be modified by the vascular SMCs (inside-out signalling) ((Beamish et al. 2010). Composition of the ECM also

varies according to the vessel type with larger arteries having more elastin which confers more elasticity and compliance to these vessels. Collagen deposition on the contrary is responsible for the strength of the vessel wall thereby lending mechanical support. Endothelial dysfunction, changes in SMC contraction or an altered ECM are underlying causes of unbalanced or abnormal forces in the vasculature such as in hypertension.

1.2 Biomechanical forces in the cardiovascular system

The predominant forces generated by the flow of blood within the vascular network include the fluid shear stress on the endothelial cells, wall tension and corresponding cyclic strain on both the endothelial cells and SMCs together with the mechanical load exerted on the heart due to return of venous blood to the heart and subsequent contraction to pump blood against the systemic vascular resistance.

1.2.1 Hemodynamic forces in blood vessels

The frictional force or shear exerted by the flow of blood along the endothelial cell layer of the blood vessel is an important factor in vascular homeostasis (Figure 1). The shear stress exerted by laminar flow of blood is proportional to the viscosity of blood and varies inversely to the third power of the radius of the blood vessel. Laminar shear stress induces alignment of endothelial cells in the direction of flow and is beneficial for proper functioning of the vessel wall by endothelial cell NO release and activating anti-inflammatory pathways (Tzima et al. 2005). Conversely, disturbed flow as in curvatures and at bifurcations activates pro-inflammatory pathways.

On the other hand, blood pressure or radial pressure exerted by the blood against the vessel wall drives wall tension which depends on the transmural pressure difference, vessel radius and the wall thickness as explained by Laplace's law (Figure 1). Short term increases in blood pressure lead to myogenic constriction of small vessels (Meininger et al. 1992), a reflex action to normalize wall tension. However, long term increases in blood pressure induce chronic remodelling of the vessel wall accompanied by outward remodelling which follows hypertrophy or hyperplasia of the vascular SMCs

in larger and smaller arteries, respectively (Osol et al. 1995, Owens et al. 1981, Prewitt et al. 2002).

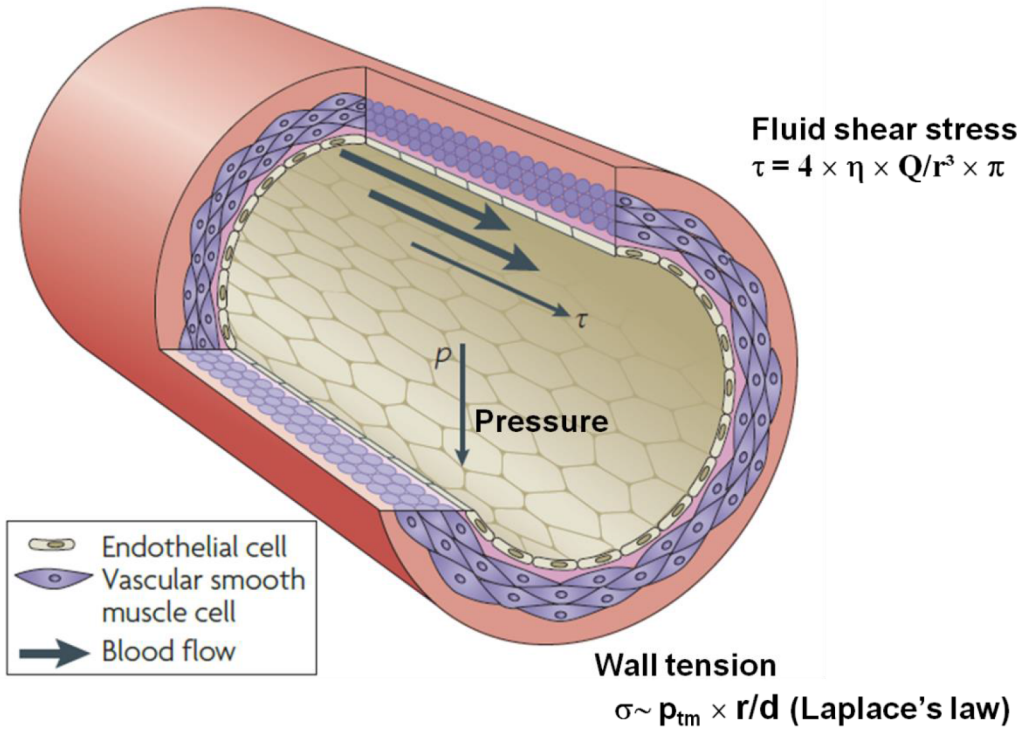

Figure 1: Hemodynamic forces in the arterial wall. Endothelial cells are exposed to both fluid shear stress and the pressure exerted by the blood flowing through the blood vessels. Vascular SMCs are exposed predominantly to changes in wall tension due to pressure exerted by the blood on the vessel wall (Modified from Hahn et al. 2009).

1.2.2 Hemodynamic forces in the heart

The force experienced by the cardiac cells at any given moment depends on the cardiac load which in turn regulates cardiac output (CO). Cardiac output is the volume of blood ejected from the left ventricle each minute and equals the product of stroke volume and heart rate. Stroke volume is the volume of blood ejected by the ventricle during each contraction. Thus, the work done by the heart depends on the preload, the contractility of the ventricular fibres and the afterload. Preload or the volume of blood in the heart prior to contraction determines the force of contraction during systole according to the Frank-Starling law. It depends on the duration of ventricular diastole and the venous return of blood to the heart. Myocardial contractility is influenced by inotropic agents

such as sympathetic stimulation through catecholamines while afterload or the pressure against which the ventricles eject blood depends on the systemic vascular resistance termed peripheral vascular resistance. Conditions such as an increase in peripheral resistance or blood volume can increase cardiac load and the resultant hemodynamic forces in the heart.

1.3 Hypertension: A case of hemodynamic forces gone awry

In order to understand the pathophysiology of hypertension, it is essential to understand the regulation of blood pressure. Blood pressure is regulated by cardiac output and the total peripheral resistance that is intricately linked to contraction of the smooth muscle cells lining the peripheral resistance arteries. There are several factors regulating blood pressure by influencing either of these two parameters. The nervous system regulates blood pressure by baroreceptor (e.g. carotid sinus) and chemoreceptor-mediated reflexes. While the peripheral chemoreceptors primarily detect changes in pO_2, the central chemoreceptors in the hypothalamus detect changes in the levels of CO_2 (pCO_2) and pH. Additionally, pressure can be regulated by hormones, the predominant mediator being the renin-angiotensin–aldosterone system, by increasing vasoconstriction and by an increase in total blood volume through enhanced sodium and water retention in the kidneys. Hormones such as norepinephrine can increase both cardiac output and peripheral resistance by acting on β_1-adrenoceptors in the heart and on α_1-adrenoceptors in the vascular SMCs. Vasodilatation can also regulate blood pressure and is induced by hormones such as atrial natriuretic peptide (ANP), metabolites such as adenosine, and ions such as K^+ that induce SMC hyperpolarization. Additionally, NO released by endothelial cells is an important vasodilator. Physical changes such as temperature or the reflex-like myogenic response of vascular SMCs are other means of blood pressure regulation. Thus, changes in the vessel diameter resulting from the above-mentioned inputs have direct influence on the pressure gradient according to Ohm's law. The resting systolic blood pressure in humans is 100-130 mmHg while the diastolic pressure is 60-80 mmHg. While systolic pressure is influenced by the cardiac output, diastolic pressure is largely determined by the total

peripheral resistance. An imbalance in any of these parameters will result in changes in blood pressure.

Systolic blood pressure greater than 140 mmHg and diastolic blood pressure greater than 90 mmHg (definitions of the WHO) are considered symbolic of clinical hypertension. A prolonged and consistent increase in blood pressure results in increased wall tension as defined by Laplace's law thereby imposing an enhanced cyclic strain on the arterial SMCs. This results in a shift in phenotype of the SMCs from a quiescent, contractile state to a proliferative and synthetic phenotype. The result is a gain in the number or size of SMCs and consolidation of the ECM, thereby increasing the wall thickness to counter the rise in wall tension. Such changes lead to fixation of the blood pressure at a higher level due to increased peripheral resistance, which increases the cardiac output resulting in a vicious cycle that promotes further remodelling. Additionally, the heart has to constantly pump blood against an increased afterload resulting in an enhanced cardiac mass termed cardiac hypertrophy. This hypertension-induced remodelling of the blood vessel wall and the heart involves a series of changes in the phenotype of the respective cells and the surrounding ECM in which they are embedded.

1.4 Hypertension-induced cardiovascular remodelling

1.4.1 SMCs in pathological remodelling of the blood vessel wall

The pathological remodelling of the blood vessel wall in hypertension manifests itself predominantly as a reduced contraction of SMCs and a resultant stiffening of the vessel wall by concomitant deposition of ECM proteins. In order to understand the process better, the mechanisms of SMC contraction have to be outlined since hypertension-induced early remodelling mechanisms impinge on the ability of SMCs to contract. SMC contraction can be initiated by electrical (voltage-gated calcium channels), chemical (via norepinephrine, angiotensin II) or mechanical stimuli (myogenic response). Intracellular calcium plays an important role in SMC contraction. Calcium entry via L-type calcium channels or release from the sarcoplasmic reticulum leads to an increase in intracellular free calcium which binds to calmodulin. The calcium-calmodulin complex activates

myosin light chain kinase (MLCK), an enzyme that phosphorylates myosin light chain allowing it to form cross-bridges with actin filaments (Wier et al. 2003). Vascular smooth muscle contraction usually is maintained in a tonic phase whereby the medial SMCs are constantly constricted. This requires the inhibition of myosin light chain phosphatase (MLCP) activity that consolidates the phosphorylation of myosin. On the contrary, activation of MLCP would decrease SMC contraction. Subsequent activation of the Rho GTPase RhoA and Rho kinase not only activates MLCK but also inhibits MLCP activity by an inhibitor protein CPI-17, which is also regulated by protein kinase C (PKC)(Kitazawa et al. 2003). Therefore, mechanisms that alter intracellular calcium or affect the activation of MLCK greatly affect SMC contraction.

G-protein coupled receptors interacting with the α-subunit of the heterotrimeric G-protein $G_{q/11}$ can activate phospholipase C (PLC)β, resulting in the formation of inositol trisphosphate (IP_3) and diacyl glycerol (DAG). IP_3 triggers calcium release from the sarcoplasmic reticulum via the IP_3 receptor while DAG can activate transient receptor potential channels C3, C6 and C7 causing influx of extracellular calcium. Receptors coupled to G_s stimulate adenylyl cyclase which catalyzes formation of cAMP. In vascular SMCs, an increase in cAMP through β2-adrenoceptor stimulation, e.g. by adrenaline, results in vasodilatation via disinhibition of MLCP. Another important vasodilator mechanism is the NO-cGMP system. NO released by endothelial cells diffuses to the vascular SMCs where it activates guanylyl cyclase, increases cGMP formation with subsequent activation of MLCP and enhanced sequestration of calcium into the ER.

The inherent contractile property of vascular SMCs is lost or reduced under conditions of remodelling along with an increase in proliferation and migration of these cells. The contractile phenotype of SMCs is associated with a number of important marker proteins like calponin, smooth muscle actin (SMA) and smooth muscle myosin heavy chain (SM-MHC) (Regan et al. 2000, Shanahan et al. 1993, Althoff et al. 2012). On the other hand, a shift to the proliferative or synthetic phenotype is marked by a decrease in expression of the aforementioned proteins and an increase in expression of vimentin, integrin β_1, collagen and different matrix metalloproteinase (MMP) isoforms (Minami et

al. 2012, Rzucidlo et al. 2007).Other important factors influencing the differentiated state of SMCs are platelet derived growth factor B (PDGF-B) and transforming growth factor β (TGF-β) (Li et al. 2011, Durante et al. 1996, Egan et al. 2005, Grainger et al. 1998, Tang et al. 2011). While PDGF-B causes increased proliferation of vascular SMCs, TGF-β maintains the contractile state of these cells through expression of SMC marker proteins.

In this context, the phenotype of vascular SMCs is strongly regulated by the myocardin family of transcription coactivators, namely myocardin, myocardin related transcription factor A and B (MRTF-A and MRTF-B) (Parmacek et al. 2007, Long et al. 2008, Wang et al. 2003, Yoshida et al. 2003, Minami et al. 2012).Although myocardin has a constitutive nuclear localization, recent work has shown that it is exported from the nucleus under conditions of hypertension (Pfisterer et al. 2012). On the contrary, MRTF-A and B which have RPEL motifs with a G-actin binding site are localized in the cytoplasm. This localization of MRTF-A and B is tightly regulated by the polymerization status of actin whereby polymerized F-actin drives their accumulation in the nucleus(Olson et al. 2010, Vartiainen et al. 2007, Miralles et al. 2003). In vascular SMCs, serum response factor (SRF) controls gene expression governing the switch between the contractile and the synthetic phenotype depending on the transcriptional co-activators that bind to it. Thus, SRF activity can be fine-tuned by changes in the relative amounts of myocardin and MRTF-A that interact with it. In the presence of these coactivators, SRF binds to the CarG box in the promoter region of its target genes. While myocardin knockout is lethal in mice, mice lacking MRTF-A or B are viable (Li et al. 2003, Li et al. 2006). This also indicates that these coactivators must have distinct functions in terms of regulating the SMC phenotype. It is noteworthy that the ternary complex factor Elk-1 competes with myocardin for binding to SRF and thus regulates its activity and the corresponding SMC phenotype (Wang et al. 2004). Apart from the changes in SMC phenotype, the remodelling process also is affected by the ECM surrounding the vascular SMCs.

1.4.2 ECM in pathological remodelling of the blood vessel wall

The extracellular matrix is an integral part of the arterial wall with endothelial cells resting on the basement membrane rich in collagen IV. Collagens and elastins are the main structural components of the vessels. Among the 26 different types of collagen known, type I and III are the major fibrillar collagens in blood vessels representing 60% and 30% of total collagens, respectively, in their wall (Prockop et al. 1995). The cross linking of collagens and elastins is regulated by an enzyme known as lysyl oxidase (LOX) which has several isoforms (Reiser et al. 1992). The expression and activity of LOX is an important determinant of the stability of the vessel wall as well as in fibrosis. The ECM also contains several glycoproteins like fibronectin, vitronectin, laminin, tenascin and thrombospondin as well as proteoglycans such as versican, hyaluronan and perlecan among others (Chothia et al. 1997). Another ECM component, tenascin C, is up regulated in arteries exposed to high pressure (not only blood pressure) and promotes migration of SMCs.

The ECM composition is regulated not only by the synthesis of the ECM proteins but also their degradation which is regulated by the matrix metalloproteinases. MMP-1, MMP-13 are collagenases, MMP-2 and 9 are gelatinases while MMP-3 rather has a broad spectrum activity. In addition, there are also membrane-type metalloproteinases (MT-MMP). The activity of MMPs is regulated by their conversion to the active form as well as by the tissue inhibitors of MMPs known as TIMPs (Feldman et al. 2001, Badier-Commander et al. 2000). In various remodelling processes, including hypertension, the expression and activity of these molecules is altered. For example, pressure-induced upregulation of MMP9 has been implicated in early hypertensive remodelling (Lehoux et al. 2004). In hypertension, there is an induction of collagen and elastin synthesis and a reduced degradation resulting in stiffening of the arterial wall. Additionally, the receptors for these ECM proteins such as integrins also contribute to the remodelling process. It is now widely accepted that integrins can receive information from the ECM and transduce signals to the cell thereby regulating cell behavior (Miranti et al. 2002).

1.4.3 Pathological remodelling of the heart in hypertension

Prolonged increase in biomechanical stress in the heart as in hypertension manifests as an increase in cardiac mass termed hypertrophy and deposition of fibrotic tissue both of which result in reduced cardiac function and ultimately heart failure. Hypertrophy is defined by an increase in cardiomyocyte size, enhanced protein synthesis and higher sarcomere organization. Induction of the fetal gene program often precedes the hypertrophic response with increase in expression of genes such as atrial natriuretic peptide (ANP), and early response genes like c-fos and c-myc. Several molecular pathways are involved in the hypertrophic response including calcineurin-NFAT signalling or the phosphoinositide 3-kinase (PI_3)-Akt-GSK-3 pathway in addition to signalling by various G-protein-coupled receptors including $G_{q/11}$, G_s and G_i signalling (Olson et al. 2000, Cantley et al. 2002, Chesley et al. 2000, Chien et al. 1999). Transcriptional regulation by MEF2/HDAC is another important mediator of cardiac hypertrophy among several other mechanisms (McKinsey et al. 2002). Additionally, TGF-β1 has been shown to play a pivotal role in the response to pressure overload in the murine heart (Koitabashi et al. 2011).

However, hypertrophy is not the sole result of prolonged cardiac stress. In addition, there is an increase in cardiac fibrosis. The fibrotic state results from an imbalance between MMPs and their inhibitors, thereby altering the composition of the ECM. Increased fibrosis in turn impairs cardiomyocyte function. In hypertensive heart disease, there is an accumulation of collagen and with enhanced cross-linking leading to fibrosis. A large part of this is contributed by myofibroblasts with collagen turnover being regulated by a combination of growth factors such as angiotensin II (ANGII), TGF-β_1 and TNF-α. Dahl salt-sensitive rats show increased expression of MMP2, TIMP1 and TIMP2 as left ventricular hypertrophy (LVH) progresses under hypertensive conditions (Iwanaga et al. 2002).Similarly, there is an increase in MMP2 activity in spontaneously hypertensive rats (SHRs) (Mujumdar et al. 2001).Apart from these molecules, various integrin receptors expressed in the heart play an important role in the remodelling process such as $\alpha_3\beta_1$ and $\alpha_5\beta_1$ that are expressed on cardiac myocytes. While $\alpha_3\beta_1$ can bind to collagen I, laminin and fibronectin, $\alpha_5\beta_1$ is a predominant fibronectin receptor.

Furthermore, integrins can activate downstream molecules such as focal adhesion kinase (FAK), small GTPases such as Rac and Rho thereby interfering with other signalling pathways.

In addition to the direct effects of cardiomyocytes and fibroblasts via the aforementioned mechanisms, cardiomyocyte apoptosis is another important mechanism which facilitates remodelling in hypertensive heart disease. Increased apoptosis has been demonstrated in hypertensive hearts in both murine and human models of hypertension (Fortuño et al. 2003). Apart from the direct effect of physical force on apoptosis, there is significant contribution from local humoral factors such as ANGII to this process. Apoptosis of cardiomyocytes may compromise contractile function, facilitate remodelling by deposition of fibrotic scar tissue and increased stiffening, impair myocardial energy production and trigger arrhythmias. Thus, an increase in cardiac stress by increased blood pressure over prolonged periods can lead to widespread remodelling and impaired function of the heart. An early step in pressure induced remodelling of both the heart and the arteries is the mechanosensing of supraphysiological biomechanical forces by the respective constituent cells.

1.5 Vascular mechanotransduction

1.5.1. Components of cellular mechanotransduction

Mechanotransduction is the process by which cells convert mechanical stimuli to chemical activity (Ingber et al. 2006). The two predominant forces in the vasculature, namely fluid shear stress and cyclic strain, have already been discussed. Both these forces transduce signals to the cell via a variety of pathways. Various cellular components such as the extracellular matrix, transmembrane integrin receptors, cytoskeleton itself and certain ion channels are candidate mechanosensors. In endothelial cells, putative mechanotransducers have been proposed such as integrins, receptor tyrosine kinases, the apical glycocalyx, heterotrimeric G-proteins, platelet/endothelial cell adhesion molecule (PECAM1) and vascular endothelial cadherin (VE-cadherin) (Tzima et al. 2001, Osawa et al. 2002, Chen et al. 1999, Tzima et al. 2005, Curry et al. 2012, Weinbaum et al. 2003, Gudi et al. 2003). Changes in

intracellular calcium are considered an important step in numerous mechanotransduction pathways. In this context, direct stretch-activated cation channels have been reported (Sachs et al. 2010). Store-operated calcium entry (SOC) pathways coupled with STIM1 and Orai proteins have also been investigated in this regard (Trebak et al. 2012, Roos et al. 2005, Vig et al. 2006).

Notably, transient receptor potential channels (TRP) have been proposed in cellular mechanotransduction, with TRPV channels reported in endothelial cell mechanotransduction while TRPC3 and TRPC6 have been associated with the myogenic response of vascular SMCs (Thodeti et al. 2009, Dietrich et al. 2005, Welsh et al. 2002). These channels have six transmembrane segments and a pore region between the fifth and sixth segment. TRPV1 has been implicated in bladder voiding, a process in which wall tension is involved (Gevaert et al. 2007). Some of these receptors and channels are shown in Figure 2.

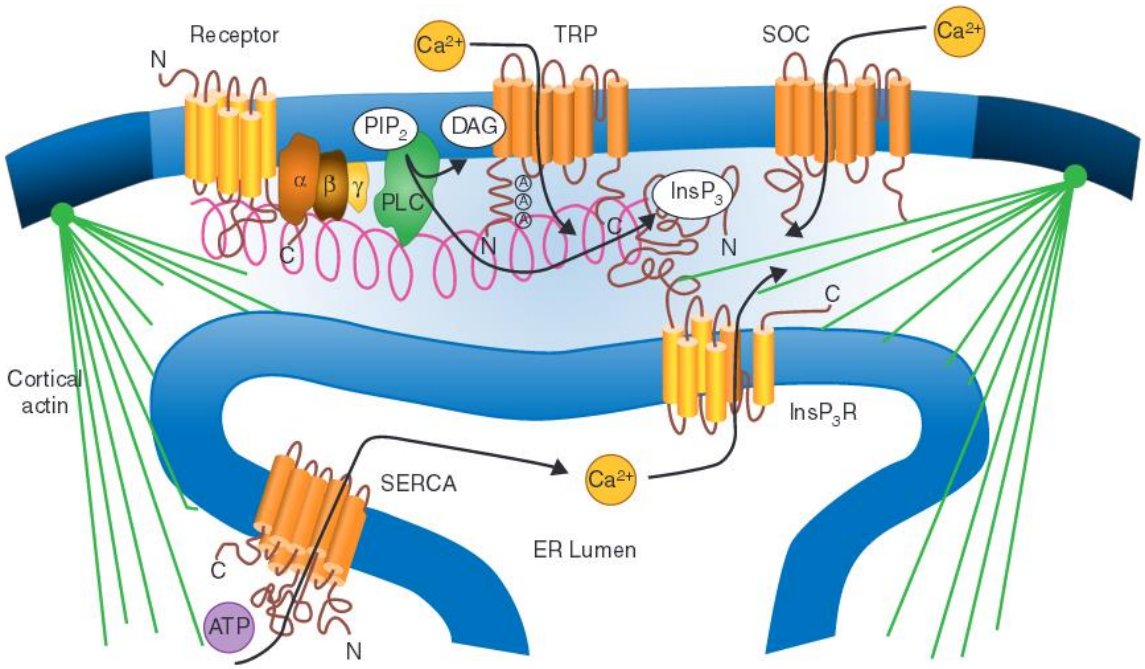

Figure 2: A representation of various channels and receptors which can cause changes in intracellular calcium in response to mechanical stimuli (From Venkatachalam et al. 2002).

More recently, GPCRs have been proposed to be mechanosensitive with ligand-independent signalling in response to membrane stretch (Mederos y Schnitzler et al.

2008, Storch et al. 2012). This is achieved by release of PLC which catalyzes formation of IP_3 and DAG. DAG in turn can activate TRPC6 channels in the plasma membrane. Recently, piezo proteins have been identified as pore forming subunits of mechanically activated channels (Kim et al. 2012, Coste et al. 2012). Most of these pathways lead to changes in the concentration of ions, e.g. calcium, within the cell thereby initiating downstream signalling cascades.

We have identified TRPC3 channels as an upstream component of the stretch-induced zyxin translocation pathway in endothelial cells and vascular SMCs (doctoral thesis of Sahana Suresh Babu, Heidelberg, 2011). The role of TRPC3 in the zyxin-mediated response of endothelial cells to cyclic stretch has been studied in greater detail in this thesis and efforts have been made to identify pathways upstream of TRPC3 in endothelial mechanosensing.

1.5.2. Mechanosensitive gene expression

Both endothelial and smooth muscle cells respond to biomechanical stimuli with robust changes in gene expression that determine the phenotype of these cells. In this context, it is noteworthy that the changes in gene expression initiated by fluid shear stress are different from the ones associated with cyclic stretch, a component of wall tension. Several mechanosensitive transcription factors have been reported in both endothelial cells and vascular SMCs. For example, fluid shear stress regulates transcription factors such as nuclear factor κB (NFκB), activator protein-1 (AP-1), and early growth response-1 (Egr-1) in endothelial cells (Partridge et al. 2007, Lan et al. 1994, Khachigian et al. 1997). In addition, shear stress-induced transcription factors such as krüppel-like factor 2 (KLF2) and nuclear factor erythroid 2-like (Nrf2) have been extensively studied (Lee et al. 2006, Chen et al. 2003, Dekker et al. 2005). Likewise, wall tension-induced stimulation of vascular cells activates several kinases such as focal adhesion kinase (FAK), Rho kinase (ROCK) and MAP kinase pathways (Lehoux et al. 1998, Li et al. 2003, Tsuda et al. 2002, Lehoux et al. 2006) which lead to activation of transcription factors such as AP-1, C/EBP, CREB, NFκB and Sp-1 (Cattaruzza et al.2001, Cattaruzza et al. 2002, Demicheva et al. 2008, Wagner et al. 2000, Wilson et

al. 1998). In rabbit jugular veins, pressure induces upregulation of preproET-1 gene expression *in situ* (Lauth et al. 2000).

However, many of these transcription factors are part of other cellular processes like inflammation and are not specific for wall tension-induced pathways. Recent work in our group has established zyxin, a component of focal adhesions, as a specifically stretch-sensitive transcription factor in endothelial cells (Wójtowicz et al. 2010). However, stretch-induced zyxin translocation in vascular SMCs follows different kinetics and has a different threshold. This work focuses in part on the stretch-induced zyxin-dependent changes in gene expression in vascular SMCs.

1.6 The zyxin family

Zyxin is a 82 kDa protein that was isolated for the first time in chicken embryo fibroblasts (Crawford et al.1991, Sadler et al. 1992). This Lin-11 Isl-1 Mec-3 (LIM) domain protein is a member of a family that includes the lipoma preferred partner protein (LPP) and the thyroid receptor-interacting protein 6 (TRIP6). Structurally, zyxin has a proline-rich region that mediates its association with α-actinin, three ActA domains which interact with members of the Ena-VASP family (Drees et al. 2000) and three zinc finger containing LIM domains (for interaction with the DNA) at the C-terminus. It also has a nuclear export sequence (NES) accounting for its constitutive extra-nuclear localization. Zyxin is involved in assembly of the actin cytoskeleton, cell division and in shuttling from the cytoplasm to the nucleus (Hirota et al. 2000, Nix et al. 1997).There are numerous reports of its role in several cellular processes such as migration, apoptosis and cell adhesion (Crone et al. 2011, Hervy et al. 2010, Sperry et al. 2010, Yamamura et al. 2013, Fraley et al. 2012, Hoffman et al. 2006). In arterial SMCs, it has been associated with mechanotransduction (Cattaruzza et al. 2004).

Zyxin fulfils the criteria for a bonafide mechanotransducer. It is located at the vicinity of integrins at the cell-ECM interphase and is ideally situated for (mechano)sensing changes in the ECM or the cell surface, it is also capable of shuttling to the nucleus in response to stretch and finally, it has been shown to interact with DNA and regulate mechanosensitive gene expression (Nix et al. 1997, Wójtowicz et al. 2010). It is also

involved in cardiomyocyte survival in response to ANP (Kato et al. 2005). Zyxin is critically involved in the stretch-induced build up and repair of stress fibres (Smith et al. 2010, Hoffman et al. 2012). Interestingly, no overt phenotypes have been reported for mice lacking either zyxin or LPP with no available knockout mice for TRIP6. This is presumably due to the redundancy among the different family members owing to structural similarities between them (Figure 3).

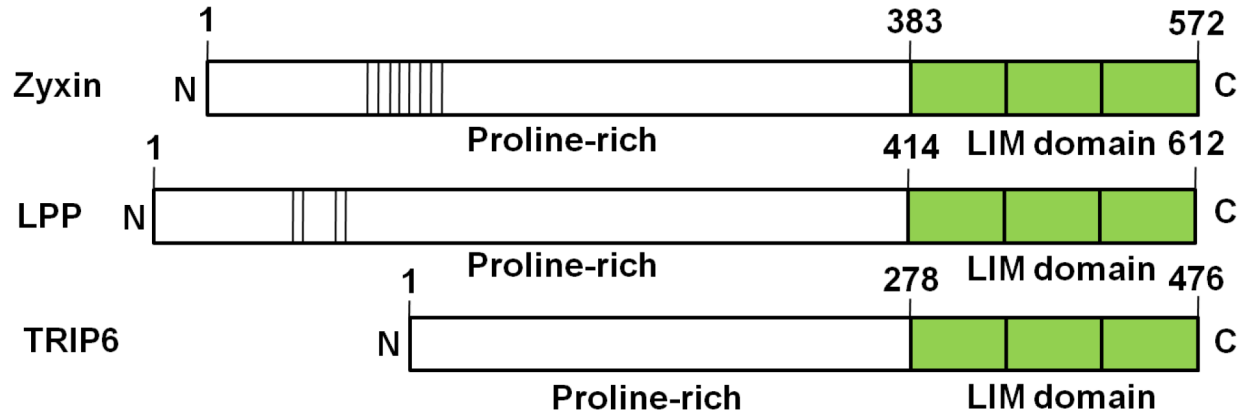

Figure 3: Domain similarity of closely related zyxin family members zyxin, LPP and TRIP6 (Adapted from Petit et al. 1999).

1.7 Aims of the project

In the context of the present study, it is important to consider the aforementioned role of zyxin as a mechanotransducer. The stretch-induced nuclear translocation of zyxin, an integral part of this mechanotransduction cascade, has been found to be TRPC3-dependent in vascular cells. However, the mechanism by which stretch activates TRPC3 channels, e.g. in endothelial cells upon stretch is not clear. Furthermore, although the zyxin-dependency of stretch-induced gene expression in endothelial cells has been characterized, the exact role of zyxin in stretched vascular SMCs along with the phenotype of zyxin-null SMCs has not yet been investigated. Finally, considering the lack of a prominent phenotype in zyxin-null mice, and the putative role of zyxin as a mechanotransducer, it becomes almost intuitive to study its role in a model of cellular stress. Accordingly, the following points have been investigated and elaborated in the present study.

a) The consequences of TRPC3 channel activation in endothelial cells on zyxin-mediated signalling and the elucidation of stretch-induced signalling pathways upstream of TRPC3 activation.

b) A genome-wide microarray analysis of stretch-induced gene expression in wild type and zyxin-null SMCs followed by pathway analysis to define zyxin-dependent pathways in stretched SMCs.

c) Characterization of the phenotype of zyxin-null SMCs *in vitro* to elucidate the consequences of zyxin-induced changes in gene expression.

c) The *in vivo* function of zyxin in mice using a model of experimental hypertension to define the role of zyxin in hypertension-induced cardiovascular remodelling.

2 MATERIALS

2.1 Equipments

2.1.1 Miscellaneous equipments

Table 1: Miscellaneous equipments used in this study

Equipment	Model	Company	Method
Agarose gel electrophoresis power supply	PowerPack P25	Biometra	Molecular biology
Anaesthetic pump	Isotec5	Datex Ohmeda	Animal surgery
Autoclave	5050 EL	Tuttnauer	Sterilization
Bacterial incubator	Innova 4230	New Brunswick Scientific	Molecular biology
Balance	BP121S	Sartorius	Weight measurements
CO_2 incubator	Innova CO-170	New Brunswick Scientific	Cell culture
	BB-16	Heraeus Instruments	
Cooling plate	EG1140C	Leica	Histology
Flexercell system	FX-5000	Flexcell® International	Biomechanical stretch
Micropipette puller	P-87	Sutter Instrument Co.	Myography
Heating block	HBT-1131	HLC-Haep Labor Consult	Miscellaneous
Heating chamber	U40	Memmert	Histology
Laminar flow	HS18 Hera safe	Heraeus Instruments	Cell culture

Equipment	Model	Company	Method
Light cycler	LightCycler 1.5	Roche	Molecular biology
Luminescent image analyzer	ImageQuant LAS 4000 mini	GE	Molecular biology
Magnetic stirrer	IKAMAG	Janke & Kunkel GmbH	Miscellaneous
Microtome	HM430	Microm International GmbH	Histology
NanoDrop	ND-1000	PeQlab Biotechnologie GmbH	Molecular biology
Nitrogen tank	Arpege 140	Air Liquide	Storage and preservation
Nucleofector®	Nucleofector® II	Amaxa	Transfection
Paraffin embedding system	EG1120	Leica	Histology
PCR cycler	Thermocycler	Biometra	Molecular biology
Peristaltic pump	Ismatec Reglo	TSE systems	Organ preparation
pH meter	pH 720	inolab	Molecular biology
Plate reader	PowerWave XS	BIO-TEK	Molecular biology
Power supply for gel chamber	PowerPac HC	BIORAD	Molecular biology
Pressure myograph system	110P	DMT	*In situ*arterial physiology
SDS-PAGE chamber	Mini-Protean	BIORAD	Molecular biology
Sonicator	UP50H	dr. hielscher GmbH	Molecular biology

Equipment	Model	Company	Method
Sterile bench	UVT-S-AR	Grant	Cell and tissue isolation
Transfer chamber	Mini-Protean	BIORAD	Molecular biology
Transilluminator	Gel Doc™	BIORAD	Molecular biology
Vortex	Vortex-2 Genie	Scientific Industries Inc.	Miscellaneous
Water bath	E11	Dinkelberg analytics	Miscellaneous

2.1.2 Centrifuges

Table 2: Centrifuge types and models used in this work

Centrifuge	Model	Company	Method
Cooling centrifuge	Z323K	HERMLE	Molecular biology
Centrifuge	Universal 32	Hettich Zentrifugen	Cell culture
Mini centrifuge	SPROUT™	Biozym	Miscellaneous
Table top centrifuge	Pico 21	Heraeus	Molecular biology
Table top cooling centrifuge	Mikro22R	Hettich Zentrifugen	Molecular biology

2.1.3 Microscopes

Table 3: Microscopes used in this study

Microscope	Model	Company	Method
Light microscope	M5-51845	Wild Heerbrugg	Organ isolation
	Axiovert 25	Zeiss	Cell culture
	CKX41	Olympus	Histological analysis
			Functional assays

Microscope	Model	Company	Method
Confocal microscope	IX81	Olympus	Immunofluorescence analysis
Stereomicroscope	Wild M650	Heerbrugg	Animal surgery

2.1.4 Specialized equipments

Table 4: Equipments used for monitoring physiological parameters in mice

Equipment	Model	Company	Method
High resolution ultrasound	Vevo2100	VisualSonics	Echocardiography and femoral artery resistivity measurements
Pressuremeter (Tail cuff)	LE5001	Panlab	Blood pressure recording
Radiotelemetry	PA-C10	DSI	Blood pressure recording

2.2 Materials for surgery and ultrasound imaging

Table 5: Materials used for surgical and imaging procedures in mice

Materials	Type	Supplier
Cannula	Venofix® 25G	B Braun
Cannulation forceps	00608-11	F.S.T
Deoxycorticosterone acetate (DOCA)	M121	Innovative Research of America
Electrode cleanser	Cleanisept® wipes	Dr. Schumacher GmbH
Electrode gel	Skintact®	Leonhard Lang GmbH
Eye cream	Bepanthen	Bayer
Forceps and tweezers	Dumont	F.S.T
Hair removal cream	SNÄ Epil	Rufin cosmetic
Isoflurane	HDG9623	Baxter

Materials	Type	Supplier
Microvessel clips	FD562R	Aesculap
Rectal lubricant	Aquagel®	Parker laboratories
Skin antiseptic spray	Kodan tinktur forte	Schülke & Mayr GmbH
Skin antiseptic cream	Betaisodona Salbe	Mundipharma GmbH
Surgical suture	G-6, 30 cm 6-0 Perma-hand Seide	Ethicon
Syringe	Luer-lok™ (20 ml)	BD-plastipak
Syringe	Luer (1 ml)	BD-plastipak
Ultrasound gel	PZN 8825881	Dahlhausen

2.3 Miscellaneous disposable materials

Table 6: Disposable materials used in the present study

Materials	Supplier
Bacterial culture tubes	Sarstedt
Cell culture dishes	TPP
Cell culture flasks (T25, T75)	Sarstedt
Cell culture plates	Sarstedt, Greiner
Cell scraper	Sarstedt
Cover slips for calcium imaging	11.8 mm diameter, Thermo Scientific
Cover slips for microscopy	Thermo Scientific
Filter papers	Munktell
Microscope slides	Thermo Scientific
PCR tubes	Sarstedt
Pipette tips	Sarstedt
Plastic pipettes	Sarstedt
PVDF transfer membranes	Immobilon®-P (Merck Millipore)
Safe lock tubes	Sarstedt
Sterile filters	GE Healthcare

2.4 Miscellaneous non-disposable materials

Table 7: Non-disposable re-usable materials used in this work

Materials	Supplier
Glass beaker	Schott Duran
Glass bottles	Schott Duran
Glass Erlenmeyer flasks	Schott Duran
Glass measuring cylinders	Duran
Hemocytometer	Neubauer SUPERIOR

2.5 Chemicals

2.5.1 Miscellaneous chemicals

Table 8: List of chemical reagents used in this study

Product	Supplier	Product	Supplier
Agar	Roth	Lysis buffer	Cytoskeleton
Agarose	Sigma	Deoxyribonuclease I	Worthington
Ampicillin	Sigma Aldrich	Paraformaldehyde	Sigma
APS	Roth	Chemiluminescence substrate	Luminata™ Forte (Merck Millipore)
Bacto-tryptone	BD	Yeast extract	Roth
Boric acid	Sigma Aldrich	Penicillin	Gibco
BSA	Sigma	Glycerol	VWR
Calcium chloride	Merck	Xylene	Sigma Aldrich
Casein	Sigma	Sodium orthovanadate	Sigma

Product	Supplier	Product	Supplier
Collagenase Type 2 (Lot: 43D14200A)	Worthingon	Mowiol 4-88	Fluka
Competent cells	Invitrogen	M-MLV reverse transcriptase	Promega
DABCO	Sigma	Zinc acetate dihydrate	Roth
DAPI	Invitrogen	Taq polymerase	Bioron
DNA ladder	Thermo Scientific	Oligo dT	Promega
Ethidium bromide	Roth	KCl	AppliChem
Fura- 2 AM	Life technologies	Zinc chloride	Merck
Gelatin	Merck	Calcium-free medium	M8167 Sigma
Glucose	Merck	Tris hydrochloride	Roth
Glycine	Sigma Aldrich	Methanol	Sigma Aldrich
Hanks BSS	Gibco	Disodium hydrogen phosphate	Roth
HEPES	Sigma	EDTA	AppliChem
Laminin	L2020 Sigma Aldrich	Horse serum	Gibco
Leupeptin A	Sigma	Triton-X 100	Sigma
L-glutamine	25030 Life technologies	DAKO® pen	Dako Denmark
Nonidet-P-40	Fluka	EGTA	Roth
Opti-MEM	Gibco	PBS	Life technologies
Pefabloc	Fluka	Pepstatin A	Sigma
Polyacrylamide	Roth	Tween 20	Roth
Potassium dihydrogen phosphate	Riedel- de Haën	Calcium acetate	Roth
RNAlater RNA stabilization reagent	Qiagen	Matra-A reagent	IBA

Product	Supplier	Product	Supplier
SDS	Serva	DTT	Roth
SOC medium	Invitrogen	Dispase	Gibco
Sodium chloride	Sigma Aldrich	Sodium fluoride	Riedel- de Haën
Sodium hydrogen carbonate	J.T.Baker	Paraffin	Paraplast®Plus™ Leica
Streptomycin	Gibco	Fungizone	Gibco
TEMED	Roth	Sodium hydroxide	Sigma Aldrich
Trypsin	Gibco	FCS	Gibco

2.5.2 Stimulants and inhibitors

Table 9: List of stimulants and inhibitors used in this study

Product	Concentration	Catalog number	Supplier
TRPC3,6,7 channel activator (Oleyl acetyl glycerol; OAG)	100 µM	O6754	Sigma Aldrich
Endothelin receptor agonist (Endothelin-1 or ET1)	100 nM	E7764-10UG	Sigma Aldrich
IP3 receptor agonist (Thrombin)	4 U/ml	T6884	Sigma-Aldrich
Murine Fas L-strep	400 ng/ml	2-3951-010	IBA
Recombinant TGF-β_1	10 ng/ml	7666-MB-005	R&D
PKC inhibitor (GF109203X)	10 µM	0741	Tocris biosciences
PLC inhibitor (U73122)	5 µM	U6756	Sigma Aldrich
TRPC3 channel inhibitor (Pyr3)	10 µM	P0032	Sigma Aldrich
IP3 receptor blocker (Xestospongin C; XeC)	10 µM	1280	Tocris biosciences
Gadolinium (III) chloride	100 µM	439770	Sigma Aldrich
Losartan	10 µM	61188	Sigma Aldrich

2.6 Kits

Table 10: List of kits used in this study

Product	Catalog number	Supplier
QIAprep spin miniprep kit	27104	Qiagen
QIAprep Plasmid midi kit	12143	Qiagen
Maxiprep kit	740424.10	Macherey-Nagel
RNAeasy mini kit	74104	Qiagen
Sensiscript RT kit	205211	Qiagen
Basic nucleofector kit (SMC)	VPI-1004	Lonza
RhoA/Rac1/Cdc42 activation assay combo biochem kit	BK030	Cytoskeleton
In situ cell death detection kit, Fluorescein	11684795910	Roche
Cystatin C mouse ELISA kit	RD291009200R	Biovendor
pCR®2.1-TOPO® cloning kit	K4500-02	Invitrogen
QuantiTect SYBR Green® kit	204243	Qiagen
RT^2 Profiler array kit	PAMM-120ZA-12	Qiagen

2.7 Oligonucleotides

2.7.1 Primers

Table 11: List of primers used in this study for Real time PCR# and RT-PCR**

Gene	Primer sequence	Annealing temperature	Supplier
Mouse RPL32 #	GGGAGCAACAAGAAAACCAA	60°C	Invitrogen
	ATTGTGGACCAGGAACTTGC		
Human/mouse Gapdh #	GACCACAGTCCATGCCATCACTGC	60°C	IBA
	ATGACCTTGCCCACAGCCTTGG		

Gene	Primer sequence	Annealing temperature	Supplier
Mouse Cyclin E2 #	ACC AGC CAG ACT CTC CGC AA	60°C	IBA
	CTC CAG ACA GTA CAG GTG GCC A		
Mouse CD95 or Fas #	TGG ATC TGG GCT GTC CTG CC	60°C	IBA
	TTT CAC GAA CCC GCC TCC TCA		
Mouse MMP13 #	CTTCTTCTTGTTGAGCTGGACTC	55°C	Biomers.net
	CTGTGGAGGTCACTGTAGACT		
Mouse RGS5 #	GCGGAGAAGGCAAAGCAA	60°C	Sigma
	GTGGTCAATGTTCACCTCTTTAGG		
Mouse Inta8 #	TCA AGG CGA GGA ACA GCA A	58°C	IBA
	CCT TGG GAA CCC GAT GGT		
Human IL-8 #	TAGCCAGGATCCACAAGTCC	58°C	IBA
	GCTTCCACATGTCCTACAA		
Mouse CTGF	GCGAAGCTGACCTGGAGGAA	58°C	Biomers.net
	TTGGCGATTTTAGGTGTC		
Mouse Itgb1	TGGCAACAATGAAGCTATCGTG	56°C	Biomers.net
	GTAGGACAGTCTGGAGTCTCCACA		
Mouse ANP #	Undisclosed (QT00250922)	55°C	Qiagen
Mouse BNP #	Undisclosed (QT00107541)	55°C	Qiagen
Zyxin **	GGCCATGGCGGCCCCCCGC	61°C	IBA
	TCAGGTCTGGGCTCTAGCGGAGTG		

Table 12: List of primers used for genotyping

Gene	Primer sequence	Supplier
Zyxin WTR	TGGACGAAGTTTCCGTGTGTTG	IBA
Zyxin WTF	TACAAGGGCGAAGTCAGGGCGAGTG	
Zyxin NEOF	GACCGCTTCCTCGTGCTTTAC	

2.7.2 Small interfering RNAs

Table 13: Small interfering RNAs (siRNAs) used in this study

Gene	Target sequence	Supplier
Mkl1 or MRTF-A (mouse)	GGGCTCTGCCCATGCTTTT	Sigma
Zyxin (human)	AAGGTGAGCAGTATTGATTTG	Qiagen
PLC β_1 (human)	TCGAGATTACATGGATGTTAA	Qiagen
PLC β_3 (human)	CACGCTTGTCAACTACATCGA	Qiagen
PLC γ_1 (human)	CACCCTTACCACCAAGATCAA	Qiagen
Scrambled siRNA	Proprietary (undisclosed)	Qiagen

2.8 Antibodies

2.8.1 Primary antibodies

Table 14: Primary antibodies used in this study

WB: Western blot, ICC: Immunocytochemistry, IHC: Immunohistochemistry

Antibody	Species reactivity	Dilution	Application	Supplier
Rabbit polyclonal anti-zyxin	Mouse, human	1:1000 1:250	WB ICC	Prof. Mary Beckerle, USA
Rabbit polyclonal anti-MRTF-A	Mouse	1:200	ICC	Abcam (ab49311)
Goat polyclonal anti-MRTF-A	Mouse	1:1000	WB	Santa Cruz (sc-21558)
Rabbit polyclonal anti-TG2	Mouse	1:100	IHC	Neomarkers (RB-060-P)
Rabbit polyclonal anti-collagen I	Mouse	1:200	IHC	Abcam (ab34710)

Antibody	Species reactivity	Dilution	Application	Supplier
Rabbit polyclonal anti-PCNA	Mouse	1:200	IHC	Abcam (ab2426)
Mouse monoclonal anti-PLC β_1	Human	1:1000	WB	Abcam (ab77743)
Rabbit polyclonal anti-PLC β_3	Human	1:1000	WB	Abcam (ab1254735)
Rabbit polyclonal anti-PLC γ_1	Human	1:1000	WB	Abcam (ab4828)
Mouse monoclonal anti-beta actin	Mouse, human	1:2000	WB	Abcam (ab6276)
Rabbit polyclonal anti-tubulin	Mouse	1:1000	WB	Cell signalling #2144
Rabbit polyclonal anti-histone H3	Mouse	1:1000	WB	Abcam (ab1791)
Rabbit polyclonal anti-FAK	Mouse	1:1000	WB	Cell signalling #3285
Rabbit polyclonal anti-phospho FAK (pY^{397})	Mouse	1:1000	WB	Invitrogen 44-624G
Rabbit polyclonal anti-Akt	Mouse	1:1000	WB	Cell signalling #9272
Rabbit polyclonal anti-phospho Akt (Ser473)	Mouse	1:1000	WB	Cell signalling #9271
Rabbit polyclonal anti-integrin α_5	Mouse	1:1000	WB	Cell signalling #4705
Rabbit polyclonal anti-integrin β_1	Mouse	1:1000	WB	Cell signalling #9699
Rat monoclonal anti-PECAM1	Mouse	1:100	IHC	Santa Cruz

Antibody	Species reactivity	Dilution	Application	Supplier
Mouse monoclonal anti- α - actinin	Mouse	1:800	ICC	Sigma Aldrich A7811

2.8.2 Secondary antibodies

Table 15: List of secondary antibodies used in this work

Antibody	Species reactivity	Dilution	Application	Supplier
Cy2-conjugated donkey IgG (H+L)	Rat	1:200	ICC	Dianova
Cy3-conjugated donkey IgG (H+L)	Rabbit	1:200	ICC	Dianova
Goat IgG peroxidase	Rabbit	1:5000	WB	Sigma (A6154)
Donkey IgG peroxidase	Goat	1:5000	WB	Sigma (A5420)
Goat IgG peroxidase	Mouse	1:5000	WB	Sigma (A4416)

2.9 Growth media, buffers and solutions

Table 16: List of media used for cell culture and bacterial growth

Media	Purpose	Composition
Neonatal medium	Cardiomyocyte isolation and culture from neonatal mice hearts	(Dulbecco's modified Eagle's medium nutrient mixture F-12 Ham; D6421+ 2mM L-glutamine + Penicillin + Streptomycin + 5% horse serum

Media	Purpose	Composition
Growth medium	Propagation of HUVECs	Endothelial cell basal medium (PromoCell) + 5% FCS + Penicillin/Streptomycin/Fungizone + supplement (without hydrocortisone)
Growth medium	Propagation of VSMCs and cardiac fibroblasts	DMEM (1x) + GlutaMax^{TM}-I + 15% FCS +Penicillin/Streptomycin/Fungizone
Luria-Bertani (LB) agar	Propagation of bacteria	1.5 % (w/v) Agar in LB medium with 50 µg/ml ampicillin
Luria-Bertani (LB) medium	Propagation of bacteria	1.0 % (w/v) Bacto-tryptone 0.5 % (w/v) Yeast extracts 1.0 % (w/v) NaCl

Table 17: List of buffers and solutions used in this study

Buffer/Media/Solution	Composition
Agarose gel loading buffer	10 mM Tris HCl, pH 7.5 10 mM EDTA, pH 8.0 30% Glycerol 0.01% Bromophenol blue 0.01% Xylene green
Blocking buffer for ICC/IHC	0.25 % Casein 0.1 % BSA 15 mM NaN_3 50 mM Tris, pH 7.6
Blocking buffer for WB	5 % milk powder or Blotto® in TBST
Dnase I solution	0.5% (w/v) solution in PBS

Buffer/Media/Solution	Composition
Collagenase solution (Type 2)	2% (w/v) solution in PBS
Lysis buffer (whole cell lysates)	10 mM Hepes, pH 7.9 10 mM KCl 0.1 mM EDTA 0.1 mM EGTA 0.1 M DTT 50 µM Pefabloc 25 µM Protease inhibitors
Lysis buffer I for nuclear extraction	10 mM HEPES 10 mM KCl 0,1 mM EDTA 0,1 mM EGTA 0,15 % Nonidet-P-40 20mM Na_3VO_4 Pefa und Proteaseinhibitormix
Lysis buffer II for nuclear extraction	20mM HEPES 400 mM NaCl 0,01 mM EDTA 0,01 mM EGTA 0,15 % Nonidet-P-40 20 mM Na_3VO_4 Pefabloc and Protease inhibitor mix
Membrane stripping buffer	0.2 M NaOH
Mounting medium for ICC/IHC	0,1 M Tris HCl, pH 8,5 10 % Mowiol 4-88 25 % Glycerin 2,5 % DABCO

Buffer/Media/Solution	Composition
Phosphate-buffered saline (PBS)	8.0 g NaCl 0.2 g KCl 1.44 g Na_2HPO_4 0.2 g KH_2PO_4
Pefabloc	15 mM HEPES Puffer, pH 7,4 4 % Pefabloc-SC
Protease inhibitor mix (PIM)	1 % Pepstatin A in 20 % DMSO und 80 % 15 mM Hepes, pH 7,4 1 % Leupeptin in 20 % DMSO und 80 % 15 mM Hepes, pH 7,4
Ringer's solution	154 mM NaCl, 5.6 mM KCl 2.4 mM $CaCl_2$, 6 mM $NaHCO_3$ 5.6 mM Dextrose, 30 mg/l Nitroprussiate 27 mg/l Adenosine
Running buffer for SDS-PAGE	25 mM Tris HCl, pH 8.3 192 mM Glycine 0.1% SDS
5x TBE buffer	450 mM Tris 450 mM Boric acid 20 mM EDTA, pH 8.0
Tris-buffered saline (TBS)	6.1 g Tris (0.5 M) 8.75 g NaCl (1.5 M) in 1 litre H_2O
TBST	0.05 % Tween 20 in TBS
Transfer buffer	25 mM Tris 192 mM Glycine, pH 8.3
Zinc fixation	0.1 M Tris HCl, pH 7.4 3.2 mM $Ca(CH_3COO)_2(H_2O)$ 22.8 mM $Zn(CH3COO)_2.2H_2O$ 35.9 mM $ZnCl_2$

3 METHODS

3.1 *In vitro* methods using isolated cells

3.1.1 Cell isolation and culture

Isolation and culture of human umbilical vein endothelial cells (HUVECs)

The isolation of HUVECs from fresh umbilical cords was approved by the local ethics committee (#336/2005). Briefly, the two ends of the umbilical vein were cannulated and the blood was flushed out with 20 ml of Hanks buffer. The endothelial cells were isolated using dispase solution (3.1 g/l) by filling the cords through the cannula and tying up the two ends. The cords filled with the dispase solution were incubated at 37°C for 30 minutes. Finally, the contents were emptied into a 50 ml falcon tube. The vein was flushed with Hanks buffer to collect the residual cells. The tube was centrifuged for 5 minutes at 1000 rpm. The cell pellet was re-suspended in endothelial cell growth medium. The cells were routinely cultured on standard 6-well plastic plates or collagen type I-coated Bioflex elastomer plates (Flexcell®) which were additionally coated with 2% (w/v) gelatin solution. Cells were allowed to grow in a CO_2 incubator at 37°C. P0 cells were used for all experiments for measurements of calcium transients. For all other experiments, cells were passaged once (P1).

Isolation and culture of human umbilical artery-derived vascular smooth muscle cells (HUASMCs)

Human arterial smooth muscle cells were isolated from human umbilical cord arteries. The umbilical artery was cannulated and washed with Hanks buffer to remove the residual blood. The artery media was cut into small pieces and placed in a Petri dish. The arterial fragments were covered with DMEM medium containing 15% FCS and antibiotics. Smooth muscle cells usually took 10-14 days to grow out of the artery. These cells were detached from the Petri dish by treatment with trypsin for 5 minutes at 37°C followed by centrifugation for 5 minutes at 1000 rpm. The cell pellet was re-suspended in DMEM medium containing 15% FCS and antibiotics and transferred into a T75 cell culture flask. Cells were allowed to grow in a CO_2 incubator at 37°C. Only cells

cultured up to passage 3 were used for the experiments to avoid artifacts due to prolong sub-culture of smooth muscle cells.

Isolation and culture of mouse aortic smooth muscle cells (mAoVSMCs or vascular SMCs)

For the isolation of mouse arterial smooth muscle cells, the thoracic aorta of WT and zyxin-null mice were used. The aorta was isolated, cleared from surrounding fat and connective tissue and cut into small fragments. They were washed with Hanks BSS solution and transferred to one well of a 6-well plate containing 1.4 ml of DMEM/SMC growth medium 2 (1:1, Promocell, Heidelberg, Germany) which was supplemented with 5% FBS and containing 250 µl collagenase solution. The arterial fragments were digested overnight and the medium was replaced the next day. The cells were allowed to grow to 70-80% confluence. Finally, the cells were trypsinized and centrifuged for 5 minutes at 1000 rpm. The cell pellet was suspended in DMEM medium containing 15% FCS and antibiotics. These cells were seeded in a T25 or T75 flask and propagated. For the experiments, cells were either seeded on plastic plates or collagen type I-coated Bioflex elastomer plates (Flexcell®). Cells were allowed to grow in a CO_2 incubator at 37°C. Only cells cultured up to passage 3 were used for the experiments to avoid artifacts due to prolong sub-culture of smooth muscle cells.

Isolation and culture of neonatal cardiomyocytes from mouse hearts

For isolation of neonatal cardiomyocytes and cardiac fibroblasts, 1-2 day old neonates were used. The pups were sacrificed by removing the head with sharp scissors. The pups were placed on their backs, a midline sternotomy was performed and pressure was applied to the chest cavity with the fingers. This allowed the heart to ‘pop’ out, which was then excised easily. The hearts were placed in ice cold PBS/2G. Usually, 10 hearts were used for isolating sufficient number of cardiomyocytes. The hearts were washed 2-3 times with cold PBS/2G to remove red blood cells and debris. The solutions for digesting the hearts were prepared in parallel. DNAse/collagenase mix was placed on ice. 5-7 falcon tubes containing 5 ml each of DF20 medium were placed on ice. PBS/2G was warmed in a water bath at 37°C. The hearts were chopped into fine pieces

on ice and transferred to a 50 ml falcon tube. The digestion mixture was prepared by adding 500 µl of DNAse/collagenase mix to 4.5 ml of pre-warmed PBS/2G. The hearts were digested with this mixture in steps of 15 minutes each in a CO_2 incubator with constant rotation of the tube for efficient mixing. After 15 minutes, the mixture was allowed to settle for 1 minute and the supernatant containing the cells was transferred to a tube containing 5 ml of DF20 medium to stop the digestion reaction. This process was repeated 5-6 times for complete digestion of the tissue fragments. Finally, the cell suspensions were pooled together and centrifuged at 1000 rpm for 5 minutes in a cooling centrifuge at 4°C. The supernatant was discarded and the cell pellet was re-suspended in plating medium (neonatal cardiomyocyte growth medium). The cell suspension was transferred to a 10 cm Petri dish and incubated at 37°C for 1 hour. This step allows the fibroblasts to adhere to the bottom of the dish. The enriched supernatant containing mostly cardiomyocytes was taken off and distributed in 12-well plates for further experiments. Cardiomyocytes were either seeded on glass cover slips (for immunofluorescence analysis) or on a plastic surface (for RNA isolation) coated with 1% laminin solution. The fibroblasts adhering to the 10 cm Petri dish were grown in DMEM medium containing 15% FCS and antibiotics. Unless otherwise stated, cardiomyocytes were allowed to adhere overnight and then serum-starved for 24 hours before further experiments. While cardiomyocytes were used within 3 days of isolation, cardiac fibroblasts were grown till 70-80% confluence. Routinely, cardiomyocytes were checked for their quality and purity (cardiomyocyte beating and alpha-actinin staining respectively).

3.1.2 Measurement of calcium transients in HUVECs

3.1.2.1 Measurement of calcium transients in static HUVECs

Semi-quantitative measurements of intra-cellular calcium concentrations can be obtained from ratiometric fluorescent dye-based monitoring of calcium levels in cells. Since changes in intra-cellular calcium concentrations are one of the early events following exposure of cells to biomechanical forces, these measurements provide a tool to identify ion channels that may be regulated by such forces. In this method, dyes which bind calcium and undergo changes in their fluorescence enable detection of

changes in intra-cellular calcium concentrations. Such changes can be detected using a photomultiplier or microscopic imaging. The latter provides the advantage of single cell measurements and detection of fluorescence artifacts. Thus, an increase in fluorescence intensity of single cells with increasing calcium concentrations can be used to detect calcium transients in individual cells. Fura-2 belongs to the group of dyes used for such ratiometric measurements (Grynkiewicz et al. 1985). The Fura-2 dye was in form of an acetoxymethyl ester which is cleaved by cellular esterases to generate the active dye. The reversible binding of calcium to the dye results in a shift in absorption maximum to 340 nm. The fluorescence emission at 360 nm (isobestic point) is however independent of binding to calcium. As such, when Fura-2 is excited at two alternating wavelength of 340 and 360 nm, the signal intensity at 340 nm is dependent on calcium as well as calcium-independent factors such as loading of the dye, cellular deformation, variation in light intensity and perfusion artifacts. The signal intensity corresponding to 360 nm is solely dependent on these calcium-independent external factors. The ratio of emission intensity at 340 and 360 nm offers a true measure of changes in calcium concentration independent of such artifacts. However, the time resolution of this system is limited by the time taken for a shift in wavelength from 340 to 360 nm and rapid changes in the scale of less than 200 ms cannot be recorded accurately. The instrument comprised of a xenon laser, a condenser, 10x objective, CCD camera, filters, and an electrical circuit driving the shift in excitation wavelength. These experiments were done with the help of expert advice and technical inputs from Prof. Rainer Nobiling (University of Heidelberg). The device was designed and assembled at the Institute of Physiology and Pathophysiology, University of Heidelberg. The camera software allowed a control of the frame rate and binning affecting temporal and lateral resolution respectively.

The cells were seeded on a glass cover slip which was placed in an open perfusion chamber. The cells were under continuously flowing medium pre-warmed and fed by a syringe pump. A suction pump was used to remove the excess medium so that the liquid level in the perfusion chamber remained constant. The stimulus (in solution) was applied through another motor-driven syringe which could be interchangeably switched on or off by a switch (Figure 4). The flow rate was maintained at 0.5 or 1 ml/minute.

Where appropriate, the cells were pre-incubated with the inhibitors and the perfusion medium was also loaded with the specific concentration of the inhibitor.

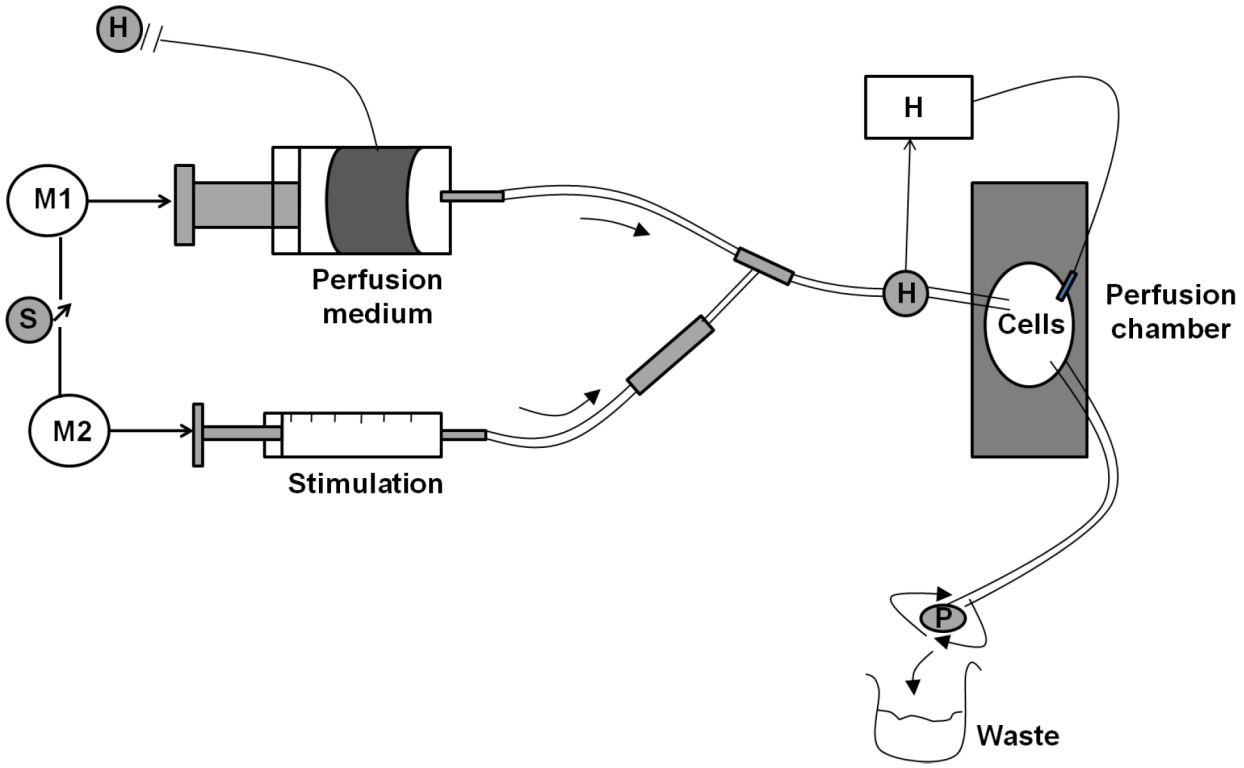

Figure 4: Working diagram of the flow set-up used for measuring calcium transients in HUVECs. M1, M2 indicate motors driving the syringes, 'S' represents the switch for directional control, 'H' indicates heating device, 'P' indicates a pump for removing excess used medium.

The following sequence of events were used: a) loading of cells with Fura-2 AM dye at 37°C in a CO_2 incubator for 5 minutes b) placement of the cover slip seeded with the cells in the perfusion chamber under flow for 5 minutes to stabilize the cells c) focal plane was adjusted to the level of the cells d) image acquisition was started e) after 150 seconds, the first stimulus (1 ml) was added followed by a period of stabilization f) after 500 seconds, the histamine stimulus (1 ml) was applied and the imaging was stopped at 750 seconds. Images were analyzed using ImageJ software whereby individual images were stacked together. The cells to be analyzed were defined as regions of interest (ROI) and the intensity values were obtained using the 'Ratio ROI Manager' plugin. The fluorescence intensity value of the background was subtracted from that of selected

cells and the final ratio of intensity at 340 and 360 nm was obtained for each time unit. The initial value was normalized to 1for all the calcium transients.

3.1.2.2 Measurement of calcium transients in stretched HUVECs

For the measurement of calcium transients in stretched HUVECs, the above mentioned device was modified to accommodate fluorescence measurements in combination with cyclic stretch. For these experiments, cells were seeded on elastic membranes. After loading with the fluorescent dye, the membrane was cut into thin slices which could be fixed onto the stretch set-up (Figure 5).

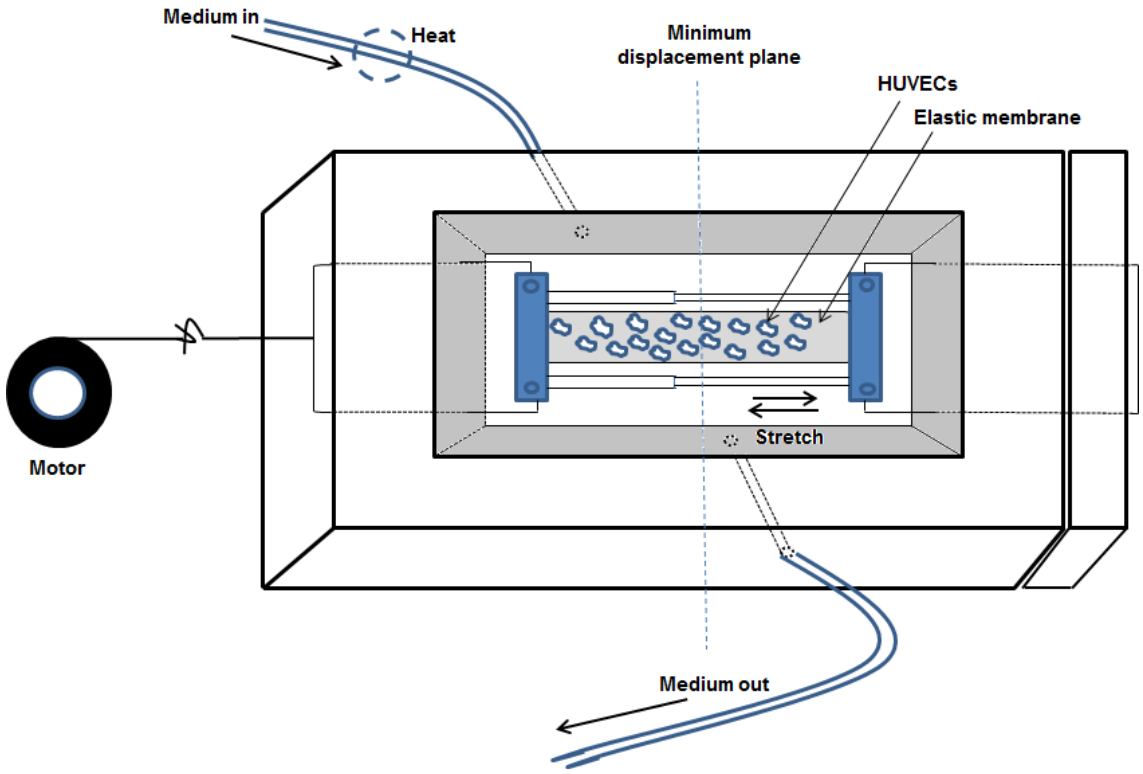

Figure 5: Design of the set-up for application of biomechanical stretch during the measurement of calcium transients in HUVECs.

Using a combination of a motor and a wire-guided movable framework (Designed by Prof. Rainer Nobiling and built at the Institute of Physiology and Pathophysiology, University of Heidelberg), the membrane (and thus, the HUVECs seeded on it) could be stretched in a cyclic fashion. The frequency of the motor-driven stretch protocol was in sync with the changes in excitation wavelength between 340 and 360 nm. The cells

were under constant flow of medium. Selective inhibitors were added directly to the perfusion chamber. Alternatively, cells were pre-treated with siRNA targeting specific genes. The sequence of events was as follows: a) loading of cells with Fura-2 AM at 37°C for 5 minutes in a CO_2 incubator b) membrane was cut with a scalpel into thin slices c) one such rectangular piece of membrane with cells was mounted onto the stretch framework and fixed in place d) the flow of medium was initiated e) cells were allowed to stabilize for 5 minutes f) the motor was triggered, the focal plane was adjusted and the field of view was moved to the region of the membrane where the cells showed minimal lateral displacement during stretch g) the motor was switched off and cells were allowed to stabilize for another 5 minutes h) the image acquisition was started i) after 150 seconds, the cells were stretched for 50 seconds j) a static period followed for 200 seconds k) the cells were stretched again for 50 seconds and imaging was stopped at t=500 seconds. The images were analyzed as discussed in section 3.1.2.1 except that small clusters of cells were analyzed together. Analysis of individual cells was not possible due to motion artifacts.

3.1.3 Biomechanical stretch model

HUVECs and vascular SMCs were seeded on collagen I-coated Bioflex™ elastomers (Flexercell Inc., USA). HUVECs were exposed to 10% cyclic elongation for 6hours at 0.5 Hz with a sinusoidal profile using a Flexercell FX-5000 strain unit (Figure 6).

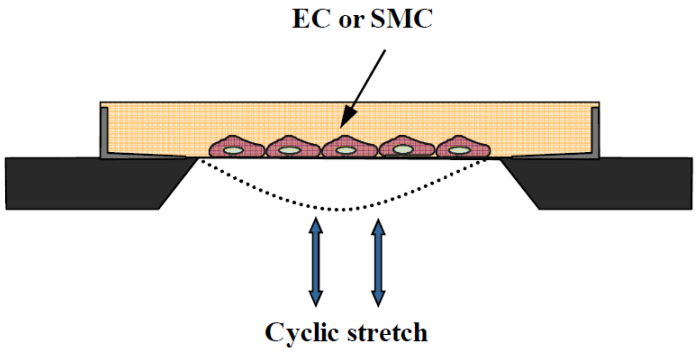

Figure 6: Device for exposing endothelial or smooth muscle cells to cyclic stretch using vacuum (From doctoral dissertation of Sahana Suresh Babu, Heidelberg, 2012).

For vascular SMCs, the same strain unit was used but cells were exposed to 13-15% cyclic elongation unless otherwise stated for specific time periods depending upon the experimental design. This method has been used in the literature to mimic an increase in circumferential wall tension (Suresh Babu et al. 2012, Arnold et al. 2014). Following exposure to cyclic stretch, the cells were either used for immunofluorescence analyses or lysed for isolation of RNA and proteins.

3.1.4 Microarray analysis

Smooth muscle cells isolated from the aorta of age-matched WT and zyxin-null mice were used for microarray analysis. Cells were allowed to grow to 90% confluence and were subjected to 10% cyclic elongation at a frequency of 0.5 Hz for 6hours. Three independent experiments were performed for each experimental group (Static vs stretch). Biological replicates rather than technical replicates were used for each experiment. High quality RNA was isolated as described elsewhere and stored at -80°C. A volume of 15 µl (equivalent to 5-10 µg total RNA) were used for microarray analysis.

The GeneChip measurements were performed at the microarray facility in Mannheim (Prof. Norbert Gretz, Dr. Carsten Sticht, ZMF, Mannheim). Gene expression profiling was performed using the GeneChip® Mouse Genome 430 2.0 Array from Affymetrix. A custom CDF Version 17 with Entrez-based gene definitions was used to annotate the arrays. The raw fluorescence intensity values were normalized applying quantile normalization. A commercial software package SAS JMP10 Genomics, version 6, from SAS was used to analyse differential gene expression based on ANOVA. A false positive rate of a=0.05 with FDR correction was taken as the level of significance. Analytical settings and conditions of the microarray are available at http://www.ma.uniheidelberg.de/inst/zmf/affymetrix/ablauf_e.html. Gene Set Enrichment Analysis (GSEA) was used to determine whether defined lists (or sets) of genes exhibit a statistically significant bias in their distribution within a ranked gene list (see http://www.broadinstitute.org/gsea/for details) (Subramanian et al. 2005). Gene Ontology terms related to molecular function (GO_mf) were used and pathways belonging to various cell functions were obtained from public external databases (KEGG, http://www.genome.jp/kegg/). The raw and normalized data are deposited in

the Gene Expression Omnibus database (http://www.ncbi.nlm.nih.gov/geo/; accession No. GSE60447).

3.1.5 Transfection

Two separate methods were used for transfection of siRNA and the zyxin expression construct respectively in vascular SMCs.

3.1.5.1 Magnet-assisted transfection

For each well of a 6-well plate, 3 µg of siRNA was diluted in Opti-MEM medium to give a final volume of 200 µl. Thereafter, 4 µl of MATra-si reagent (containing magnetic beads) was added to the diluted siRNA and allowed to incubate at room temperature for 20 minutes. The SMCs were washed with Hanks buffer and were incubated with 2 ml of Opti-MEM medium. The siRNA-magnetic beads mixture was added dropwise to the cells and the plate was immediately placed on a powerful magnet (Universal Magnet Plate, IBA) for 30 minutes to allow the beads to penetrate the cells. The efficiency of gene knockdown was measured at the protein level after 72 hours on a western blot.

3.1.5.2 Nucleofection

Transfection of larger constructs in vascular SMCs is difficult to achieve with magnet-assisted transfection resulting in very low transfection efficiency. Therefore, a Nucleofector^{TM} technology based on momentary application of an electric pulse is used for higher transfection efficiencies. Accordingly, transfection of the zyxin expression construct was achieved using a Nucleofector^{TM} kit (Lonza) according to manufacturer's instructions. For each transfection cycle, $2x10^6$ cells were used for transfection with 4 µg of plasmid DNA or pmaxGFP^{TM} (as a control for transfection). After the transfection process, these cells were seeded in two separate wells of a 6-well plate. The program U025 resulted in higher transfection efficiency and was used in all subsequent experiments. After 48 hours of transfection, the cells were analyzed.

3.1.6 Standard analytical methods

3.1.6.1 Isolation of RNA from cultured cells

Cells were rinsed with ice-cold Hanks BSS and lysed with 350 µl lysis buffer containing 1% β-mercaptoethanol. Total RNA was isolated using a RNA extraction kit (MachereyNagel) according to manufacturer's instructions. The RNA was eluted in 30-35 µl of RNase-free water. The concentration and quality of the RNA was determined using a spectrophotometer (NanoDrop ND-1000).

3.1.6.2 Reverse transcription

500 ng of the RNA template (a volume of 13 µl) was mixed with 1 µl of oligo dT primer (10 pmol/µl). The formation of hybrid formation with the polyA-tails of mRNA was facilitated by heating the mixture at 70°C for 10 minutes. The mixture was chilled in ice and briefly centrifuged. A freshly prepared mixture containing 4 µl of 5x first strand buffer, 1 µl of 10 mM dNTPs and 1 µl of 0.1 M Moloney murine leukemia virus reverse transcriptase (M-MLV RT) was prepared. The resultant final mixture was incubated at 42°C for 50 minutes for first strand cDNA synthesis. Thereafter, the reaction was inactivated by incubating at 70°C for 10 minutes and cooled on ice. The resultant cDNA (20 µl) was diluted 1:5 or 1:10 with Dnase-free water for conventional and real time PCR respectively.

3.1.6.3 Quantitative real time polymerase chain reaction (Real time PCR)

Real time PCR was performed using a LightCycler instrument (Roche Diagnostics, Germany) by using the QuantiTect SYBR Green® kit. Briefly, 5 µl cDNA (2.5 ng/µl), 1 µl each of forward and reverse primer (10-20 µM), 3 µl of RNase-free water, and 10 µl of SYBR Green were added to obtain a final reaction volume of 20 µl. The annealing temperatures used for respective primer pairs are tabulated in Table 11. The quantification of changes in gene expression was done using an absolute quantification (based on number of copies of the gene product) or by using the (delta) (delta) Ct method (based on the number of cycles required for crossing a certain threshold of expression) (Livak et al. 2001).

The fold change in gene expression was calculated as follows.

$$\text{Ratio} = \frac{2^{Ct(\text{target, untreated}) - Ct(\text{reference, untreated})}}{2^{Ct(\text{target, treated}) - Ct(\text{reference, treated})}}$$

For absolute quantification, a standard curve is required based on serial dilutions (of known concentration) of the plasmid DNA encoding the amplified gene sequence. This is achieved by amplification of the desired sequence by conventional RT-PCR and cloning into a vector for bacterial transformation. These techniques will be discussed in the following sections. GAPDH or the 60S ribosomal protein L32 (RPL32) was used as a house keeping gene for normalizing the changes in gene expression.

3.1.6.4 Conventional RT-PCR

In this study, the expression of various genes has been studied by quantitative real time PCR. However, conventional RT-PCR has been used at different stages to amplify gene sequences for cloning or genotyping. The PCR reaction mixture (Table 18) was loaded in an automatic thermocycler (Biometra) which was programmed as follows (Table 19).

Table 18: Composition of the reaction mixture for PCR

Ingredients	Volume	End concentration
Water	35.5 µl	-
10x PCR buffer	5 µl	1x
$MgCl_2$	0.75 µl	1.5 mM
dNTPs (20 mM)	1.5 µl	0.6 mM
Primer (forward/reverse)	1 µl each	1 µM
Taq polymerase (5U/µl)	0.2 µl	0.02 U/µl
cDNA (5 ng/µl)	5 µl	25 ng

Table 19: Conditions for semi-quantitative PCR

PCR step	Temperature (in °C)	Time
Pre-denaturation	95°C	5 minutes
Denaturation Annealing Synthesis	95°C 56-60°C (primer specific) 72°C	30 seconds 60 seconds (35-45 cycles) 2 minutes
Extension	72°C	5 minutes

3.1.6.5 Expression plasmids

The zyxin expression plasmid was constructed by subcloning a full-length PCR fragment including the first stop codon (positions 305 to 1999; NM_011777) derived from VSMC complementary DNA (cDNA) into the cDNA 6.2/N-EmGFP TOPO 5.9-kb vector, with the TOPO cloning reaction used according to the manufacturer's recommendations (TOPO Mammalian Expression Vector Kit, Invitrogen). The conditions for the RT-PCR were slightly modified with annealing at 61°C for 5 minutes, synthesis at 72°C for 10 minutes and extension at 72°C for 10 minutes. Similarly, for construction of real time PCR standards, PCR amplified fragments were ligated into the pCR®TOPO 2.1 vector using the TOPO TA cloning® kit according to manufacturer's instructions. In both cases, 2 µl of the TOPO vector containing the PCR fragment was mixed with 20 µl of Top10F™ competent cells followed by incubation in ice for 30 minutes. The cells were exposed to heat shock at 42°C for 40 seconds and immediately placed on ice. Thereafter, 250 µl of SOC medium was added to the cells and the resulting suspension was incubated at 37°C for 1hour with continuous shaking at 300 rpm. Ampicillin (20 µg/ml) containing sterile LB-agar plates were pre-warmed at 37°C followed by addition of 50 and 100 µl of transformed bacterial cells respectively to two separate plates. Bacterial colonies were allowed to grow overnight at 37°C in an incubator.

Transformed colonies were randomly picked by a sterile pipette tip and transferred to tubes containing 7 ml of LB medium with appropriate antibiotics. These tubes were

shaken overnight at 37°C. Plasmids were purified using the QIAPrep® Spin Miniprep kit according to manufacturer's instructions. In case of real time PCR standards, clones were randomly sent for sequencing since directionality of the insert is of no consequence in this case. However, for cloning of the expression construct for over expressing zyxin, the directionality of the insert was verified by digestion of the plasmids with restriction enzymes (3.1.4.6) followed by agarose gel electrophoresis (3.1.4.7). Only the plasmids which had the insert ligated in the correct orientation (initiation codon proximal to the promoter) were sent for sequencing. For the correct plasmids, the corresponding bacterial colonies were further propagated by adding 200 µl of cell suspension to 200 ml of LB medium (with appropriate antibiotics). The resultant suspensions were agitated overnight at 37°C in Erlenmeyer flasks to promote bacterial growth. A QIAPrep® Maxiprep kit was used to obtain purified plasmid DNA according to manufacturer's instructions. All clones were sequenced prior to downstream applications.

3.1.6.6 Plasmid digestion by restriction endonucleases

The construct containing the zyxin coding sequence was digested with the restriction endonucleases NspI for 2 hours at 37°C in presence of 1x CutSmart™ buffer. This digestion process gives five fragments having sizes of approximately 4097, 1380, 1309, 644 and 72 bp respectively (for correct orientation of the insert with the initiation codon proximal to the promoter). Likewise, an incorrect orientation of the insert results in fragments of sizes 3107, 1634, 1380, 1309 and 72 bp respectively upon enzymatic digestion. The products of this digestion reaction were loaded on an agarose gel and separated by electrophoresis. The clone corresponding to the correct size of the DNA fragments was selected for further purification (in this case termed clone 12).

3.1.6.7 Agarose gel electrophoresis

It is a method used for the separation of nucleic acids. Agarose gels of different density (1-2% agarose) were used depending on the size of the DNA fragment. Briefly, agarose was melted in 100 ml of TBE buffer followed by addition of 4 µl of ethidium bromide to label the DNA fragments. The resultant solution was poured in an electrophoresis

chamber. Samples (PCR products or restriction digests) were mixed with 6x loading buffer and added to loading pockets in the agarose gel. Electrophoresis was carried out at 120 V for approximately 45 minutes. A DNA standard ladder was used to verify the size of the separated DNA fragments. The bands were imaged using a GelDoc XR unit in combination with a Quantity One software package version 4.06 (Biorad, Germany).

3.1.6.8 Immunofluorescence analysis

Unless otherwise specified, cells were fixed with methanol for 15 minutes at -20°C. Thereafter, cells were air-dried for 30 minutes and washed with PBS. The fixed cells were permeabilized with 0.1% Triton X-100 for 10 minutes and were incubated with casein blocking solution for 45 minutes to reduce unspecific binding of antibodies. This was followed by incubation with primary antibodies (diluted in the blocking solution) overnight at 4°C. The cells were washed with PBST three times to remove excess unbound antibodies and incubated with secondary antibodies (conjugated with Cy2 or Cy3) for 1 hour at room temperature. This was followed by washing twice with PBST and once with PBS finally to remove traces of detergent which would interact with the nuclear staining dye DAPI used in the subsequent step. After incubation with DAPI for 5 minutes, cells were washed twice with PBS and then mounted with mowiol using cover slips. Images were obtained using an IX81 confocal microscope equipped with an IX-DSU disk unit and analyzed with the cell^R software package.

3.1.6.9 Protein biochemistry

For isolation of total cellular protein, cells were washed with ice-cold Hanks buffer. 100 µl of cell lysis buffer was added to each well of a 6-well plate and the cells were scraped off using a cell scraper (Sarstedt) into 1.5 ml tubes placed on ice. 2.5 µl of Triton X-100 was added for each 50 µl of lysis buffer and incubated for 10 minutes. The resulting lysate was centrifuged at 3000 rpm for 5 minutes at 4°C to remove any debris. The lysate was either snap frozen and stored at -80°C or used for further analysis. The protein concentration was measured using a Bradford assay using a colorimetric plate reader. Where applicable, the cell lysate was separated into cytosolic and nuclear fractions for determination of sub-cellular localization of proteins. Mouse aortic VSMCs

were lysed using buffer I. The lysates were centrifuged (12,000x*g* at 4°C for 15 minutes) and the supernatant (cytosolic fraction) was transferred to a new tube and used for Western blot analysis. The residual pellet containing the nuclear fraction was washed twice with ice-cold Hanks buffer, dissolved in 40 µL buffer II and sonicated 2 times for 5 seconds at 50 Watts on ice. After centrifugation (12,000×*g* at 4°C for 15 minutes), the supernatant containing the nuclear fraction was transferred to a new tube and used for Western blot analysis.

Protein samples were separated by sodium dodecylsulfate polyacrylamide gel electrophoresis (SDS-PAGE). 8-12% gels were prepared depending on the size of the proteins to be separated. Proteins were denatured by addition of 4x sample loading buffer (Roth) followed by heating at 95°C for 10 minutes. The proteins were separated by electrophoresis using a running buffer at a voltage of 75 V for stacking of the proteins followed by 120 V for separation. A protein standard was used to estimate the approximate molecular mass of the separated protein bands. The separated protein bands were transferred onto a PVDF membrane which was pre-activated with methanol. The transfer was done using a transfer buffer at a constant current of 350 mA for 60-90 minutes. After the transfer, the membrane was immersed in blocking solution (5% milk or Blotto® in TBST) for 1 hour followed by incubation with primary antibody overnight at 4°C. Thereafter, the membrane was washed thrice with 0.05% (v/v) TBST for 5 minutes each and incubated with secondary antibodies conjugated to horseradish peroxidase for 60 minutes at room temperature. Finally, the membrane was washed twice with TBST and once with TBS and developed using a chemiluminescence substrate with 5 minutes of incubation. Images were obtained using an 'ImageQuant LAS 4000 mini' imaging system and the band intensities were quantified using ImageJ software.

3.1.7 Functional assays using cultured cells

Cell migration assay

Mouse aortic VSMCs (1.5×10^5) were plated in 6-well plastic plates and grown to confluency in DMEM medium containing 15% FBS. The monolayer was wounded by

scratching with a pipette tip and the distance between the edges was measured at x4 magnification. This was considered as the starting time point (t=0). After 24 h (t=24), measurements were made again. Migration velocity was calculated in µm/h.

Proliferation assay

Mouse aortic VSMCs were seeded into 6-well plastic plates (20,000 cells/well). After 6 h, cells in a single well were fixed and stained with DAPI (4',6-diamidino-2-phenylindole) and photographed to determine the cell number at the starting time point (t=0). The remaining cells were serum starved for 24 hours. The medium was replaced by fresh DMEM medium with 15% FBS and images were taken in the same manner after 72 h. A 0-13% cyclic elongation was used for the stretch stimulation where appropriate. The nuclei were counted using a specially designed algorithm with the help of ImageJ software. 5 images were taken for each well, 3 technical replicates were used for each individual experiment. For statistical analysis, the figure ‘n’ represents the number of biological replicates.

Collagen gel compaction assay

Type I collagen prepared from rat tails was diluted 1:5 with DMEM. Mouse aortic VSMCs were added to the collagen solution previously neutralized using 0.1 M NaOH, at a density of 5,000 cells per 0.5 mL in each well of a 48-well plate. After 2 h incubation at 37°C, the gels were gently detached and diameters were measured at x4 magnification (considered as the starting time point; t=0). The contraction was monitored after 24 h. Alternatively, the medium was replaced with fresh medium containing endothelin-1, epinephrine or norepinephrine (each at 100 nmol/L).

Stress fiber quantification

VSMCs were fixed with 4% PFA for 15 minutes at 4°C. Thereafter, the cells were washed with Hanks BSS to remove additional PFA. Phalloidin labelled with Alexa fluor 488 was used to specifically stain for F-actin stress fibres in the cells. Immunofluorescence images were taken and the intensity of stress fibres was quantified

by the cell^R software package (Olympus). Additionally, the number of condensed actin spots was manually counted using 4-5 comparable fields of view.

Apoptosis assay

Apoptosis was detected in VSMCs using the *in situ* cell death detection kit (Roche) based on TUNEL staining according to the manufacturer's instructions. Briefly, cells were seeded into 6-well BioFlex^{TM} plates. They were serum starved for 24 hours. The serum-free DMEM medium was replaced with fresh DMEM medium containing 15% FBS followed by treatment with trimeric Fas ligand (400 ng/mL) (IBA). Cells were exposed to 18% cyclic elongation at 0.5 Hz for 18 hours. This higher intensity of stretch was used to induce more visible and reproducible apoptosis of the cells. The cells were fixed and stained with DAPI in combination with the above kit and TUNEL positive nuclei were counted.

3.2 *In situ* methods

Although vascular smooth muscle cells in culture offer a useful tool for studying the phenotype of these cells, there are inherent limitations due to the artificial environment which might not completely reflect the behavior of the cells embedded in the three dimensional ECM of the arterial wall. Therefore, isolated arteries might better reflect the functional behavior of these cells. As such, femoral arteries were isolated from mice and analyzed as follows.

Perfusion of isolated femoral arteries from mice

The hind limbs of euthanized mice were immersed in perfusion buffer (Table 1 and 2). Under a stereomicroscope, the femoral artery was separated from the adjacent vein and nerve and cleared of connective tissue. Femoral artery segments were mounted on glass capillaries (diameter 120 µm) fitted to a pressure myograph system 110P (DMT, Denmark). The capillaries were pulled from 0.15 mm glass cannulas using a device programmed to generate a specific force and temperature, thereby achieving a final tip-diameter of 120 µm. The capillaries were cut to a length of approximately 1.5 cm. The pressure transducer along with the MyoView^{TM} software allowed a continuous

monitoring of the temperature of the buffer, pressure and diameter of the arteries. After equilibration of the artery at 10-30 mmHg for 1 hour, the pressure gradient (∆p) was increased in small increments of 20 mmHg to a value of 60 mmHg (inflow pressure set at 90 mmHg and outflow pressure at 150 mmHg). Changes in vessel diameter were recorded after every 15 minutes. The perfusion chamber was continuously refilled with pre-warmed perfusion buffer. With the intraluminal pressure set at 60 mmHg, arterial segments were pre-constricted with cumulative doses of phenylephrine (10 nmol/L to 1 µmol/L). Pre-constricted vessels were tested for dilator response with acetylcholine (100 nmol/L to 1 µmol/L) added to the perfusion chamber. This was followed by constriction with endothelin 1(ET1) (10 nmol/L to 1 µmol/L). Vasoconstriction was manifested as a decrease in vessel diameter while treatment with acetylcholine was measured as a gradual increase in diameter.

The perfusion buffer was freshly prepared for each working day by adding 40ml of 25x solution II dropwise to 800 ml water plus 40 ml solution I (Tables 20 and 21) with continuous stirring.

Table 20: Perfusion buffer pH 7.4 (1x)

Solution I		Solution II	
Chemical	**Concentration (mmol/L)**	**Chemical**	**Concentration (mmol/L)**
NaCl	119.00	$MgSO_4$. $7H_2O$	1.17
$CaCl_2$	1.25	$NaHCO_3$	2.10
KCl	4.70	KH_2PO_4	1.18

Table 21: Perfusion buffer pH 7.4 (25x)

Solution I		Solution II	
Chemical	**Concentration (g/l)**	**Chemical**	**Concentration (g/l)**
NaCl	173.850	$MgSO_4$. $7H_2O$	7.390
$CaCl_2$	5.875	$NaHCO_3$	52.10
KCl	8.760	KH_2PO_4	4.08

The final volume of the buffer was adjusted to one liter with ddH_2O and the solution was saturated with carbon dioxide and oxygen (95% O_2 and 5% CO_2) for 20 minutes. The pH was adjusted to 7.4 and the solution was completed with addition of EDTA (260 µl/l) and D-glucose (2 g/l).

3.3 *In vivo* methods

In order to test if the changes observed *in vitro* in cultured cells and *in situ* in isolated femoral arteries in the absence of zyxin could in fact have an effect under physiological and pathophysiological conditions, following methods were used to monitor and compare vital parameters between WT and zyxin-null mice. A model of experimental hypertension was used in combination with the following experimental tools to induce pathophysiological stress in the mice. All animal experiments were approved by the local ethics committee (Ethics approval G101/09).

3.3.1 DOCA-salt model of hypertension

The DOCA-salt model is a renovascular volume-overload model which induces an increase in blood pressure by retention of sodium and water in the kidneys (Iyer et al. 2010). There are other variants of this model involving removal of one of the kidneys in addition to the DOCA-salt treatment to induce a strong increase in blood pressure. However, in this study, the DOCA-salt treatment has been used alone because of better animal survival rates and ease of application. Accordingly, the increase in arterial blood pressure (both systolic and diastolic) is modest compared to higher values in the literature with the one-kidney model. Briefly, age matched WT and zyxin-null mice were anaesthetized using isoflurane. The hair over the neck was removed and the skin was disinfected. A small incision was made and the DOCA-salt pellet (50 mg) was placed under the skin in a small subcutaneous pocket. The pellets contained a biodegradable matrix which released the active ingredient in a sustained manner over a period of 21 days. The incision was closed with sutures and the animal was allowed to regain consciousness. The body temperature of the animal was maintained at 37°C during the entire procedure. In order to complement the effect of DOCA-salt on blood pressure, the

drinking water was supplemented with 1% w/v NaCl. Changes in blood pressure were measured by the following methods.

3.3.2 Blood pressure measurements in mice

Two distinct methods have been used in this study to measure blood pressure in mice.

3.3.2.1 Tail-cuff method

The tail-cuff method is a non-invasive method of blood pressure measurement in mice. Briefly, the mice were individually placed in a restrainer with the tail available for the placement of a pressure sensing cuff. The animals were trained in this position for a week to enable them to adapt to this method. The whole set up was placed inside a dark chamber maintained at 37°C to keep the animal warm. The method records the first appearance of a pulse while deflating the occlusion cuff or the disappearance of pulse upon inflation of the occlusion cuff. It also simultaneously records the heart rate of the mice. At least 5 recordings were made for both systolic and diastolic arterial blood pressure for each animal. Values which differed by more than 2 times the standard deviation were discarded. The advantage of this method is that it is non-invasive. However, it has potential limitations such as artifacts caused by movement of the animal and the lack of measurements in unrestrained mice.

3.3.2.2 Telemetry

To overcome the potential limitations of the tail-cuff method, radiotelemetry was used to accurately measure blood pressure in mice (Kaïdi et al. 2007). This technique offers the advantage of continuous blood pressure recordings in unrestrained mice. However, the technique is invasive and expensive. Briefly, age matched WT and zyxin-null mice were anaesthetized using isoflurane. The animal was placed on a heating plate maintained at 37°C during the surgical procedure. A thread was tied to the upper incisors and the animal was slightly stretched to allow a better visualization of the carotid arteries. The limbs were secured with tape following the monitoring of pain reflex. The hair was removed from the throat region and the skin disinfected. An incision was made and the salivary glands were gently separated. The surrounding fat was cleared and the left

common carotid artery was separated carefully from the nerve and the adjacent vein. After a cranial permanent ligature just below the bifurcation of the carotid artery, a caudal occlusion was made with a microvessel clip to temporarily stop the blood flow in this segment of the artery. A small incision was made in the artery and the catheter (PA-C10, DSI) was inserted in the artery by simultaneously removing the clip. The length of the catheter insertion was reproduced by monitoring the position of a notch in the catheter which should ideally be placed inside the incision immediately proximal to the opening. This ensured that the tip of the catheter reached the arch of the aorta and was exposed to the circulating blood. The catheter was tied in this position by sutures and the body of the device was placed in a subcutaneous pocket on the lateral left flank of the mice. The skin incision was closed with sutures and the animal was allowed to regain consciousness on the warm plate. Thereafter, the animal was place in its cage and exposed to infra-red light for at least 1 hour to keep it warm. The initial weight of the animal was routinely monitored after the surgery. A 7-8 day period was allowed for the mice to regain normal circadian rhythm. Baseline blood pressure readings were measured for two days followed by implantation of the DOCA-salt pellets with continuous monitoring of blood pressure for 21 days post treatment.

3.3.3 High resolution ultrasound measurements in mice

In order to analyze the cardiac function and the resistivity of femoral arteries in WT and zyxin-null mice, high resolution ultrasound imaging (VisualSonics) was used.

3.3.3.1 Echocardiography

Echocardiography or high resolution ultrasound measurements of cardiac function was done using the MS-550D micro scan transducer (40 MHz) using the VisualSonics Vevo 2100 imaging system. The animal was anaesthetized using 3% v/v isoflurane for induction and 2% v/v for maintenance of this state. The animal was positioned on the platform in the supine position. Eye lubricant was placed to prevent drying of the area. ECG gel was placed on the copper leads on the platform and the paws were taped to them to obtain information regarding the ECG and respiratory behaviour of the animal. A rectal probe was lubricated and inserted to monitor the body temperature of the

animal during imaging. The hair on the chest was removed using a hair removal cream and a generous amount of warm ultrasound-compatible gel was applied both on the chest and the transducer head while avoiding any air bubbles. The platform was slightly tilted towards the left and the transducer head was placed at close proximity to the chest (although not touching the animal skin). With the notch on the transducer pointing towards the head of the mouse, the transducer was rotated at an angle of approximately 35 degrees counter clockwise to the midline offering a long axis view of the heart. Images were taken in the brightness mode or B-mode and the motion mode or M-mode. While the B-mode offers two-dimensional images of an area of interest, the M-mode acquires an image in one dimension over time. For the short axis view, the transducer was rotated approximately 90 degrees clockwise from its present position. The images were analyzed using the analysis software from VisualSonics. The measurements available in the M-mode include the left ventricular (LV) anterior wall thickness during systole and diastole, LV internal diameter in systole and diastole, LV posterior wall thickness in systole and diastole, intraventricular septum thickness in systole and diastole. Based on these parameters, the software uses inbuilt algorithms to calculate ejection fraction, fractional shortening, stroke volume and cardiac output of the heart.

3.3.3.2 Measurement of resistivity index of femoral arteries

For measuring the resistivity of the femoral arteries, the animal was prepared on the platform as previously described. Hair was removed from the hip and the groin region down the hind limb. The transducer head was placed parallel to the femoral artery (already visible after hair removal). The position of the transducer was fine tuned by using the B-mode and the colour Doppler mode. In this mode, blood flowing towards the transducer is represented by red while blood flowing away is represented by blue. Thus, it offers the directionality of the blood flow in addition to the mean velocity allowing a distinction between the femoral artery and the vein. The animal and the transducer probe are positioned in such a way that the angle between the blood flow and the transducer (and thereby, the ultrasound beam) is less than 60 degrees for accuracy of velocity measurements. The Vevo 2100 analysis software allows measurements of the

peak systolic velocity and the end diastolic velocities. These values can be used to calculate the resistivity index (RI).

RI = (Peak systolic velocity – End diastolic velocity)/ Peak systolic velocity

The RI indicates the resistivity of the vascular bed distal to the vessel under investigation.

3.4 *Tissue-based* methods

3.4.1 Tissue preparation and histological staining

After the mice were sacrificed, the chest was opened to expose the heart. A small opening was made in the right ventricle and the left ventricle was cannulated for perfusion with Ringer's solution as well as zinc fixative where applicable. Except for the purpose of TUNEL staining (where PFA fixation was used), tissues were fixed with zinc fixative overnight. They were dehydrated using a series of increasing concentrations of ethanol (70, 85 and 99%) followed by treatment with Isopropanol. Thereafter, the tissues were incubated in melted paraffin at 60°C overnight. The following day, the tissues were embedded in paraffin blocks and stored at room temperature. A microtome was used to cut fine sections of the tissues (5 µm in thickness) which were dried and immobilized on the glass slides by incubating at 42°C overnight. Masson's trichrome staining was used for the detection of collagen fibres in the heart. Briefly, the paraffin sections were deparaffinized using xylol and rehydrated with increasing dilutions of ethanol (96, 85 and 70% respectively) followed by immersion in ddH_2O. The tissue was fixed in Bouin's solution for 1 hour at 56°C and rinsed with tap water for 5-10 minutes to remove the yellow colour. Next, the sample was stained with Weigert's iron hematoxylin solution for 10 minutes followed by rinsing in running warm tap water for 10 minutes and washing with distilled water. Tissues were immersed in a Biebrich scarlet-acid fuchsin solution for 12 minutes, washed in distilled water and differentiated in freshly prepared phosphomolybdic-phosphotungstic acid solution (1:1) for 20 minutes. The sections were directly transferred to aniline blue solution for 5 minutes, rinsed briefly in distilled water and differentiated in 1% acetic acid solution for 4 minutes. Finally, after washing in distilled water, the samples were dehydrated very quickly through 95% and absolute

ethyl alcohol and cleared in xylol. The specimens were mounted with a resinous mounting medium (Eukitt®) and imaged using a light microscope. Collagen stained blue, nuclei appeared black while muscle and cytoplasm appeared red.

3.4.2 Immunohistochemistry

Prior to immunostaining, the paraffin sections were deparaffinized using xylol and rehydrated with increasing dilutions of ethanol (96, 85 and 70% respectively) followed by immersion in ddH_2O. When PFA-fixed samples were used, an additional antigen retrieval step was used involving microwave irradiation of the samples (350 W for 5 minutes) immersed in 0.1M citrate buffer at pH 6. The tissue samples were encircled with a DAKO pen by drawing a water repelling circle around the specimen. Thereafter, the same process of immunostaining was performed as described in section 3.1.6.8.

3.4.3 RNA isolation and cDNA preparation from tissues

Immediately after isolation, tissues were placed in RNA later stabilization reagent overnight. A RNeasy® mini kit (Qiagen) was used for isolating RNA according to manufacturer's instructions. For femoral arteries, 100 µl of lysis buffer (containing 1% β-mercaptoethanol) was used while 600 µl was used for heart tissue. The tissue was chopped into small pieces using clean micro scissors and sonicated several times (5 seconds each at 50 Watts) on ice until the tissue appeared lysed. This lysate was used for RNA isolation using the kit. DNA was prepared from purified RNA by using the Sensiscript® reverse transcription kit (Qiagen) according to manufacturer's instructions.

3.4.4 Protein isolation from tissues

After tissue isolation, the samples were snap frozen and stored at -80°C prior to use. The tissues were lysed with RIPA buffer containing a cocktail of protease inhibitor mixture (PIM), pefabloc, sodium orthovanadate (1 mmol/l) and sodium fluoride (1 mmol/l). Cardiac tissues were lysed with 500 µl of lysis buffer and the lysate was centrifuged at 12,000 rpm at 4°C for 15 minutes. The supernatant was collected, snap frozen and stored at -80°C for further protein analysis.

3.4.5 RT^2 profiler PCR array

RNA was isolated from the hearts of untreated as well as DOCA-salt-treated C57BL/6J and zyxin-null mice after 10 days of treatment as described in section 3.4.3. The cDNA was synthesized by using the RT^2 First Strand kit (Qiagen) according to manufacturer's instructions. The cDNA was mixed with a RT^2 SYBR Green mastermix and dispensed into the wells of a 96-well plate containing primer pairs designed for genes involved in cardiac fibrosis (Mouse fibrosis RT^2 profiler^{TM} PCR array PAMM-120ZA-12). The plate was tightly sealed with optical thin-walled 8-cap strips, centrifuged briefly and gene expression changes were monitored using a real-time cycler according to manufacturer's instructions (Applied Biosystems model 7500; Molecular immunology laboratory of Prof. Bernd Arnold at DKFZ, Heidelberg). C_t values were used for further analysis using a web-based PCR array data analysis software (SABiosciences).

3.5 Statistical analysis

All results are expressed as means±SEM of *n* individual experiments. For analyzing differences between two individual experimental groups, an unpaired Student's *t* test was used with $p< 0.05$ considered statistically significant. Differences among 3 or more experimental groups were analyzed by one-way ANOVA, followed by a Tukey's multiple comparison test for selected pairs of groups with a probability value of $p<0.05$ considered statistically significant.

4 RESULTS

4.1 Role of TRPC3 channels in mechanosensing by ECs

In order to better understand the mechanism of stretch-induced zyxin activation in both vascular endothelial and smooth muscle cells and thereby its functional consequences, the nature and kinetics of the mechanosensing cascade upstream of this process were studied in greater detail. In the experimental set up used to measure calcium transients generated by cyclic biomechanical stretch, use of vascular SMCs was technically difficult compared to ECs because of poor loading of the fluorescent calcium-sensitive dye Fura-2 in vascular SMCs, necessitating higher cytotoxic concentrations. To circumvent this problem, human umbilical vein endothelial cells (HUVECs) were used as a cell model for measuring such calcium transients owing to their availability and ease of Fura-2 loading.

4.1.1 *Pharmacological activation of TRPC3 channels in ECs*

Using a combination of pharmacological tools and *in situ* measurements using femoral arteries from mice deficient in one or more TRPC channel isoforms, stretch-induced zyxin activation in ECs and vascular SMCs was shown to be TRPC3-dependent (doctoral thesis of Sahana Suresh Babu, Heidelberg, 2012; Suresh Babu et al. 2012). To further investigate if activation of TRPC3 channels is sufficient to induce nuclear translocation of zyxin and hence its activation, oleyl-acetyl-glycerol (OAG), an analogue of diacylglycerol (DAG) was used to activate these channels. OAG induced prominent calcium transients in HUVECs (Figure 7A and B). Protein kinase C mediates TRPC channel closure by a negative feedback loop following stimulation with OAG. Accordingly, the effect of OAG was further accentuated by the inhibitor of protein kinase C (GF109203X; Figure 7A and B). OAG-induced channel activation was comprehensibly blocked by Pyr3, a specific inhibitor of TRPC3 channels (Figure 7A and B). The non-specific cation channel blocker gadolinium completely blocked calcium transients in these cells. This indicates that the OAG-induced calcium transients in HUVECs are predominantly TRPC3 channel-dependent. The increase in intracellular

calcium can result from release from intracellular stores (store-operated) or by entry of extracellular calcium through membrane-bound cation channels.

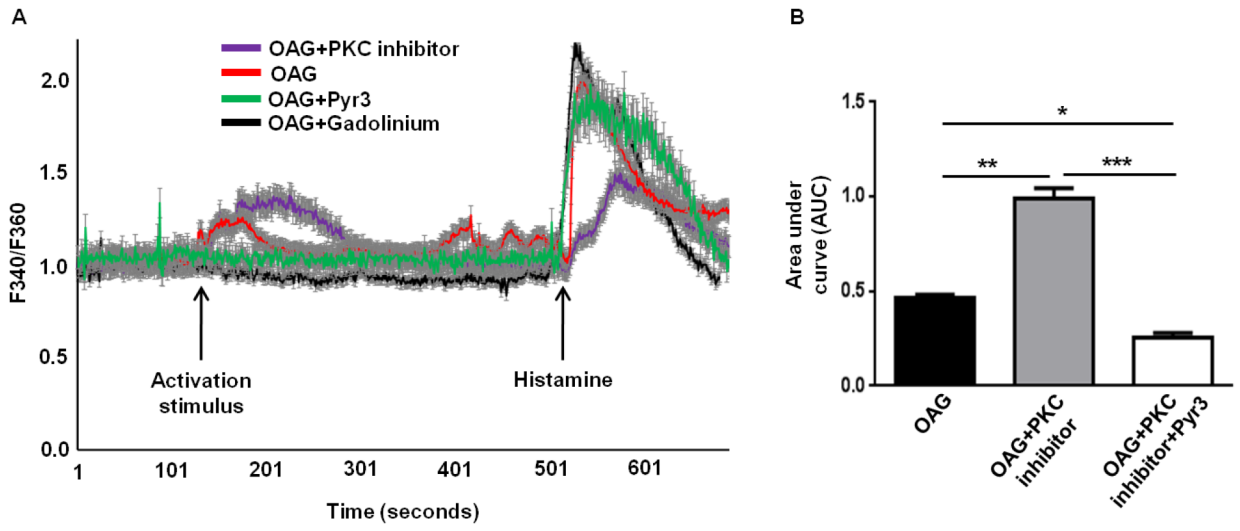

Figure 7: OAG-induced calcium transients in HUVECs are TRPC3-dependent. A, Representative calcium transients induced in HUVECs by activators of TRPC3 channels (100 µM OAG and 10 µM PKC inhibitor GF109203X) as measured by Fura-2 ratio imaging at 340 and 360 nm, respectively. Stimulation with histamine (1 µM) was used as a control to normalize activation efficiency of different batches of cells. **B,** Quantitative analysis of TRPC3 channel activation in HUVECs and its inhibition by Pyr3 (10 µM). The non-selective cation channel blocker gadolinium (100 µM) completely abolished OAG-induced calcium transients. Area under the curve (AUC) was measured for each treatment; *p<0.05, **p<0.01 and ***p<0.001 as indicated, n=3 for each group.

4.1.2 *The OAG-induced calcium transients are independent of calcium release from intracellular stores*

The release of calcium from intracellular stores by phospholipase C (PLC)-mediated release of inositol phosphate (IP_3) and its subsequent activation of the IP_3 receptor is an important mechanism regulating calcium signalling. To confirm the origin of the OAG-induced calcium transients, cells were pre-incubated with a specific blocker of the IP_3 receptor, xestospongin C (XeC, 10 µM) prior to treatment with OAG. XeC had no effect on OAG-induced calcium transients (Figure 8A, C). The efficacy of XeC in this experimental set up was validated by its successful inhibition of thrombin (4U/ml) –

mediated calcium transients (Figure 8B, C) which are known to be IP_3 receptor-dependent. Therefore, dependency of the OAG-induced rise in intracellular calcium on extracellular calcium was investigated.

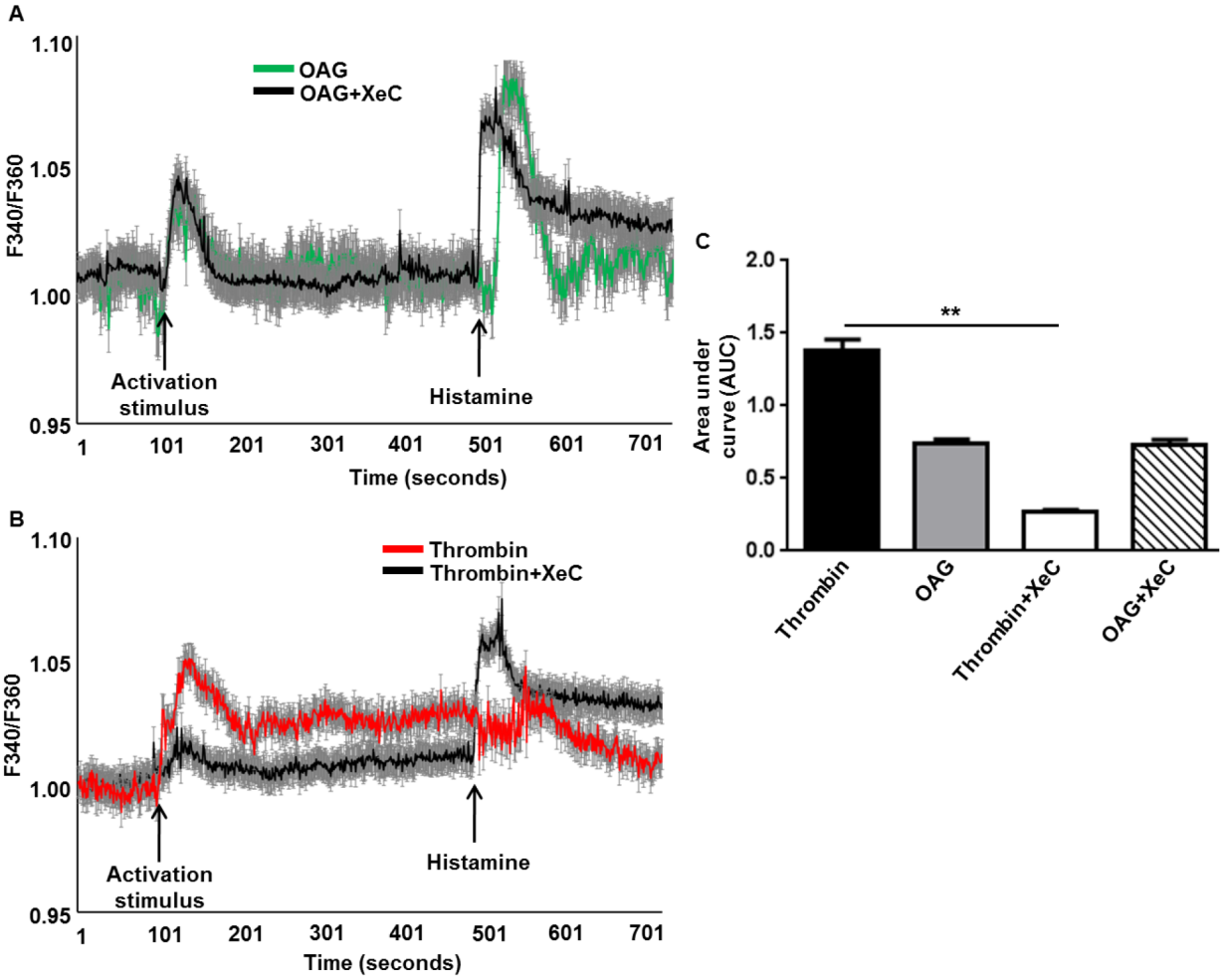

Figure 8: OAG-induced calcium transients are independent of IP_3 receptor-mediated release of intracellular calcium. A, Representative calcium transients induced in HUVECs treated with OAG (100µM) alone or after 6 hours pre-incubation with XeC (10 µM). Stimulation with histamine (1 µM) was used as a control to normalize activation efficiency of different batches of cells. **B,** Representative calcium transients induced in HUVECs treated with thrombin (4U/ml) alone or after 6 hours pre-incubation with XeC (10 µM). **C,** Summary of the quantitative analysis of calcium transients in HUVECs. Area under the curve (AUC) was determined for each treatment; **p<0.01 as indicated, n=3 for each group.

4.1.3 *The OAG-induced calcium transients are dependent on extracellular calcium*

To further corroborate the aforementioned findings and examine the source of OAG-induced calcium transients in HUVECs, the same experiments were performed in the absence or presence of extracellular calcium. OAG-induced calcium transients were completely abolished in the absence of extracellular calcium in the perfusion medium (Figure 9). Replacement of calcium in the medium led to a transient activation of the cells. Therefore, subsequent measurements were done after a period of 5 minutes following stabilization of the cells. Indeed, OAG reproducibly induced calcium transients in the presence of extracellular calcium (Figure 9).

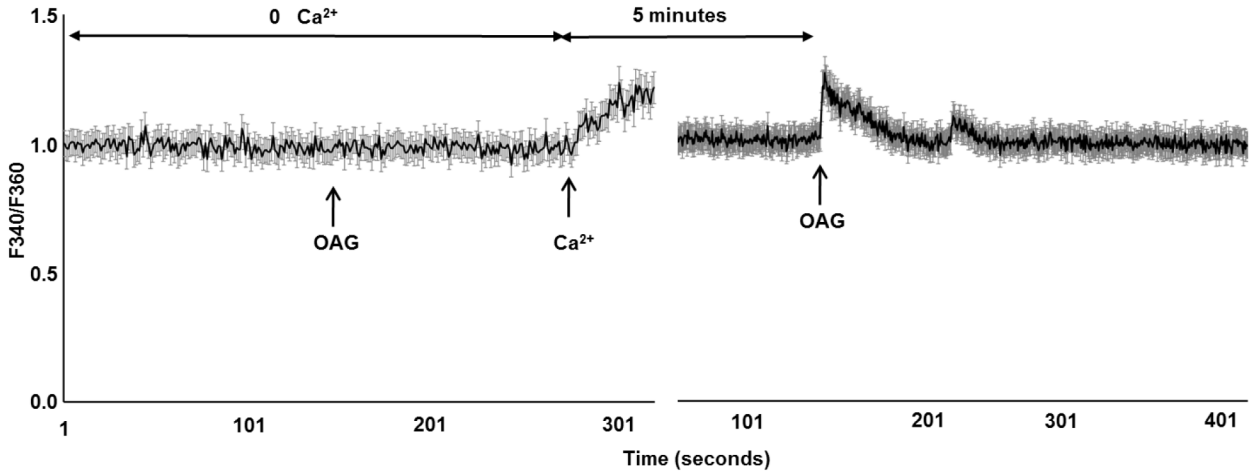

Figure 9: OAG-induced calcium transients are dependent on extracellular calcium. Representative calcium transients in HUVECs measured in the absence (calcium-free medium) or presence of extracellular calcium. OAG (100 µM) was used for TRPC3 channel activation; n=3.

4.1.4 *OAG is sufficient to induce nuclear translocation of zyxin and subsequent gene expression*

The aforementioned results indicate the existence of functional TRPC3 channels in HUVECs which are responsive to stimulation with OAG. Since TRPC3 has been implied in stretch-induced zyxin translocation to the nucleus, the ability of OAG to stimulate zyxin activation independently of stretch was tested in the cultured HUVECs. TRPC3 channel activation by OAG in fact strongly induced the translocation of zyxin from focal

adhesions to the nucleus (Figure 10B and D). Interleukin 8 (IL-8) is a downstream target of zyxin activation and is a read-out for zyxin activation in ECs (Wójtowicz et al. 2010). Accordingly, OAG induced an upregulation of IL-8 gene expression in HUVECs (Figure 10E), albeit slightly lower than that observed with stretched ECs. Both these effects were blocked by the TRPC3 inhibitor Pyr3 (Figure 10C, D and E)

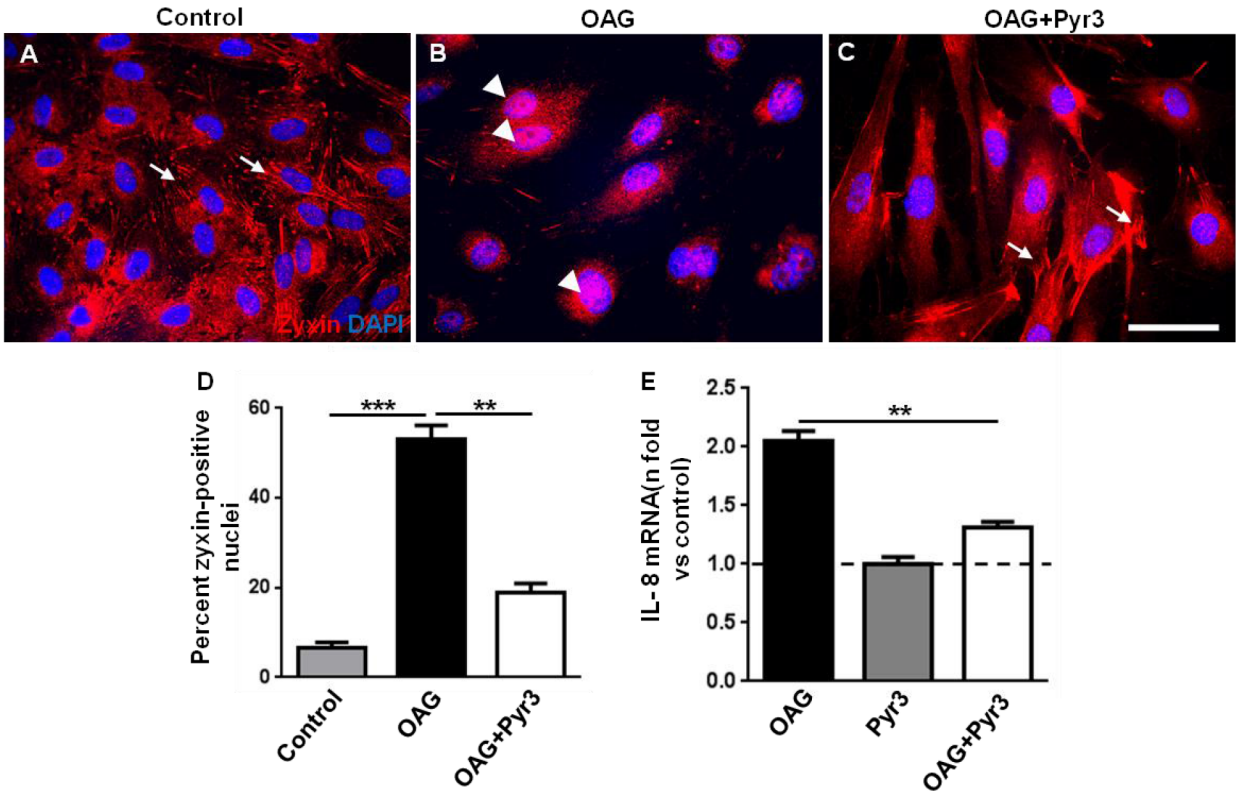

Figure 10: OAG-induced zyxin activation in HUVECs. A-C, Representative confocal immunofluorescence images (IF) of the sub-cellular localization of zyxin in HUVECs in control cells and after treatment with OAG (100 µM) alone for 24 hours or following a 6 hours pre-incubation with Pyr3 (10 µM).**D,** Summary of the quantitative analysis of zyxin-positive nuclei in HUVECs, **p<0.01, ***p<0.001 as indicated, n=3 for each group. **E,** Analysis of IL-8 gene expression in HUVECs following the same treatment, **p<0.01 as indicated, n=4 for each group.

These findings confirm a role forTRPC3 in zyxin activation in ECs. However, it is unclear if TRPC3 itself is directly involved in mechanosensing or is regulated following a sequence of events upstream of its activation. Furthermore, the kinetics of stretch-

induced calcium transients in vascular cells, in particular, the participation of TRPC3 therein has not been studied in detail.

4.1.5 *Kinetics of calcium transients induced by cyclic stretch in ECs*

Recent evidence suggest a ligand-independent activation of certain GPCRs, particularly in vascular SMCs by biomechanical stretch (Storch et al. 2012). These GPCRs are known to activate TRPC channels, e.g. TRPC6, by a mechanism which involves activation of phospholipase C (PLC). In the present study, the kinetics of stretch-induced calcium transients in HUVECs seeded on elastic membranes was investigated in the presence of pharmacological inhibitors of PLC and TRPC3 channels. Additionally, isoforms-selective knock down of PLC using specific siRNAs was used to study the contribution of individual isoforms to this process. Cyclic stretch induced a characteristic calcium transient with a rapid peak increase (phase I) in intracellular calcium followed by a gradual phase with a negative slope (phase II) indicating a biphasic response (Figure 11A, B).This resulted in a baseline that was shifted to higher levels of resting calcium. Subsequent cycles of stretch led to a step wise increase in calcium. The stretch-induced calcium transients were completely abolished by gadolinium. U73122, a compound which blocks all isoforms of PLC, had an effect on phase II leading to a rapid decay of the calcium signal in this phase. A similar albeit less severe effect was observed with knock down of the PLC isoform β_1 (PLC β isoform 1; PLCβ_1) or the specific TRPC3 channel blocker Pyr3 (Figure 11A, B). Each of these treatments led to a failure of the step wise increase in calcium at subsequent cycles of stretch (Figure 11A). Knock down of other PLC isoforms (PLCβ_3 and PLCγ_1 respectively) had no significant effect on the kinetics of this process (Figure 11A, B).The angiotensin II receptor (a GPCR) antagonist losartan (10 µM) also had no significant effect (slope of the tangent to the curve was -0.181±0.004). The difference between the peak calcium levels after stretch and the resting calcium levels preceding that stretch cycle was found to be the same for each treatment group. HUVECs were pre-incubated with the inhibitors for 6 hours prior to stretch and the inhibitor was also present in the perfusion medium during the application of cyclic stretch. Stretch was limited to two cycles to avoid loss of cells which would result in measurement artifacts.

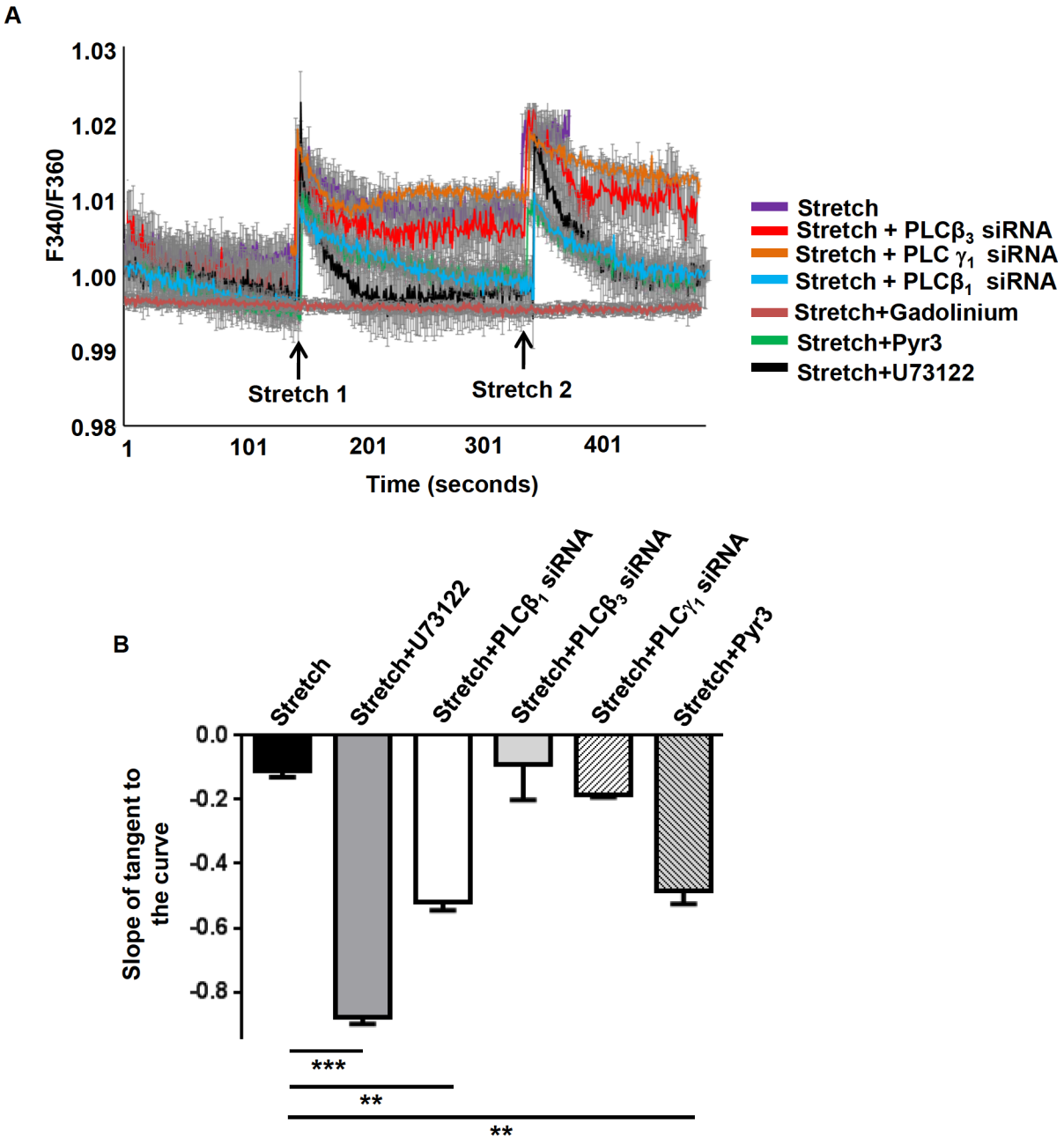

Figure 11: Effect of PLC and TRPC3 inhibition on stretch-induced calcium transients in HUVECs. A, Cyclic stretch-induced calcium transients in HUVECs stretched for 50 cycles using elastic membranes. 5 μM each of U73122 and Pyr3 and 100 μM of gadolinium was used. **B,** Quantitative analysis of the rate of decay of phase II of the stretch-induced calcium transient in HUVECs, **p<0.01 and ***p<0.001 as indicated, n=4 for each group. The slope of the tangent to the curves was used as a measure of the rate of decay of the calcium transient.

The knock down of PLC isoforms by specific siRNA was validated by Western blotting. The residual amounts of $PLC\beta_1$, $PLC\beta_3$ and $PLC\gamma_1$ following knock down was approximately 42, 35 and 38%, respectively (Figure 12). Scrambled siRNA was used as a control.

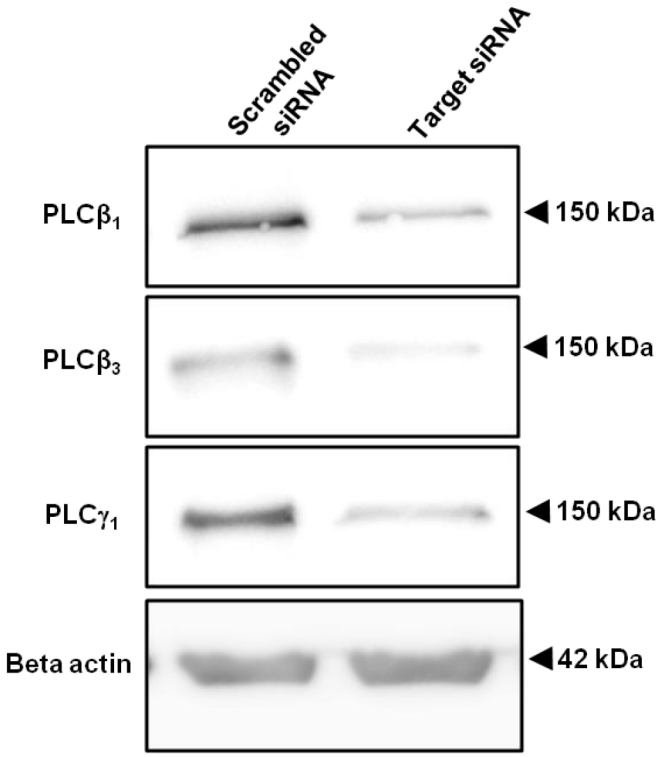

Figure 12: Knock down of PLC isoforms in HUVECs by siRNA. PLC isoforms were knocked down by specific siRNA using magnet-assisted transfection. Protein amounts were measured 72 hours post transfection. Beta actin was used as a loading control.

Since Pyr3 affects only phase II of the stretch-induced calcium transient in HUVECs, its ability to interfere with zyxin activation was investigated under conditions of cyclic stretch. Pyr3 in fact revealed a pronounced inhibitory effect on nuclear translocation of zyxin and the expression of IL-8 upon stretching of the HUVECs (Figure 13A through E). Pyr3 was thus able to block the activation of TRPC3 in response to both OAG stimulation and cyclic stretch of HUVECs.

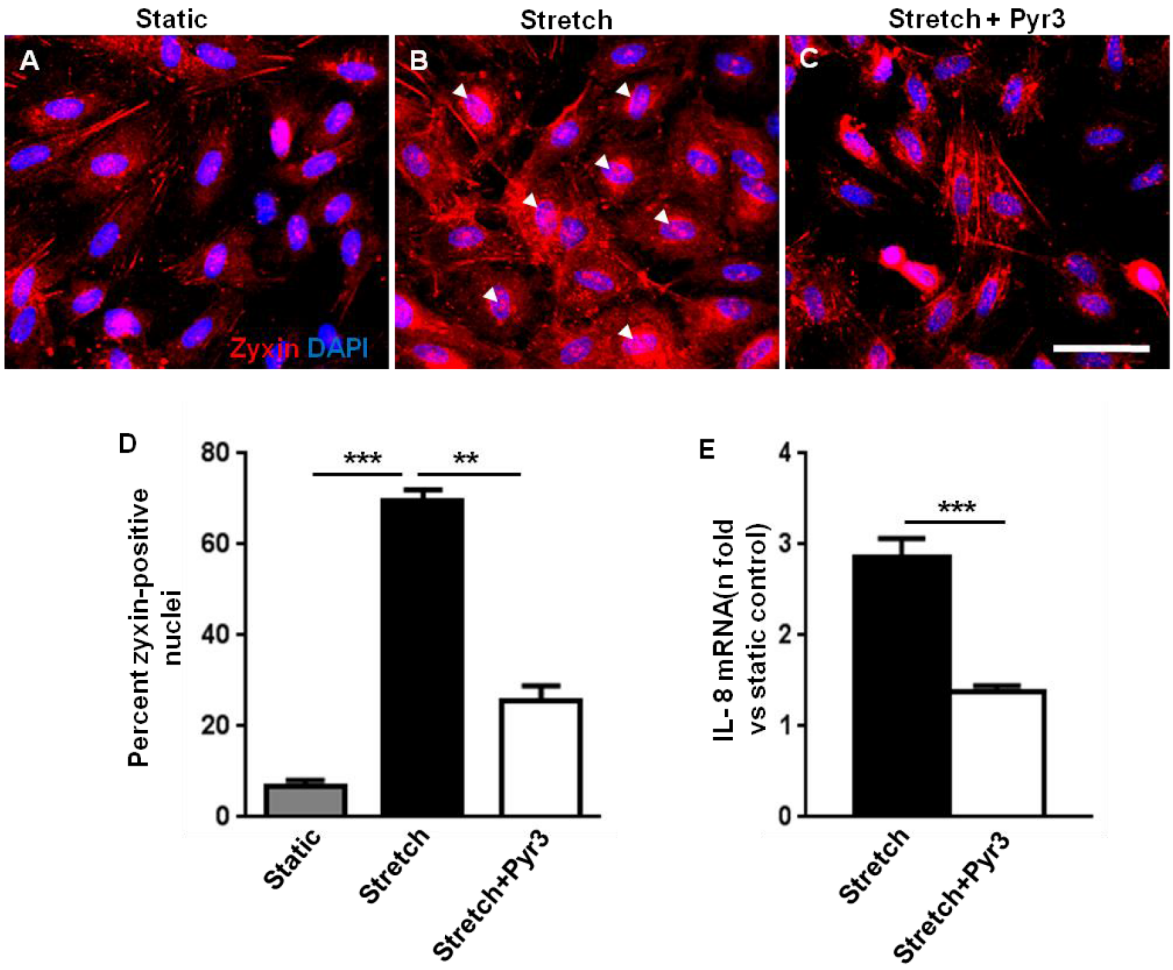

Figure 13: TRPC3 channel inhibition by Pyr3 strongly reduces stretch-induced zyxin activation. A-C, Representative confocal IF images of static and stretched HUVECs in the absence or presence of Pyr3 (10 µM). Zyxin-positive nuclei are marked by white arrow heads. Scale bar represents 100 µm. **D,** Quantitative summary of the percentage of zyxin-positive nuclei in HUVECs treated as above, **p<0.01, ***p<0.001 as indicated, n=3 for each group. **E,** Statistical summary of the effect of Pyr3 on IL-8 gene expression in stretched HUVECs, ***p<0.001 as indicated, n=3 for each group.

These data point to a complex regulation of stretch-induced zyxin activation in HUVECs that is not driven solely by global changes in intracellular calcium. Although angiotensin II receptors are considered mechanoresponsive in vascular SMCs acting predominantly through TRPC6, the prominent effect of PLC but not angiotensin II receptor blockade on stretch-induced calcium transients in HUVECs suggests the existence of a different set of mechanoreceptors. Thus, the responses of ECs and vascular SMCs to stretch in

terms of zyxin activation might be very different. With substantial work already done to elucidate the effects of zyxin activation in ECs (Wójtowicz et al. 2010,Suresh Babu et al. 2012), subsequent parts of the present study focused on the role of zyxin in vascular SMCs and its *in vivo* function.

4.2 Functional consequences of the loss of zyxin in vascular SMCs

In order to outline the effects of zyxin on stretch-induced gene expression in vascular SMCs, it is essential to understand the subtle differences between zyxin activation in ECs and vascular SMCs and thus interpret the present data in the light of previously published work in ECs.

4.2.1 *Differential threshold and kinetics of zyxin activation by stretch in ECS and vascular SMCs*

Biomechanical stretch induces the nuclear accumulation of zyxin in vascular SMCs (Figure 14A, B). The intensity threshold of the stretch stimulus required for this process differs between ECs and vascular SMCs. Thus, while a 10% cyclic elongation of ECs is sufficient to drive the translocation of zyxin from focal adhesions to the nucleus, a much stronger stimulus, namely 15-18% cyclic elongation is required in vascular SMCs (Wójtowicz et al. 2010,Cattaruzza et al. 2004). Furthermore, this process is essentially biphasic with zyxin shuttling in and out of the nucleus upon stretch over the course of time. Accordingly, zyxin accumulates in the nucleus of ECs within 30-60 minutes after stretch and returns to the focal adhesion after approximately 120 minutes. With persistent stretching, zyxin re-accumulates in the nucleus after 6 hours and is stably localized in the nucleus at later time points (doctoral dissertation of Agnieszka Wójtowicz, Heidelberg, 2008). On the contrary, in rat vascular SMCs, zyxin accumulated in the nucleus after 30 minutes and was completely relocalized to the focal adhesions after 6 hours of stretch (Cattaruzza et al. 2004). Therefore, a different pattern of zyxin-dependent gene expression is expected in vascular SMCs compared to ECs.

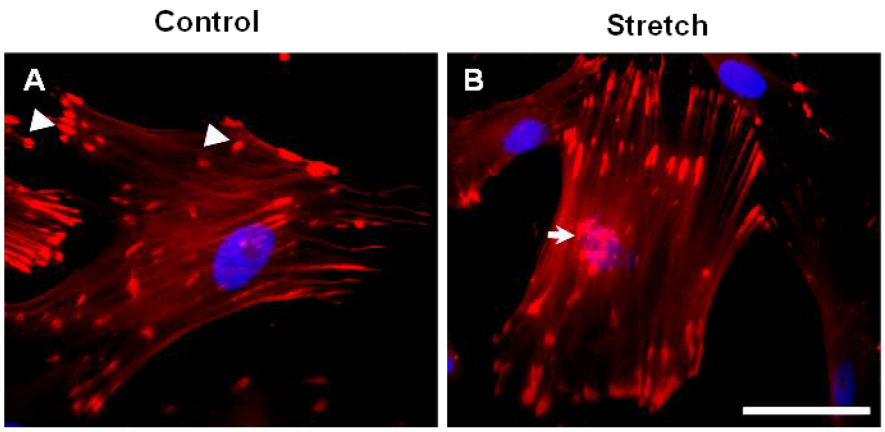

Figure 14: Cyclic stretch induces nuclear translocation of zyxin in vascular SMCs. A, Confocal IF images of aortic SMCs from wild type mice show a punctate distribution of zyxin at focal contact points to the substrate (indicated by white arrowheads) in static control cells. **B,** Mouse aortic SMCs exposed to 15% cyclic elongation at 0.5 Hz for 1 hour show a marked translocation of zyxin from focal adhesions to the nucleus (indicated by white arrow). Scale bar indicates 50 μm.

4.2.2 *Role of zyxin in stretch-induced gene expression in vascular SMCs*

Nuclear zyxin is responsible for approximately 68% of stretch-sensitive genes in human endothelial cells (Wójtowicz et al. 2010). Based on the differences in the kinetics of zyxin activation between ECs and vascular SMCs, a genome-wide DNA microarray analysis was done to test if zyxin is equally important in vascular SMCs. Static and stretched aortic SMCs isolated from wild type (WT) and zyxin-null mice ($zyxin^{-/-}$) were used for this array. Approximately 90% of the stretch-responsive genes in vascular SMCs were zyxin-dependent (Figure 15A through C). Selected genes were validated by real-time PCR. These genes were selected because of their putative association with at least one of the critical pathways regulating vascular SMC behaviour, namely proliferation, migration, contraction and apoptosis. Expression of all five candidate genes, namely cyclin E2, tumour necrosis factor receptor superfamily member 6 (Fas or CD95), integrin α8 (Itga8), matrix metalloproteinase 13 (MMP13) and regulator of G-protein signalling 5 (RGS5) was found to be stretch-sensitive and zyxin-dependent (Figure 15D).Gene Set Enrichment Analysis (GSEA) based on KEGG (Kyoto

Encyclopedia of Genes and Genomes) and GO (Gene Ontology) revealed that zyxin regulates distinct pathways in response to cyclic stretch.

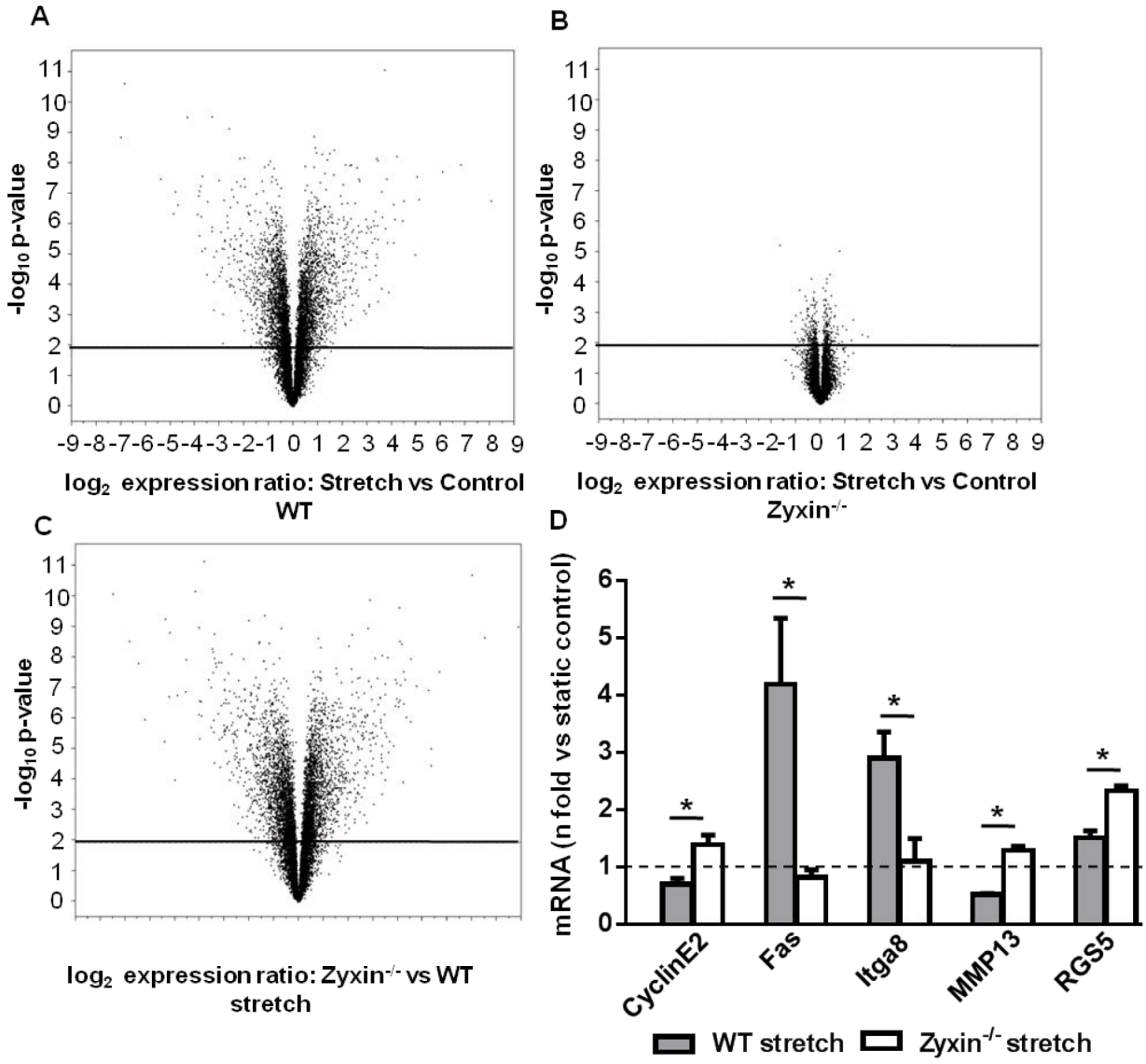

Figure 15: Zyxin regulates a vast majority of stretch-responsive genes in vascular SMCs. A-C, Volcano plot analysis of changes in expression of genes in stretched wild type (WT) and zyxin$^{-/-}$aortic SMCs (fold expression vs calculated probability). Genes which were differentially and significantly regulated ($p<0.01$) are displayed above the black solid line (n=3 for all experimental groups). 4718 genes were stretch-responsive in wild type compared to only 315 in zyxin$^{-/-}$vascular SMCs. D, Verification of 5 microarray target genes by real time RT-PCR, *$p<0.05$ as indicated, n=3 for all experimental groups.

4.2.3 *Regulation of vascular SMC phenotype by zyxin in vitro*

Out of the several pathways found to be zyxin-dependent, four broad pathways were selected based on their importance in determining the phenotype of vascular SMCs especially under pathophysiological conditions. Accordingly, proliferation, apoptosis, migration and contractility of zyxin-deficient vascular SMCs was analyzed in further detail by *in vitro* functional assays to determine the significance of the observed changes in gene expression. Furthermore, where possible, rescue experiments were performed by re-expressing zyxin in the zyxin-deficient vascular SMCs to see if such processes were strictly zyxin-dependent.

4.2.3.1 *Loss of zyxin results in increased proliferation of vascular SMCs*

Out of the several genes found to be zyxin-.dependent in vascular SMCs, cyclin E2 and MMP13 are associated with cell proliferation being involved in cell cycle regulation and in promoting growth. Since both these genes were found to be up regulated in zyxin-null vascular SMCs, the proliferation of these cells was monitored *in vitro*. Accordingly, the number of nuclei was counted after 72 hours in both static and stretched vascular SMCs. Zyxin-null vascular SMCs displayed a remarkable shift to a growth-promoting phenotype even under static conditions with a 1.6 fold higher proliferation as compared to WT vascular SMCs (Figure 16). Stretch had little effect on the proliferation rate of zyxin-null vascular SMCs which was apparently near maximum. However, stretch led to a decrease in the number of WT vascular SMCs thereby resulting in a 2.2 fold increase of zyxin-deficient vascular SMCs over their WT counterparts. The zyxin-dependency of this process was tested by re-expression of zyxin in zyxin-null vascular SMCs. Re-expression of zyxin led to normalization of the proliferation rate to near WT levels with no significant effect following expression of green fluorescent protein used as a transfection control (Figure 16). However, stretch led to a significant loss of transfected cells. As such, the consequences of zyxin re-expression could not be tested in this setting. One of the reasons for the increased proliferation might be an altered rate of apoptosis in these cells. Consequently, this was tested in the following experiments.

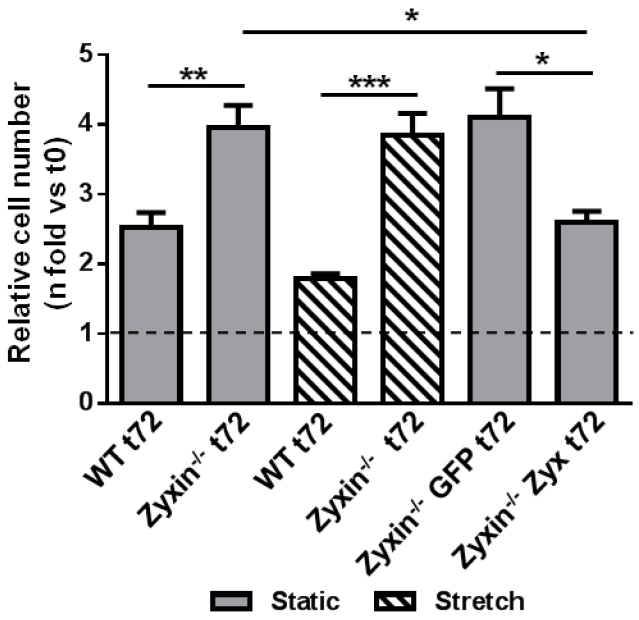

Figure 16: Zyxin-null vascular SMCs proliferate faster than their WT counterparts. The number of DAPI-stained nuclei was counted at 0 hours (t0) and after 72 hours (t72). For stretching the cells, a 13% cyclic elongation was used. Vascular SMCs with transgenic expression of green fluorescent protein and zyxin are denoted as zyxin$^{-/-}$ GFP and zyxin$^{-/-}$Zyx, respectively. *p<0.05, **p<0.01 and ***p<0.001 as indicated, n=5 for all groups except for zyxin$^{-/-}$ GFP t72 and zyxin$^{-/-}$Zyx t72 where n=3.

4.2.3.2 *Zyxin promotes Fas ligand (FasL)-induced apoptosis in stretched vascular SMCs*

Based on the selective up regulation of the Fas receptor (Figure 15D) in WT vascular SMCs upon stretch, the rate of apoptosis in stretched WT and zyxin-null vascular SMCs was tested in the presence of a trimeric Fas ligand (FasL). In the absence of stretch, exposure to FasL had no significant effect on vascular SMC apoptosis. However, stretched zyxin-null vascular SMCs showed significantly lower rates of apoptosis compared to WT cells exposed to FasL. TUNEL-positive nuclei were considered as positive for apoptosis (Figure 17A through I). Re-expression of zyxin could not be tested in this setting because transfection by electroporation induces apoptosis of vascular SMCs which would interfere in the accurate assessment of FasL-induced apoptosis in these cells. Migration of vascular SMCs is a critical factor which often accompanies

proliferation and affects SMC behaviour. Thus, the migration potential of zyxin-null vascular SMCs was investigated in further detail.

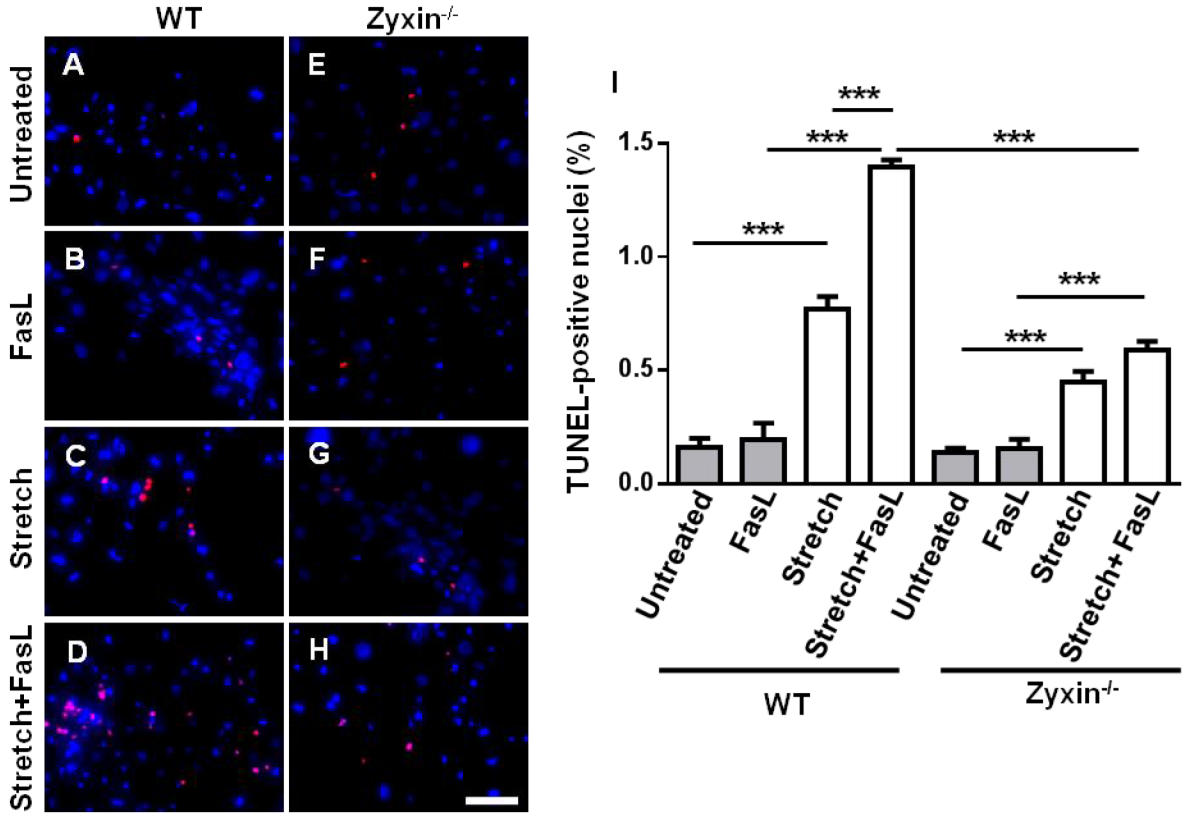

Figure 17: Stretched zyxin-null vascular SMCs are less sensitive to FasL-induced apoptosis. A-H, Detection of apoptotic nuclei by TUNEL staining (red). DAPI-stained nuclei are shown in blue. Scale bar represents 100 µm. Cells were stretched at 18% cyclic elongation for 18 hours with or without the presence of FasL (400 ng/mL). **I,** Statistical summary of apoptotic TUNEL-positive nuclei. ***p<0.001 as indicated, n=3 for all groups.

4.2.3.3 *Zyxin-null vascular SMCs are primed for migration independently of stretch*

The migration rate of WT and zyxin-null vascular SMCs was measured using a two-dimensional model of migration, namely the 2D scratch assay or the lateral sheet migration assay. The ability of the cells to migrate towards the midline of the scratch was used as a read out to assess their migratory potential (Figure 18A through H). Quantitative analysis revealed a migration speed of approximately 30µm/h in zyxin$^{-/-}$

vascular SMCs compared to 18 µm/h in WT cells (Figure 18I). Re-expression of zyxin in the zyxin$^{-/-}$vascular SMCs restored the migration speed to that observed for WT vascular SMCs while GFP overexpression had no effect on migration (Figure 18E through I). Thus, zyxin appears to negatively regulate cell motility of vascular SMCs. A characteristic feature of synthetic vascular SMCs apart from their high rates of proliferation and migration is a lack of contractility. To test if zyxin-null vascular SMCs fit this description, the ability of these cells to contract was investigated.

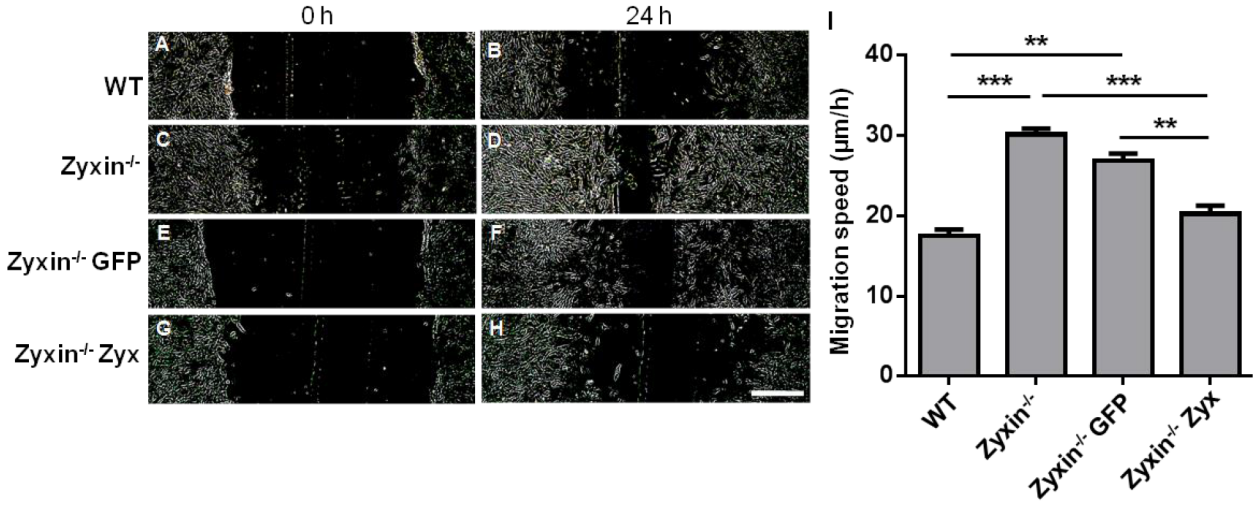

Figure 18: Zyxin$^{-/-}$ vascular SMCs are primed for migration in a two-dimensional (2D) scratch assay. A-H, Representative images of the migration of WT and zyxin$^{-/-}$vascular SMCs into a two-dimensional scratch after 24 h. Scale bar represents 500 µm. The sharpness and contrast of the images were adjusted to the same extent to clearly represent the migration front. **I,** Quantitative analysis of migration speed of the cells. The distance travelled by the cell front was divided by the time period to get the 2D migration speed. **p<0.01, ***p<0.001 as indicated. For all groups, n=5 except for zyxin$^{-/-}$ GFP and zyxin$^{-/-}$Zyx where n=3.

4.2.3.4 *Zyxin-null vascular SMCs display impaired basal and agonist-induced contraction*

Cells contract by generation of traction forces that pull against the surrounding matrix. Therefore, as an indirect means of assessing the contractility of vascular SMCs, a collagen gel compaction assay was used whereby the reduction in gel diameter was used as a read out for contractility of vascular SMCs seeded into such a collagen

matrix. Twenty four hours post seeding, zyxin-null vascular SMCs consistently showed less contractility with corresponding higher values of collagen gel diameter. Additionally, in the presence of vasoconstrictors such as endothelin 1 (ET-1), epinephrine (Eph) or norepinephrine (NE), this contractile deficit was further unmasked demonstrating a failure to adapt in the presence of a contractile stimulus (Figure 19A, B).

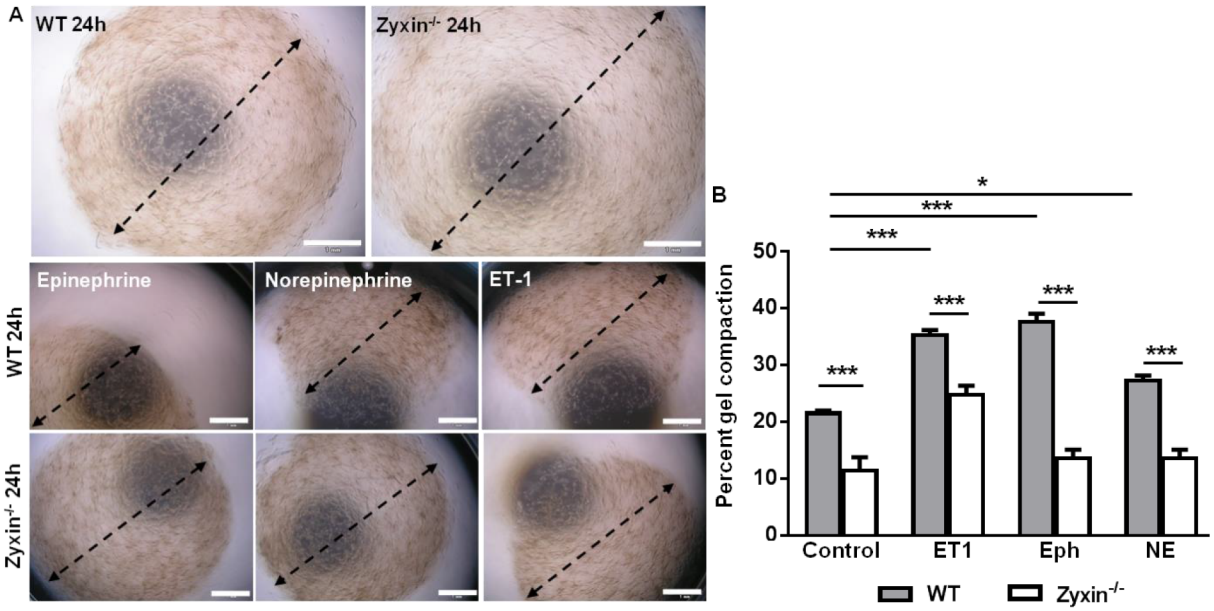

Figure19: Zyxin$^{-/-}$vascular SMCs have a basal contractile deficit which is accentuated upon pro-contractile stimulation. A, Representative images ofcollagen gels seeded with WT and zyxin-null aortic SMCs under basal and agonist-stimulated conditions 24 hours post solidification of the gels. Scale bars represent 1 mm. **B,** Analysis of the ability of WT and zyxin$^{-/-}$ vascular SMCs to pull a collagen gel thereby reducing its diameter over a time period of 24 hours, an indirect measure of the contractility of the vascular SMCs. Aortic SMCs seeded into the collagen gels were additionally stimulated with endothelin 1 (ET-1), epinephrine (Eph) or norepinephrine (NE) (100 nmol/L of each agonist). *p<0.05, ***p<0.001 as indicated, n= 4 for each experimental group.

This contractile deficit of zyxin-null vascular SMCs is in line with the reduced agonist-induced vasoconstriction of isolated femoral arteries from very old zyxin-null mice (doctoral dissertation of Agnieszka Wójtowicz, Heidelberg, 2008) To account for this inability to generate a sufficient contractile force, the assembly of actin stress fibres which are major determinants of cell contractility, was examined.

4.2.3.5 *Zyxin-null vascular SMCs display intense, poorly structured and condensed accumulation of F-actin*

There is substantial evidence regarding the role of zyxin in actin stress fibre assembly and repair. (Hoffman et al. 2012,Hirata et al. 2008,Smith et al. 2014). Zyxin is essential for building of robust stress fibres by cells in response to biomechanical stretch. Therefore, the intensity and organization of stretch-induced actin stress fibres was monitored using Alexa fluor488 tagged-phalloidin to label F-actin (Figure 20A through D).

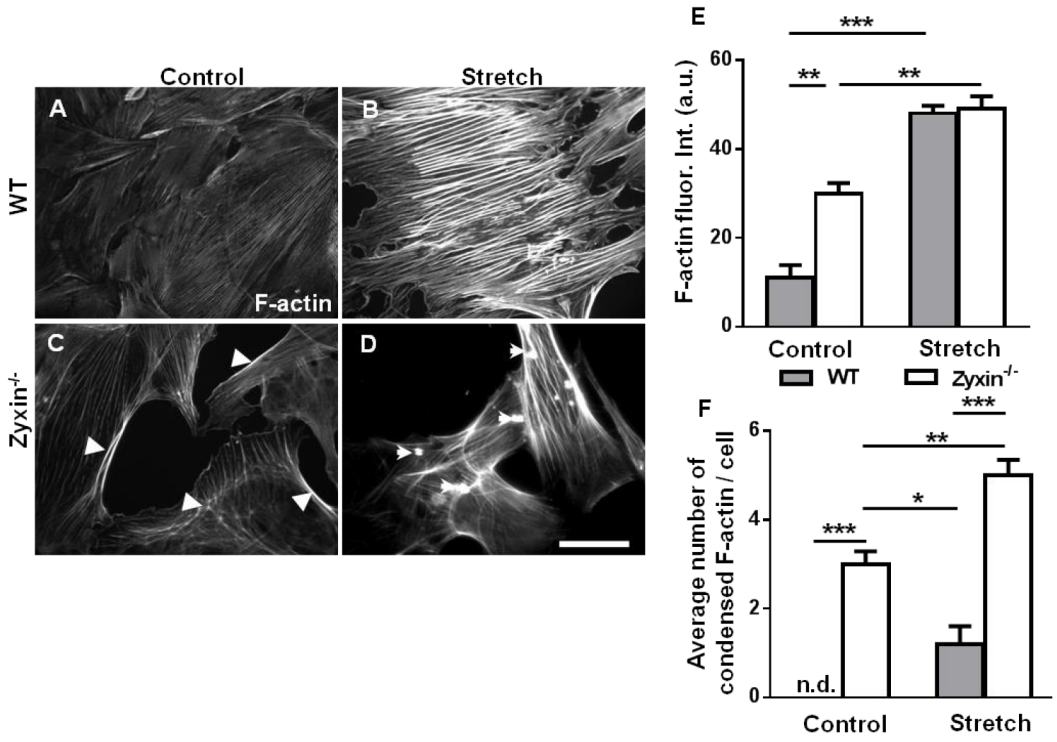

Figure 20: Zyxin$^{-/-}$ stretched vascular SMCs lack an organized actin network. A-D, F-actin stress fibres in control and stretched mouse aortic SMCs (15% cyclic elongation for 1 hour) were stained with Alexa fluor 488-labelled phalloidin (white). Scale bar represents 50 µm. **E,** Quantification of F-actin fluorescence intensity in control and stretched vascular SMCs with zyxin-deficient vascular SMCs having prominent F-actin staining along the edges of the cells (white arrowheads in Figure 20C). **p<0.01, ***p<0.001 as indicated, n=3 for each group. **F,** The average number of condensed F-actin deposits (white arrows) within the cells was quantified. *p<0.05, **p<0.01 and ***p<0.001 as indicated, n.d. indicates not detectable, n=3 for each group.

Static, unstretched zyxin-null vascular SMCs already showed a higher intensity of F-actin labelling which was localized mostly along the cell edges (Figure 20C, E). Stretch induced a robust build-up of actin stress fibres in WT vascular SMCs with characteristic parallel orientation of the fibres (Figure 20B). On the contrary, in zyxin-null vascular SMCs, there was intense accumulation of localized actin deposits appearing along the periphery or as condensed spots dispersed in the cytoplasm (Figure 20D through F). Thus, an organized actin network for efficient contraction was lacking in zyxin-deficient vascular SMCs.

These observations were reproduced in human arterial vascular SMCs (Figure 22A through E) following knock down with a siRNA targeting zyxin (Figure 21A through D).

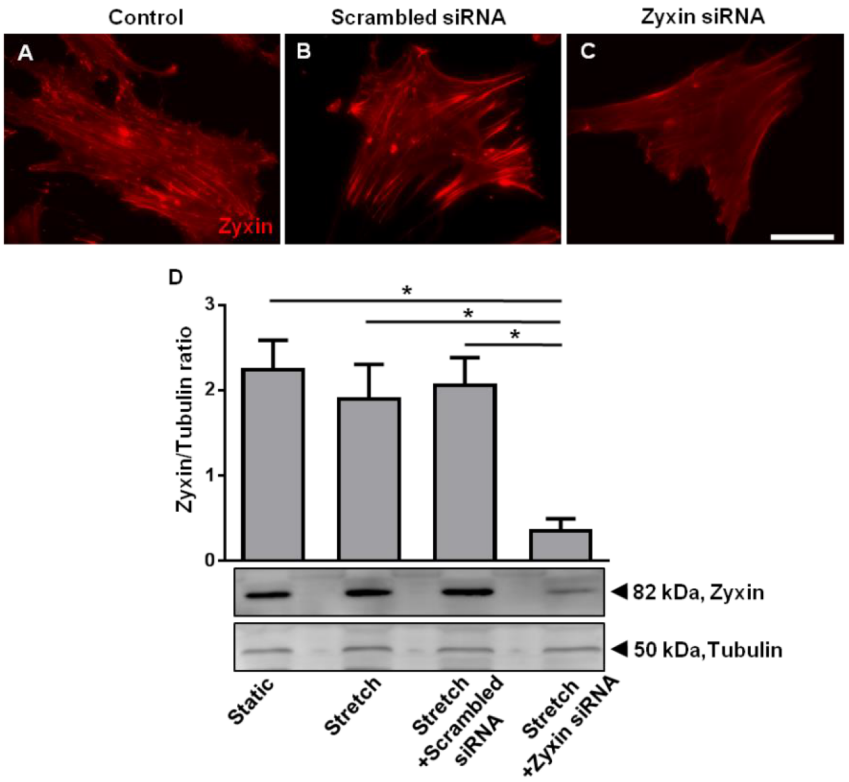

Figure 21: Zyxin silencing in human arterial vascular SMCs by using siRNA. A-C, Representative immunofluorescence images showing knock-down of zyxin in human arterial VSMCs 72 hours post transfection with a siRNA targeting zyxin. Scale bar represents 100 µm. Scrambled siRNA acts as a control for transfection of cells with a siRNA targeting zyxin. **D,** Western blot analysis of zyxin silencing (bottom) and its statistical summary (top), *p<0.05 as indicated, n=3 for each group.

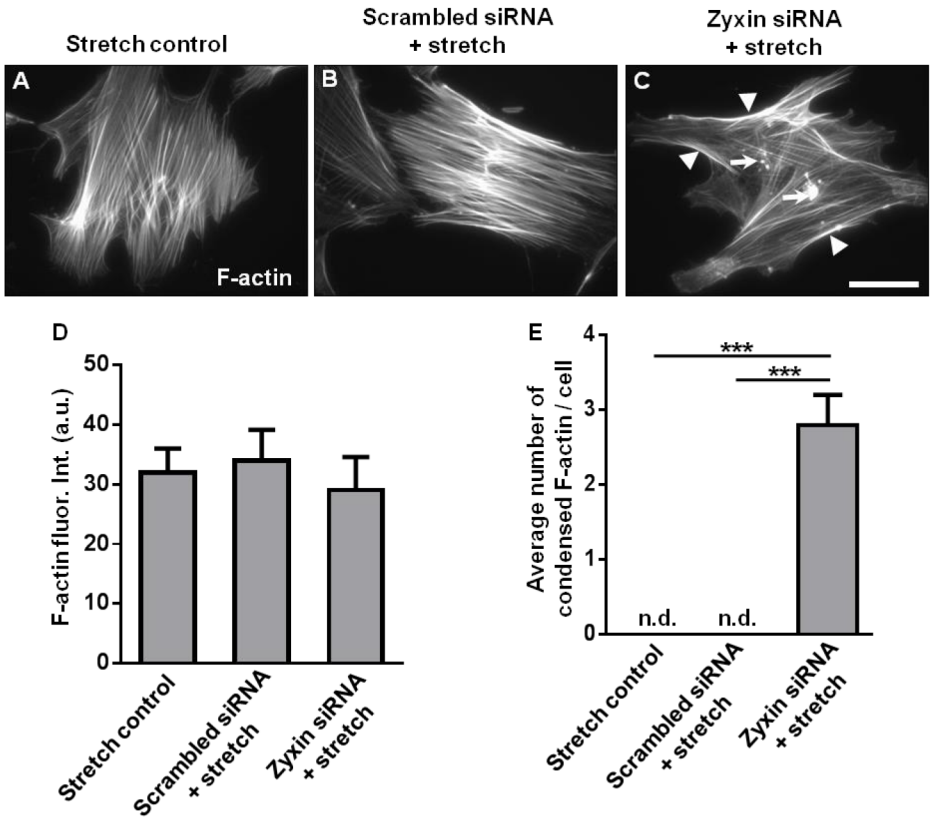

Figure 22: Knock down of zyxin results in disarray of stress fibres in stretched human arterial vascular SMCs.A-C, F-actin stress fibres in stretched humanarterial vascular SMCs (15% cyclic elongation for 1 hour) were stained with Alexa fluor 488-labelled phalloidin (white). Scale bar represents 50 µm. **D,** Quantification of F-actin fluorescence intensity in stretched human arterial vascular SMCs.Following knock down of zyxin by siRNA, prominent F-actin staining was observed along the edges of the cells (white arrowheads in Figure 22C). **E,** The average number of condensed F-actin deposits (white arrows) within the cells was quantified. ***p<0.001 as indicated, n.d. indicates not detectable, n=3 for each group.

Polymerization of actin is strongly regulated by the Rho GTPase RhoA. Consequently, the activation of RhoA was evaluated in zyxin-null vascular SMCs as a possible reason for intense F-actin staining in these cells.

4.2.3.6 Constitutive activation of RhoA in zyxin-null vascular SMCs

Following exposure of WT and zyxin-null vascular SMCs to 15% cyclic elongation for 1 hour, pull-down of active RhoA from total cell lysates resulted in significantly higher

levels of the active form of RhoA in zyxin-null vascular SMCs. The total amount of RhoA was not different between the two cell types (Figure 23A, B).

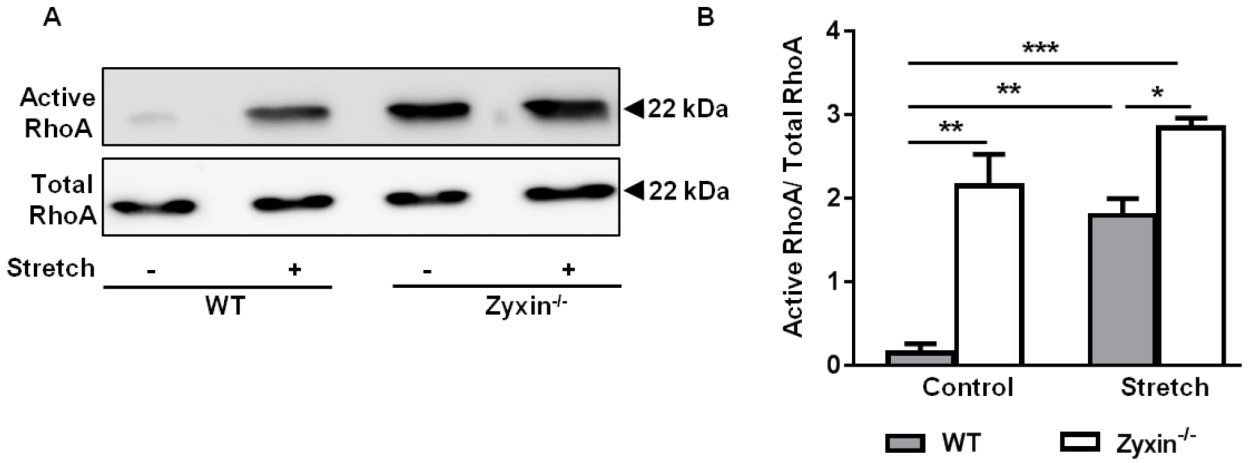

Figure 23: Zyxin$^{-/-}$vascular SMCs have higher levels of active RhoA. A, Western blot of active RhoA immunoprecipitated from total cell lysates by Rhotekin RBD beads 15 minutes after exposure of the mouse aortic SMCs to cyclic stretch (15% cyclic elongation, 0.5 Hz) or left unstretched. **B,** Quantification of active RhoA: total RhoA ratio as compared to WT vascular SMCs. Although stretch induced RhoA activation in both cell types, RhoA activity was higher in zyxin$^{-/-}$vascular SMCs; *p<0.05,**p<0.01,***p<0.001 as indicated, n=3 for each experimental group. Total RhoA remained unchanged in WT and zyxin-deficient vascular SMCs.

High RhoA activity in vascular SMCs drives the nuclear translocation of myocardin related transcription factor A (MRTF-A), a strong regulator of SMC phenotype. To test this hypothesis in zyxin-null vascular SMCs, the sub-cellular localization of MRTF-A was studied in further detail.

4.2.3.7 Nuclear accumulation of MRTF-A in zyxin-null vascular SMCs

Consistent with the high levels of F-actin and active RhoA in zyxin-null vascular SMCs, these cells displayed stronger accumulation of MRTF-A in the nucleus. Confocal immunofluorescence analysis revealed a predominant population of zyxin-null vascular SMCs with nuclear localization of MRTF-A even under basal, unstretched conditions (Figure 24A, D and G). Stretching of cells (15% cyclic elongation for 1 hour) resulted in nuclear translocation of MRTF-A in both WT and zyxin-deficient vascular SMCs albeit much stronger in zyxin-null vascular SMCs (Figure 24B, E and G).

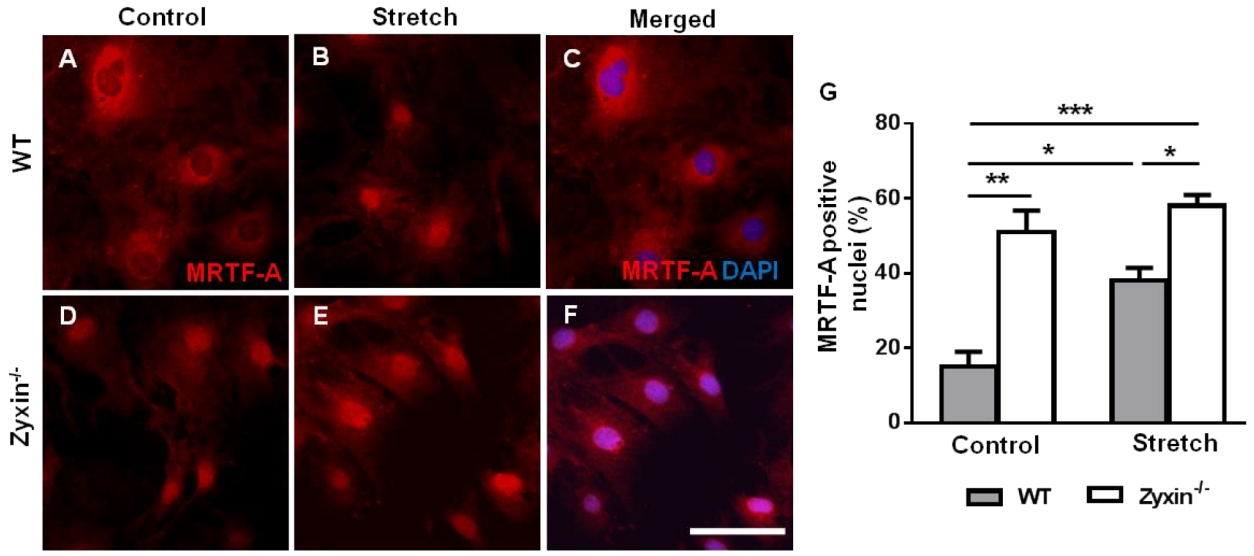

Figure 24: Stronger nuclear translocation of MRTF-A in zyxin$^{-/-}$vascular SMCs. (A,B,D and E), Representative immunofluorescence images of MRTF-A (red) localization in WT and zyxin-deficient mouse aortic SMCs. **(C,F),** Representative merged images showing MRTF-A and DAPI colocalization in stretched vascular SMCs (F) but not in control unstretched vascular SMCs (C). DAPI stained nuclei are shown in blue. Scale bar represents 100 µm. **G,** Statistical summary of stretch-induced nuclear translocation of MRTF-A in both types of vascular SMCs. *p<0.05, **p<0.01,***p<0.001 as indicated, n=3 for each group.

Western blot analyses of cytosolic and nuclear protein fractions isolated from WT and zyxin-null vascular SMCs further corroborated these findings (Figure 25H, I).

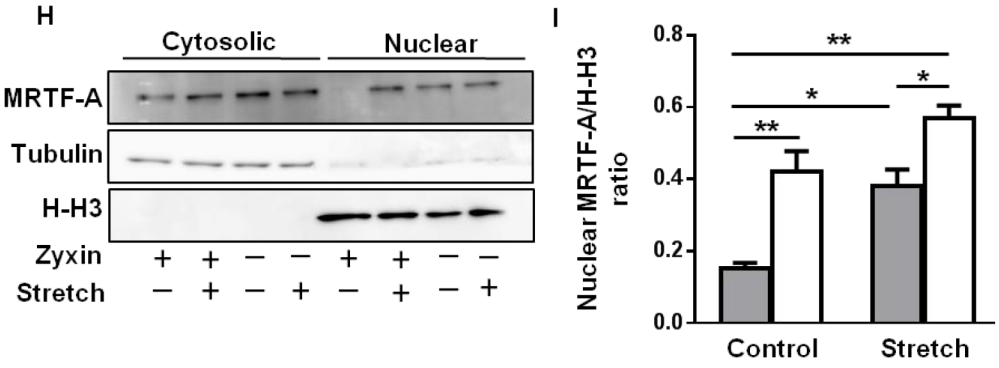

Figure 25: Statistical summary **(I)** of representative Western blot analyses (**H)** of nuclear and cytosolic fractions from WT and zyxin-null vascular SMCs demonstrating the stronger nuclear localization of MRTF-A in zyxin-null vascular SMCs, *p<0.05, **p<0.01, n=3 for each group. Histone H3 (H-H3) and tubulin were used as markers for the nuclear and cytosolic fraction, respectively.

Stretched human arterial vascular SMCs showed a similar albeit less robust accumulation of MRTF-A in the nucleus (Figure 26A through E) following transient knock down of zyxin (Figure 21).

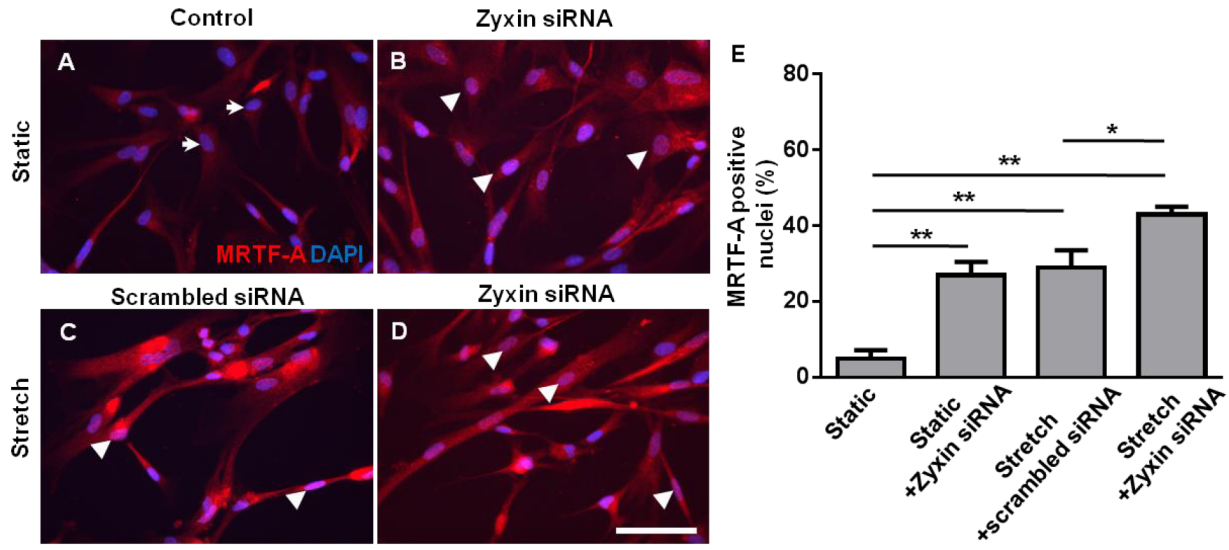

Figure 26: Stronger nuclear translocation of MRTF-A in human arterial VSMCs following zyxin silencing. A-D, Representative merged confocal immunofluorescence images of MRTF-A (red) localization in human arterial VSMCs co-stained with DAPI (blue). Scale bar represents 100 µm. White arrowheads indicate MRTF-A positive nuclei while white arrows represent nuclei negative for MRTF-A. Scrambled siRNA serves as a control for transfection of cells with siRNA targeting zyxin. **E**, Statistical summary of MRTF-A positive nuclei in human arterial VSMCs with or without zyxin silencing in the presence or absence of cyclic stretch. *p<0.05, **p<0.01 as indicated, n=3 for each group.

MRTF-A is an important transcription factor in vascular SMCs regulating gene expression by interaction with serum response factor (SRF). Therefore, its contribution to zyxin-dependent gene expression was evaluated.

4.2.3.8 *Partial reversal of zyxin-dependent gene expression by knock down of MRTF-A*

Following knock down of MRTF-A by siRNA (Figure 27A, B), the expression of all five stretch-induced zyxin-dependent genes (Figure 15D) was analyzed by real time PCR. Indeed, the expression of three out of the five genes namely cyclin E2, Itga8 and MMP13 was reversed upon knock down of MRTF-A (Figure 28).

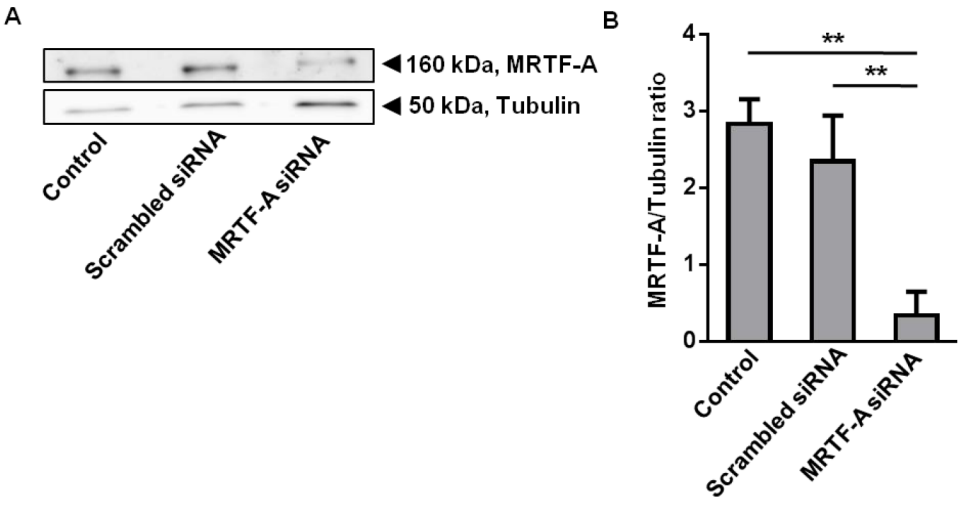

Figure 27: MRTF-A silencing by using siRNA specific for MRTF-A. A, Western blot validation of MRTF-A silencing by siRNA. Scrambled siRNA acts as a control for transfection of cells with a siRNA targeting MRTF-A. Tubulin acts as a loading control. **B,** Statistical summary of MRTF-A silencing, **p<0.01 as indicated, n=3 for each group.

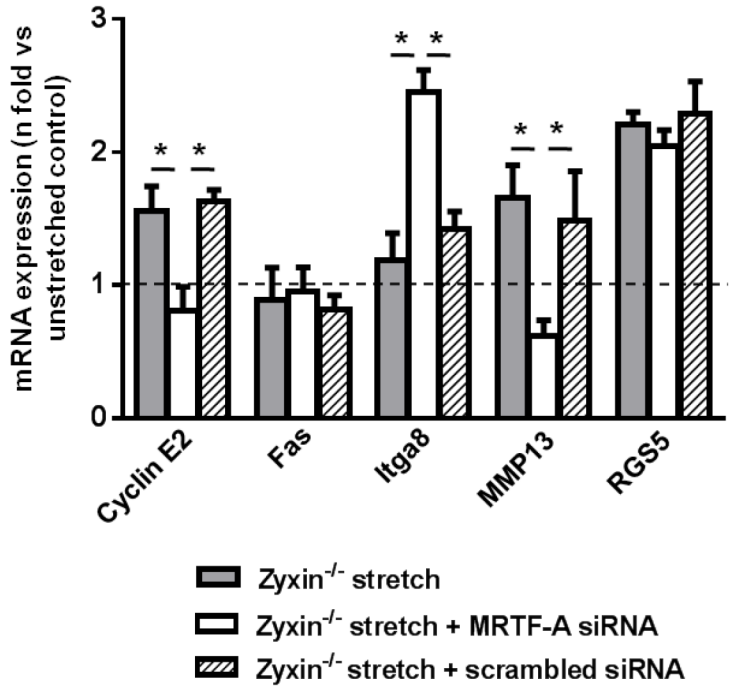

Figure 28: MRTF-A silencing partially rescues gene expression changes resulting from zyxin deficiency. Effect of MRTF-A silencing on stretch-sensitive zyxin-dependent gene expression in zyxin-deficient mouse aortic SMCs analysed by quantitative real time RT-PCR, *p<0.05 as indicated, n=3 for each group.

Thus, loss of zyxin promotes a synthetic phenotype of vascular SMCs which is further accentuated in the presence of biomechanical stretch. In view of this, subsequent efforts were made to define the role of zyxin *in vivo* using mice with global loss of zyxin. Furthermore, to induce an increased wall tension in the blood vessels to replicate the effects of exaggerated biomechanical stretch observed *in vitro*, a deoxycorticosterone acetate (DOCA)-salt model of experimental hypertension was used.

4.3 Functional consequences of loss of zyxin *in vivo* in mice

Mice with global loss of zyxin were back crossed with C57BL/6J mice for at least ten generations. All animal experiments were approved by the Regional Council Karlsruhe and were in conformance with the Guide for the Care and Use of Laboratory Animals published by the US National Institute of Health (NIH publication No. 85-23, revised 1996).Deoxycorticosterone acetate (DOCA) is a synthetic mineralocorticoid (corresponding to the human aldosterone) which causes volume-induced hypertension in mice by means of sodium and water retention in the kidneys. The increase in blood pressure was supported by supplementation of sodium chloride in the drinking water of the mice. Blood pressure was measured by a blood pressure cuff using the mouse tail or using radiotelemetry as described in the 'methods' section. Owing to the influence of zyxin on proliferation of vascular SMCs and their contractility *in vitro* along with its close proximity to the extracellular matrix (ECM), consequences of its loss on blood pressure regulation, vascular SMC proliferation, ECM content and cross-linking were measured in WT and zyxin-null mice following 21 days of DOCA-salt treatment.

4.3.1 *Loss of zyxin is dispensable in adult mice in experimentally-induced hypertension*

Experimental hypertension was induced in WT and zyxin-null mice aged 24-26 weeks. Zyxin-null mice showed comparable increase in blood pressure to WT animals following DOCA-salt treatment (Figure 29).

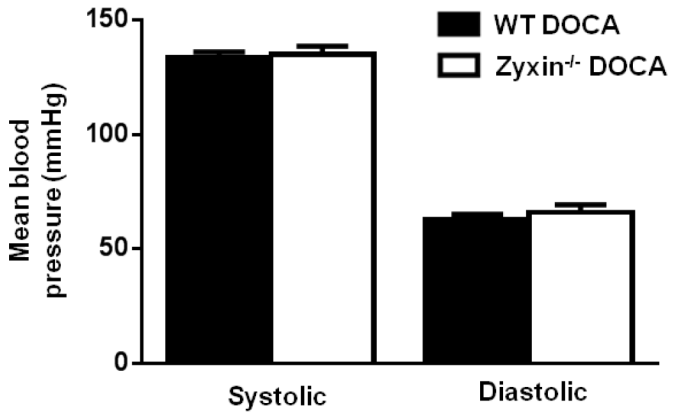

Figure 29: Blood pressure readings are comparable between WT and zyxin-null mice. Mean systolic and diastolic blood pressure values were recorded by placing a pressure cuff on the tail of the mice. DOCA-salt-treated WT and zyxin-null mice aged 24-26 weeks were compared. Data were not significantly different, n=6 for each group.

Proliferation of vascular SMCs measured by the number of proliferating cell nuclear antigen (PCNA)-positive nuclei in the media of femoral arteries from these mice was not significantly different (Figure 30A-C). Additionally, the organization of collagen I (a major ECM protein in arteries) (Figure 30D-F) and the expression of the ECM cross-linking enzyme transglutaminase 2 (TG-2) (Figure 30G-I) was comparable in both mouse strains.

Femoral arteries from older zyxin-null mice have been reported to have significant deficits in myogenic response and agonist-induced vasoconstriction (doctoral dissertation of Agnieszka Wójtowicz, Heidelberg, 2008). As such, subsequent experiments were done using old mice aged 52 weeks and very old mice aged approximately 78 weeks. These mice were monitored for changes in blood pressure by telemetry, immunohistochemistry of the femoral artery cross-sections to analyse changes in structure as well as ultrasound measurements of femoral artery blood flow to determine the resistivity of these arteries.

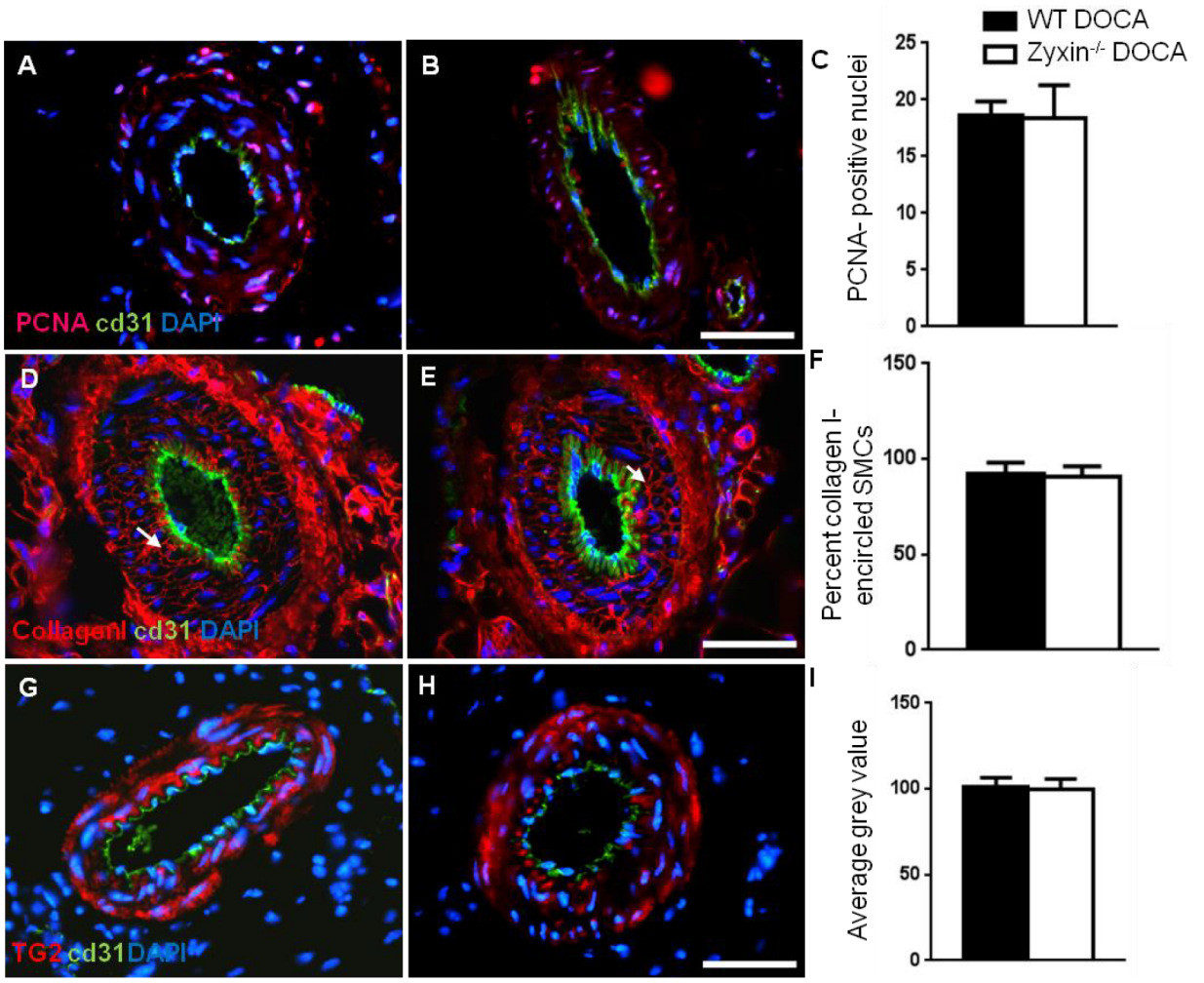

Figure 30: Femoral arteries from DOCA-treated WT and zyxin-null mice show similar remodelling. A, B, Representative confocal immunofluorescence (IF) images of femoral artery sections showing PCNA-positive nuclei (pink) of proliferative vascular SMCs. **D, E,** Representative confocal IF images of femoral artery sections showing collagen I staining (red) around the vascular SMCs and in the outer adventitial layer. The networks of fibres surrounding the vascular SMCs are marked with white arrows. **G, H,** Representative confocal IF images of femoral artery sections showing TG-2 staining (red). The endothelial cell layer is stained with CD31 (green). All scale bars represent 50 µm. **C, F and I,** Statistical summary of number of PCNA-positive nuclei, number of collagen I-encircled nuclei and of TG-2 staining intensity in grey values, respectively; n=6 for each group. Values were not significantly different between the groups.

4.3.2 *Experimental hypertension induces subtle changes in old zyxin-null mice*

Following DOCA-salt treatment for 21 days, old zyxin-null mice aged approximately 52 weeks showed a significantly lower increase in systolic arterial blood pressure as measured by radiotelemetry. However, diastolic arterial blood pressure increased in both WT and zyxin-null mice to the same extent (Figure 31).

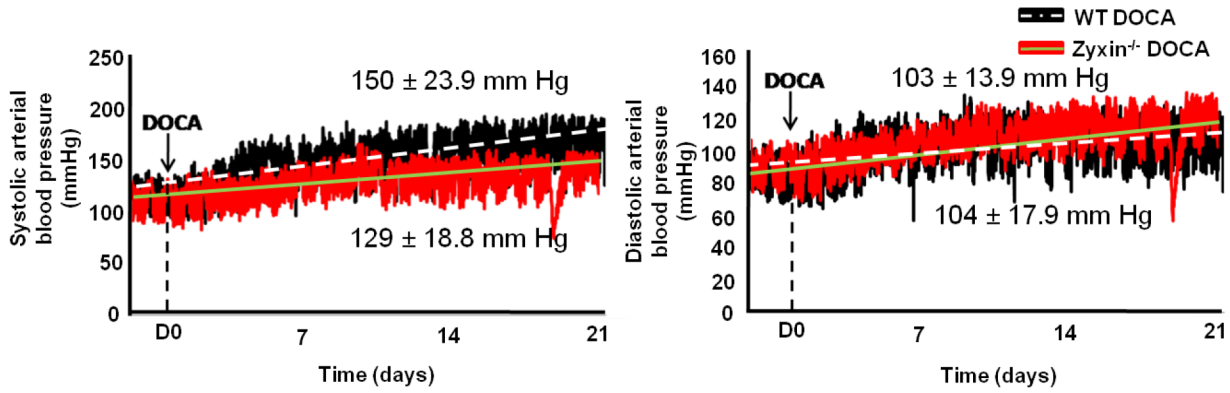

Figure 31: Measurement of blood pressure in conscious, unrestrained mice using radiotelemetry. The mean systolic and diastolic blood pressure values are shown in the figure. The white dashed line and the solid green line represent trend lines for blood pressure recordings in WT and zyxin-null mice, respectively. Mean systolic arterial pressure values were significantly different, *p<0.05, n=8 for each group.

Investigation of histological changes in femoral arteries from these mice showed subtle changes which did not achieve statistical significance (Figure 32). Diastolic pressure is affected by the constriction of small peripheral blood vessels. Although changes in diastolic blood pressure were not significant at this time point, resistivity of femoral arteries was measured using high resolution ultrasound imaging to assess any subtle functional changes in these arteries. This technique records the peak systolic velocity (PSV) and the end-diastolic velocity (EDV) of blood flow and uses an algorithm to determine resistivity of the blood vessel under investigation. No significant changes in resistivity were observed between femoral arteries from WT and zyxin-null mice (0.763± 0.03 in WT vs 0.677 ± 0.02 in zyxin-null mice, n=8).

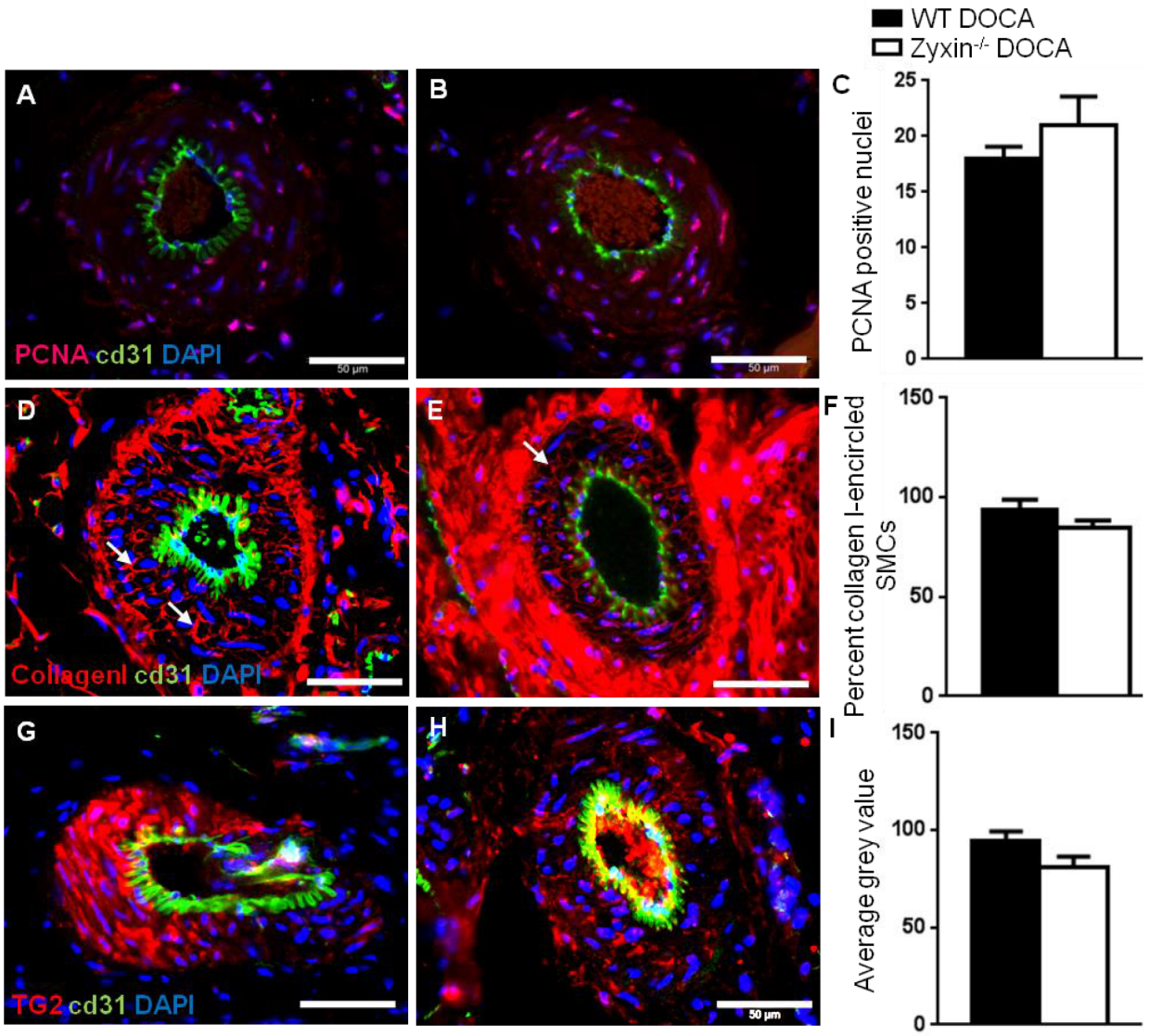

Figure 32: Femoral arteries from older DOCA-treated WT and zyxin-null mice show subtle changes in structure. A, B, Representative confocal IF images of femoral artery sections showing PCNA-positive nuclei (pink) of proliferative vascular SMCs. **D, E,** Representative confocal IF images of femoral artery sections showing collagen I staining (red) around the vascular SMCs and in the outer adventitial layer. The networks of fibres surrounding the vascular SMCs are marked with white arrows. **G, H,** Representative confocal IF images of femoral artery sections showing TG-2 staining (red). The endothelial cell layer is stained with CD31 (green). All scale bars represent 50 µm. **C, F and I,** Statistical summary of number of PCNA-positive nuclei, number of collagen I-encircled nuclei and of TG-2 staining intensity in grey values respectively, n=8 for each group. Values were not significantly different between the groups.

4.3.3 *Pronounced changes in arterial structure in very old zyxin-null mice*

DOCA-salt treatment in very old zyxin-null mice aged approximately 78 weeks led to a significantly lower increase in both systolic and diastolic blood pressure. These animals seemed resistant to a robust increase in blood pressure as compared to age-matched WT mice (Figure 33). The DOCA-salt-induced changes in blood pressure in the very old WT mice, on the other hand, were quite comparable to those in the younger WT animals.

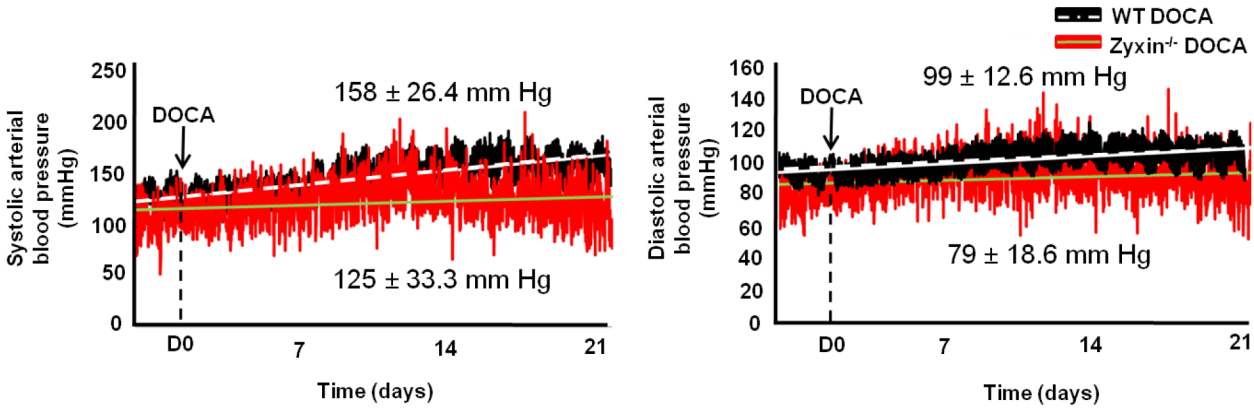

Figure 33: Representative traces of blood pressure recordings in very old WT and zyxin-null mice following DOCA-salt treatment. The mean systolic and diastolic blood pressure values are shown in the figure. The white dashed line and the solid green line represent trend lines for blood pressure recordings in WT and zyxin-null mice, respectively. Mean systolic and diastolic arterial blood pressure values were significantly different, *$p<0.05$, $n=8$ for each group.

Immunohistochemistry revealed prominent changes in the structure of the femoral arteries from zyxin-null mice along with significantly higher proliferation of vascular SMCs (Figure 34A-C). Collagen fibres surrounding the vascular SMCs were sparse which was accompanied by a decrease in TG-2 expression in these arteries (Figure 34D through I). The changes in arterial structure were thus coincident with the diminished response of the very old zyxin-null mice to an increase in blood pressure upon DOCA-salt treatment.

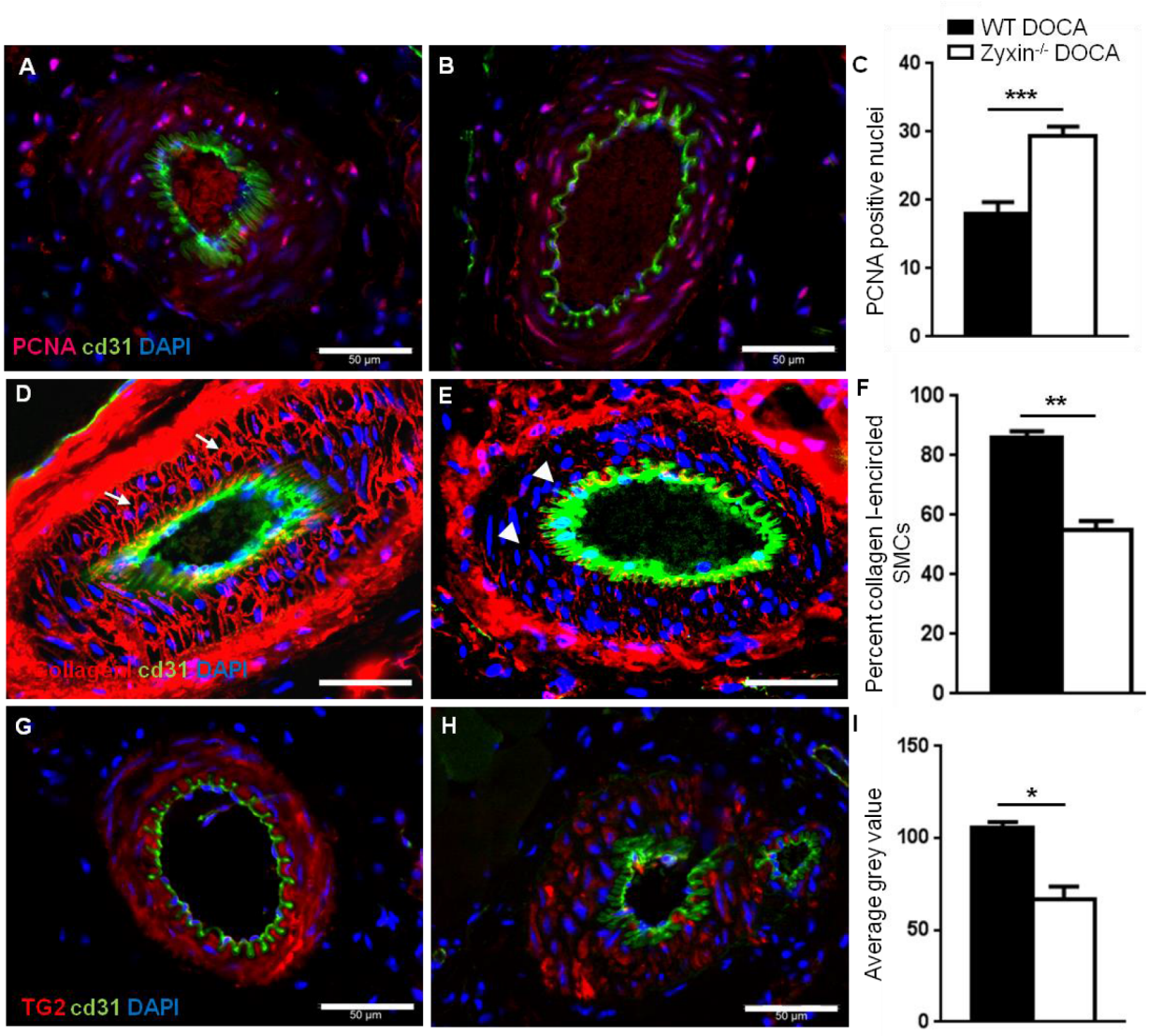

Figure 34: Pronounced structural changes in the femoral arteries from very old zyxin-null mice following DOCA-salt treatment. A, B, Representative confocal IF images of femoral artery sections showing PCNA-positive nuclei (pink) of proliferative vascular SMCs. **D, E,** Representative confocal IF images of femoral artery sections showing collagen I staining (red) around the vascular SMCs and in the outer adventitial layer. The networks of fibres surrounding the vascular SMCs are marked with white arrows. The regions showing sparse collagen fibre network are indicated by white arrowheads. **G, H,** Representative confocal IF images of femoral artery sections showing TG-2 staining (red). The endothelial layer is stained with CD31 (green). All scale bars represent 50 µm. **C, F and I,** Statistical summary of the number of PCNA-positive nuclei, number of collagen I-encircled nuclei and of TG-2 staining intensity in grey values, respectively; *p<0.05, **p<0.01 and ***p<0.001 as indicated, n=8 for each group.

Owing to the lack of a robust increase in diastolic blood pressure in zyxin-null mice along with prominent structural changes in the arterial wall, the resistivity of the femoral arteries from these mice was monitored *in vivo* following 21 days of DOCA-salt treatment. Zyxin-deficient mice displayed poor resistivity of femoral arteries which was significantly lower than that of WT animals (Figure 35). The vessel resistivity was not significantly different in these mice under baseline conditions (0.663 ± 0.042 in WT vs 0.671 ± 0.028 in zyxin-null mice, n=8).

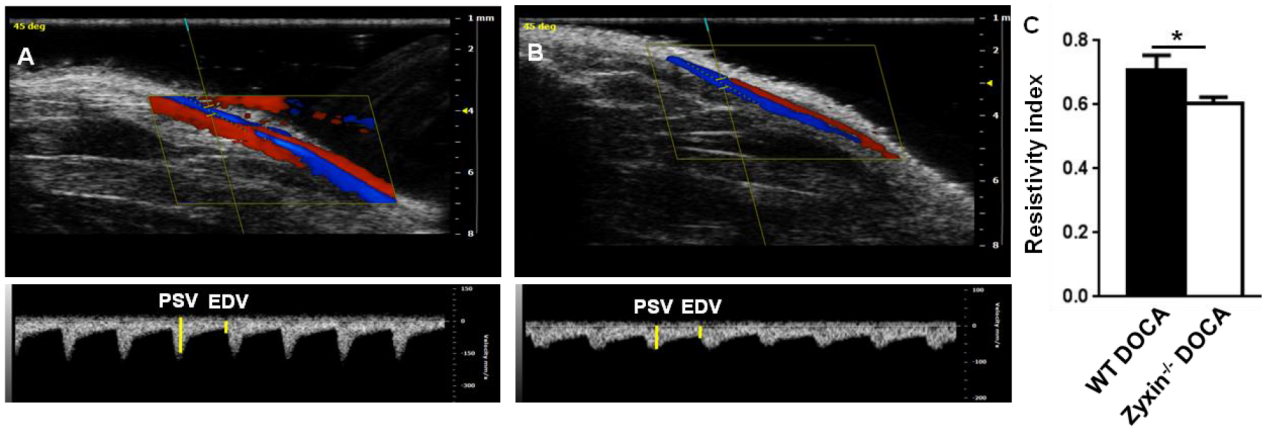

Figure 35: Femoral artery blood flow measurements using high resolution ultrasound imaging. Velocity measurements of blood flow in femoral arteries of WT **(A)** and zyxin-null mice **(B).** PSV and EDV represent peak systolic and end diastolic velocities, respectively. The colour codes red and blue represent flow of blood towards the transducer head or away from it (in this case representing the vein and the artery, respectively). C, Statistical summary of resistivity index measured from PSV and EDV values, *p<0.05 and n=8 for each group.

Therefore, reduced arterial resistivity might explain the lack of a robust increase in diastolic blood pressure in the very old mice upon DOCA-salt treatment. While total peripheral resistance influences the diastolic blood pressure, systolic pressure is also influenced by cardiac output. The zyxin-null animals have not been previously analysed for cardiac function. However, zyxin has been reported to play an important role in cardiomyocyte survival in response to atrial natriuretic peptide (ANP) (Kato et al. 2005). This along with the lack of a significant increase in systolic blood pressure already in 52 weeks old DOCA-salt-treated zyxin-null mice prompted the investigation of cardiac function in these animals.

4.3.4 *Cardiac systolic dysfunction in DOCA-salt-treated zyxin-null mice*

Cardiac systolic function was analysed in WT and zyxin-null mice (approximately 52 weeks old) both under basal conditions and 21 days post DOCA-salt treatment using high resolution echocardiography. Parameters indicative of systolic function such as cardiac output, stroke volume, ejection fraction and fractional shortening were examined. Both WT and zyxin-null mice had comparable cardiac systolic function under basal conditions (Table 22).

Table 22: Echocardiography measurements of WT and zyxin-null mice (baseline conditions)

Parameter	**WT (Mean ± SEM)**	**Zyxin-null (Mean ± SEM)**	**p-value**
Volume;s	21.2351 ± 0.8669	25.9337 ± 2.4371	p>0.05
Volume;d	65.5980 ± 2.0056	73.3503 ± 5.7209	p>0.05
Stroke Volume	44.3629 ± 2.2065	47.4166 ± 4.4959	p>0.05
Ejection Fraction	67.4477 ± 1.6887	64.6003 ± 2.3556	p>0.05
Fractional Shortening	37.0255 ± 1.3516	35.0682 ± 1.7878	p>0.05
Cardiac Output	21.7046 ± 2.2455	23.5925 ± 2.4671	p>0.05
LV Mass	125.5986 ± 2.1273	140.437 ± 5.6375	p>0.05
LV Mass Corrected	100.4789 ± 1.7019	112.3496 ± 4.5099	p>0.05

However, 21 days post DOCA-salt treatment, zyxin-null mice displayed a significant decrease in cardiac systolic parameters indicative of systolic dysfunction (Figure 36 and Table 23). It was not possible to measure diastolic function due to the increased length of the procedure owing to higher body mass and prominent sternum in older mice. Cardiac dysfunction was similarly evident in very old zyxin-null mice aged approximately 78 weeks following DOCA-salt treatment (Table 24). Measurements in short axis view of the heart were more consistent and were used in further echocardiography analyses.

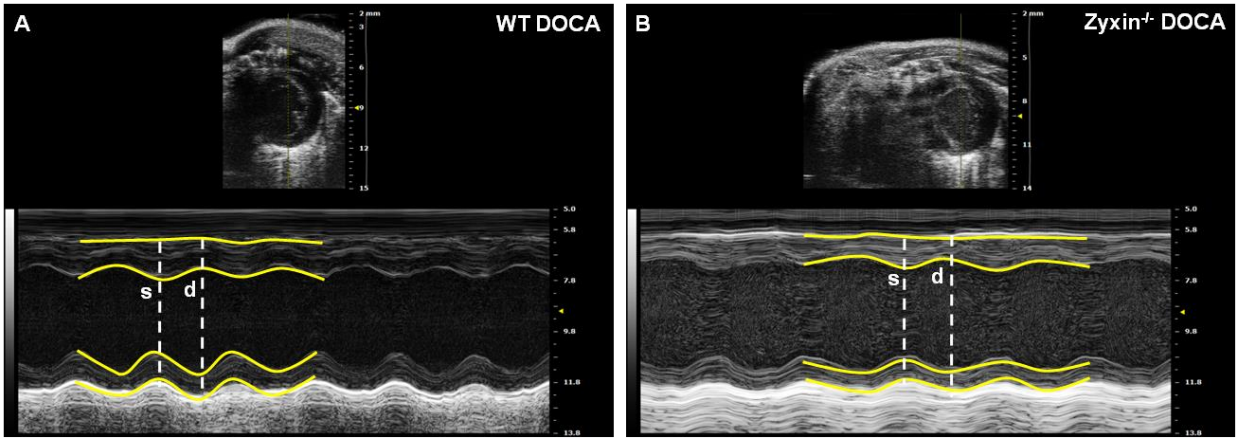

Figure 36: High resolution echocardiography measurements of systolic cardiac function in mice: DOCA-salt-treated WT and zyxin-null mice aged approximately 52 weeks were anesthetised with isoflurane and echocardiography was performed. M-mode short axis measurements are presented here for **(A)**WTand **(B)** zyxin-null mice. 's' and 'd' represent systole and diastole, respectively.Yellow lines indicate the movement of the cardiac wall.

Table 23: Echocardiography measurements in DOCA-salt-treated WT and zyxin-null mice aged approximately 52 weeks (n=8)

Parameter	WT (Mean ± SEM)	Zyxin-null (Mean ± SEM)	p-value
Volume;s	30.5791 ± 1.8945	45.5391 ± 2.4958	p<0.001
Volume;d	83.2742 ± 1.3392	91.5413 ± 2.9037	p<0.05
Stroke Volume	50.6950 ± 1.0022	42.0021± 2.3582	p<0.01
Ejection Fraction	70.6266 ± 1.8617	53.8544 ± 2.0522	p<0.001
Fractional Shortening	39.9283 ± 1.5131	28.8207 ± 1.2525	p<0.001
Cardiac Output	26.6076 ± 0.5343	15.3411 ± 1.5637	p<0.001
LV Mass	172.1988 ± 8.0991	155.8680 ± 7.3874	p>0.05
LV Mass Corrected	137.7590 ± 6.4793	124.6944 ± 5.9099	p>0.05

Measurements in very old mice (aged 78 weeks) showed an overall reduction in cardiac systolic parameters compared to mice aged 52 weeks (Table 23 and 24).

Table 24: Echocardiography measurements in DOCA-salt-treated WT and zyxin-null mice aged approximately 78 weeks (n=8)

Parameter	WT (Mean ± SEM)	Zyxin-null (Mean ± SEM)	p-value
Volume;s	34.6477 ± 2.4228	43.2350 ± 2.9132	p<0.05
Volume;d	79.8211 ± 1.4226	89.7435 ± 2.0482	p<0.01
Stroke Volume	46.9225 ± 1.7424	37.1156 ± 1.6852	p<0.01
Ejection Fraction	66.5266 ± 3.2412	52.6245 ± 2.2468	p<0.01
Fractional Shortening	36.7224 ± 1.4262	27.9812 ± 1.9842	p<0.01
Cardiac Output	24.8224 ± 1.3256	16.7560 ± 2.1556	p<0.01
LV Mass	175.6712 ± 4.6852	156.8842 ± 8.8236	p>0.05
LV Mass Corrected	141.6540 ± 7.1372	128.7742 ± 6.5342	p>0.05

To analyze the cardiac parameters in further detail, isolated working heart measurements were performed using hearts from age-matched DOCA-salt-treated C57BL6J and zyxin-null mice (approximately 52 weeks old). These experiments were performed by Dr. Jan Reil (Klinik für Innere Medizin III, Kardiologie, Angiologie und Internistische Intensivmedizin, Universitätsklinikum des Saarlandes, Germany).The data obtained from these experiments proved inconclusive. While the cardiac systolic elastance was consistently and significantly lower in zyxin-null mice (p<0.001), other parameters were more variable and did not attain statistical significance (Table 25, 26).

Table 25: Cardiac parameters from isolated working heart measurements.

	HR	SV	CO	EF
WT DOCA	414.0 ±7.214	22.9 ±1.5477	9.4 ±0.6846	47.3 ±3.133
Zyxin-null DOCA	410.6 ±9.0307	23.4 ±1.7888	9.6 ±0.7075	44.7 ±3.6748

Table 26: Cardiac contraction and relaxation measured in isolated working hearts.

	dp/dt**	(-) dp/dt**	Vo**	Ees**	K**	β**
WT DOCA	4899.6 ± 322.7962	-3429.4 ± 295.7625	-34.5 ± 7.4257	4.4 ± 0.3183	0.6 ± 0.3991	0.1 ± 0.0142
Zyxin-null DOCA	5077.2 ± 336.1198	-3677.0 ± 169.4853	-8.8 ± 14.3382	2.2 ± 0.3101	1.1 ± 0.4773	0.1 ± 0.0142

** dp/dt and (-) dp/dt are maximum and minimum rate of increase of left-ventricular pressure, Ees and Vo are slope and x-axis intercept of the end-systolic pressure-volume relationship respectively while K and β represent parameters for end-diastolic pressure volume relationship.

In order to find out any existing histological changes in the hearts, paraffin sections from these hearts were analyzed next.

4.3.5 *Consequences of loss of zyxin on cardiac cell survival and ECM remodelling and cardiac mass*

Transverse sections of hearts from DOCA-salt-treated zyxin-null mice showed signs of pronounced fibrosis as detected by Masson's trichrome staining (Figure 37A through C). Serial paraffin sections from approximately the same depth of tissue were used for comparison. The collagen fibres were stained blue and the area of fibrotic tissue was measured as a percentage of the total cross-sectional area using ImageJ. DOCA-salt-treated WT mice showed very little fibrosis consistent with the fact that the DOCA-salt model is not a strong pro-fibrotic model. Cardiac fibrosis and scar tissue deposition is often a consequence of cardiac cell death thereby leading to compromised cardiac function. Therefore, the extent of apoptosis in these hearts was analysed by counting the number of TUNEL-positive nuclei. Indeed, there was significantly higher apoptosis in

the hearts from DOCA-salt treated zyxin-null mice (Figure 38A through C).

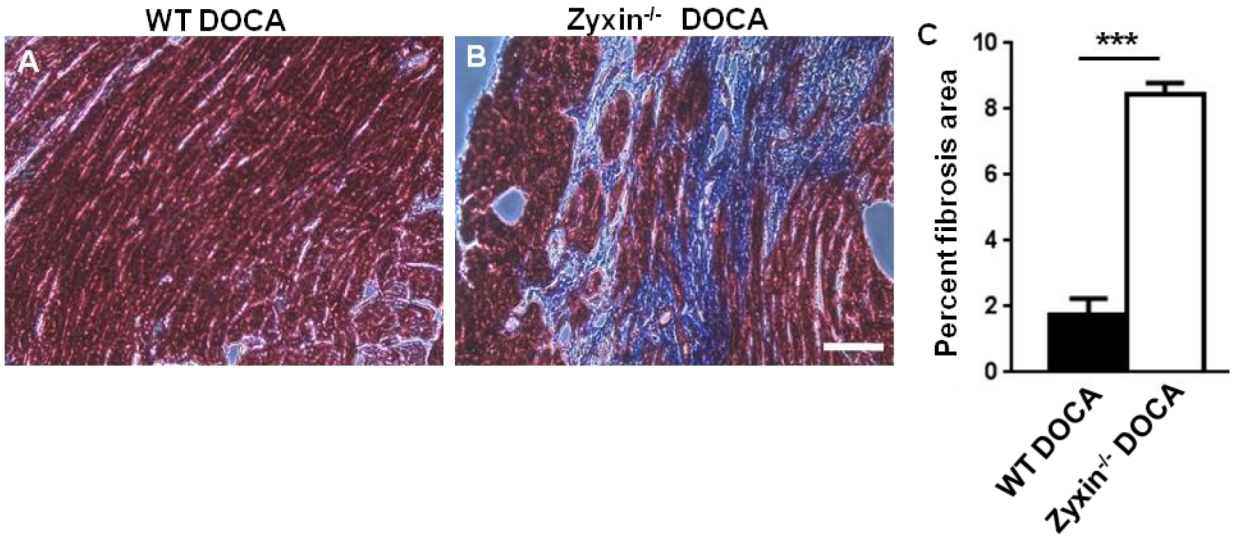

Figure 37: Pronounced interstitial fibrosis in hearts from DOCA-treated zyxin-null mice. Masson's trichrome staining of transverse sections of hearts from WT **(A)** and zyxin-deficient mice **(B)** after 21 days of DOCA-salt treatment. Fibrotic tissue is stained blue. Scale bar represents 50 μm. **C**, Statistical summary of cardiac fibrosis. ImageJ was used to calculate percent fibrosis area of the hearts for comparison, ***p<0.001 and n=6.

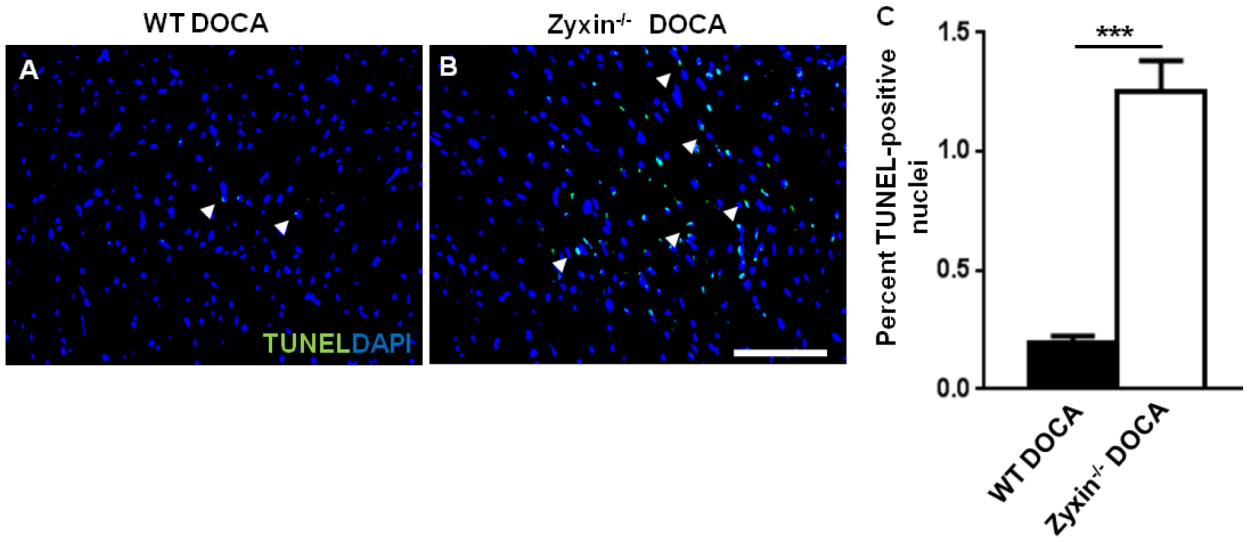

Figure 38: Detection of apoptosis in hearts from DOCA-salt-treated WT and zyxin-null mice. A, B, TUNEL-positive nuclei (green) merged with DAPI-positive nuclei (blue) in hearts from WT and zyxin-null mice, respectively following 21 days of DOCA-salt treatment. Scale bar represents 100 μm. **C**, Statistical summary of percentage of TUNEL-positive apoptotic nuclei, ***p<0.001 as indicated with n=6 in each group.

In order to find out whether the DOCA-salt-treated WT and zyxin-null mice differ in terms of cardiac mass, the ratio of heart weight (HW) to body weight (BW) was determined. However, no significant differences were observed in this context (Figure 39A). Finally, to rule out the effects of an altered kidney function on the blood volume and subsequent cardiac function, serum concentrations of cystatin c were measured using blood drawn from the mice by cardiac puncture 21 days following DOCA-salt treatment. Cystatin c is a sensitive marker of glomerular filtration rate or kidney function with elevated serum concentrations in kidney disease. Cystatin c levels were not significantly different between WT and zyxin-null mice (Figure 39B).

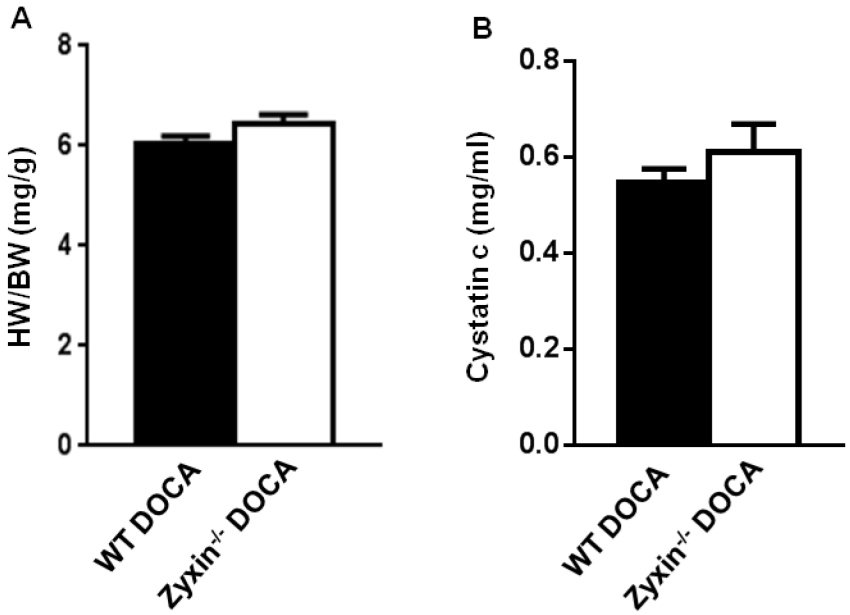

Figure 39: Measurements of cardiac mass and kidney function in DOCA-salt-treated WT and zyxin-null mice. A, Summary of heart weight to body weight ratio as an index of cardiac tissue mass in these mice. Values were not statistically significant, n=8 for each group. **B,** Quantitative analysis of cystatin c concentrations in serum derived from the blood of these mice. Data were not statistically significant, n=8 for each group.

4.3.6 *Pro-fibrotic gene expression in hearts of zyxin-deficient mice*

Molecular changes in the hearts of DOCA-salt-treated zyxin-null mice were examined to better understand the origin of fibrosis in these hearts. A real time quantitative PCR-based profiler array was used to find pro-fibrotic genes that were altered in these hearts.

To track early changes in gene expression, RNA was obtained from the hearts of untreated as well as DOCA-salt-treated WT and zyxin-null mice 10 days following DOCA-salt treatment. There was a significant upregulation of pro-fibrotic genes in hearts from zyxin-null mice as compared to WT mice (printed in bold in table 27).

Table 27: Pro-fibrotic gene expression in hearts from DOCA-salt–treated zyxin-null mice compared to their WT counterparts ($p<0.05$ and $n=3$ for each group).

Gene symbol and name	Fold change ($Zyxin^{-/-}$ DOCA vs WT DOCA)
Col1α2 (Collagen 1 isoform α2)	**3.6**
Col3α1 (Collagen 3 isoform α1)	**6.4**
CTGF (Connective tissue growth factor)	2.1
IL10 (Interleukin 10)	2.1
IL1b (Interleukin-1β)	2.2
Itgb1 (Integrin β_1)	1.9
Itgb8 (Integrin β_8)	2.5
Lox (Lysyl oxidase)	**19.3**
MMP2 (Matrix metalloproteinase 2)	1.7
MMP3 (Matrix metalloproteinase 3)	2.3
MMP9 (Matrix metalloproteinase 9)	1.5
Smad2	1.7
Ccl12 (Chemokine ligand 12)	1.9
Tgfbr1 (TGF- β receptor isoform 1)	**3.5**

Integrin expression and activation regulates the activity of focal adhesion kinase (FAK), a protein that has an important role in organ fibrosis (Lagares et al. 2012, Thannickal et al. 2003, Balasubramanian et al. 2012). Therefore, protein lysates from hearts of DOCA-salt treated zyxin-null mice (21 days of treatment) were analysed for expression of integrins and activation of FAK. Western blotting revealed an over-expression of integrin isoforms namely integrin α_5 and integrin β_1 in hearts from zyxin-null mice along with activation of FAK indicated by its increased phosphorylation (Figure 40A, B). Activation of Akt (also known as protein kinase B) which is an important mediator of cell apoptosis was similar in WT and zyxin-null mice (Figure 40A, B).

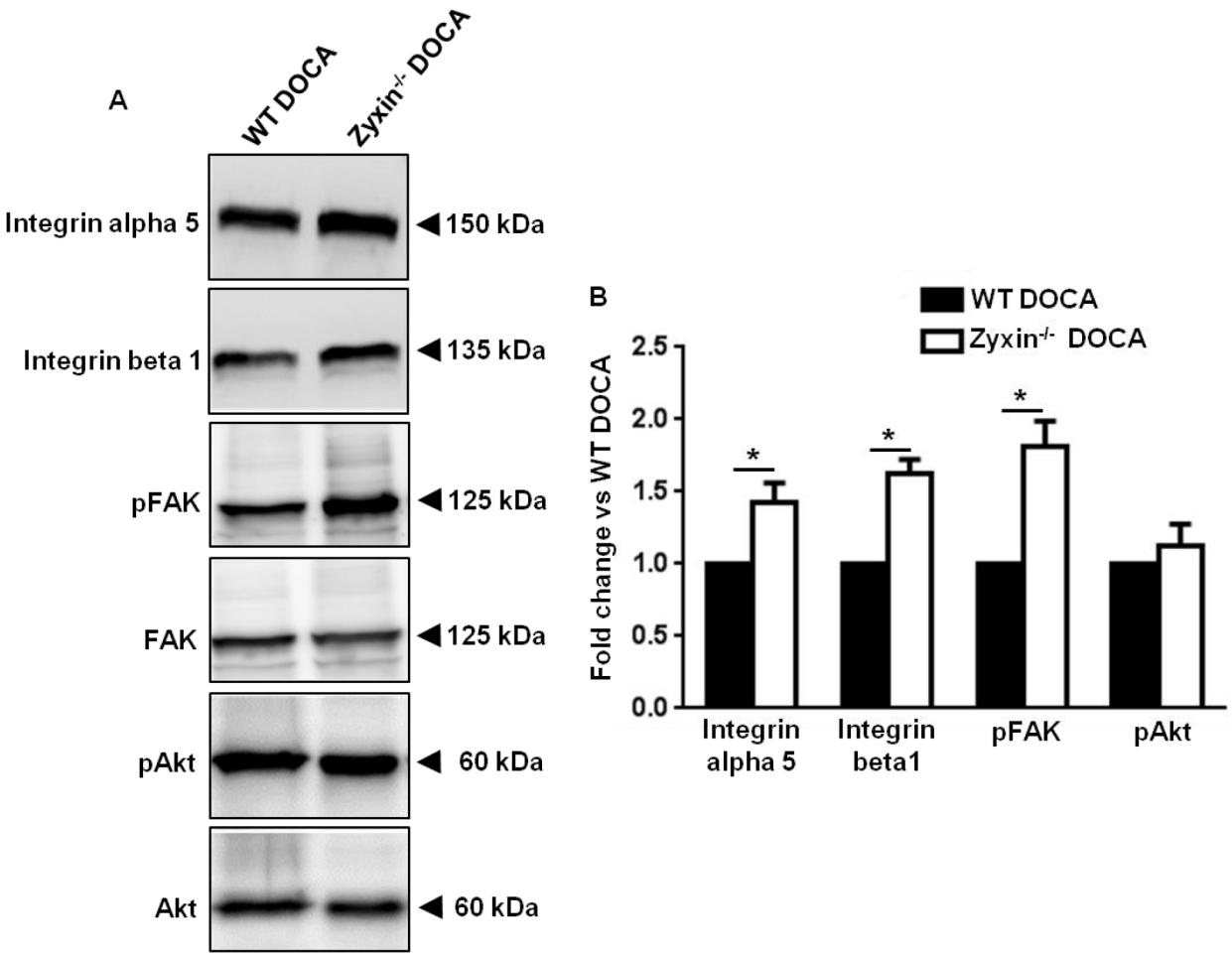

Figure 40: Over-expression and activation of integrins in fibrotic hearts from DOCA-salt-treated zyxin-null mice. A, Representative Western blots of cardiac tissue lysates from DOCA-salt-treated WT and zyxin-null mice. **B,** Statistical summary of protein expression in these hearts, *p<0.05 as indicated, n=6-8 for each group.

4.3.7 *Zyxin is dispensable for response of isolated neonatal cardiomyocytes in culture to pro-hypertrophic stimuli*

Cardiac dysfunction in zyxin-null mice upon volume overload-induced hypertension might have three sources of origin i) a dysfunction of cardiomyocytes due to exposure to increased cardiac load, ii) a pro-fibrotic response of either the cardiomyocytes or the cardiac fibroblasts or iii) a combined effect of cardiomyocyte dysfunction and a shift to a pro-fibrotic environment. To dissect the contribution of individual cell types, cardiomyocytes were isolated from neonatal hearts, serum-starved and exposed to pro-hypertrophic stimuli such as endothelin 1 (ET-1; 100 nM) for 24 hours. Expression of pro-hypertrophic genes like atrial natriuretic peptide (ANP) and B-type natriuretic peptide (BNP) were measured by real time quantitative PCR. No significant differences in expression of ANP and BNP were observed in neonatal cardiomyocytes from WT and zyxin-null mice (Figure 41).

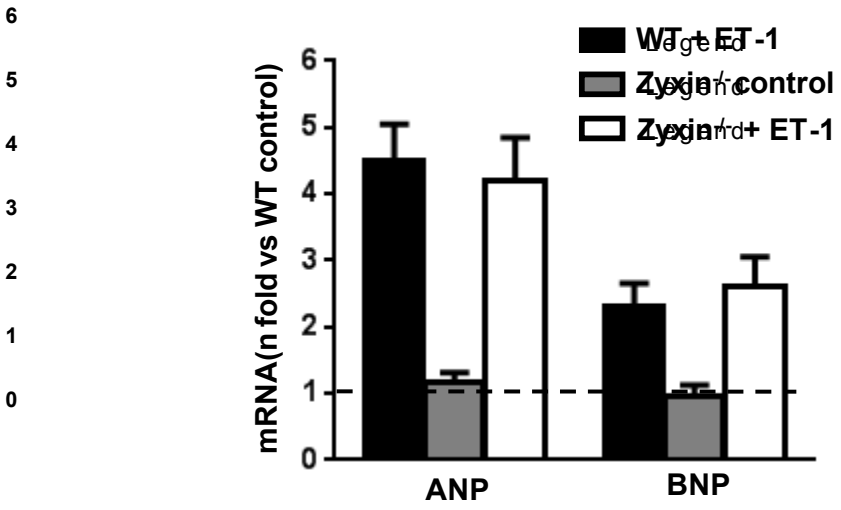

Figure 41: Expression of ANP and BNP in neonatal cardiomyocytes from WT and zyxin-null mice. Following serum starvation for 24 hours, neonatal cardiomyocytes from WT and zyxin-null mice were treated with ET-1 (100 nM) for 24 hours. Values were not significantly different between the treated groups. All groups are compared to WT control with a reference value of 1. ANP and BNP expression was not significantly different under untreated control conditions between WT and zyxin-null cardiomyocytes, n=3 for each group.

Zyxin-null mice have problems with breeding and availability of sufficient number of neonates for cardiomyocyte isolation was a major problem. Therefore, experiments involving measurements of protein expression or cell size measurements could not be done in parallel.

4.3.8 *Viability of zyxin-null cardiomyocytes in culture*

Zyxin-null mice displayed increased cardiac apoptosis after 21 days of DOCA-salt treatment (Figure 38). As such, the viability of cardiomyocytes from these mice was analysed to assess their possible contribution to the cardiac phenotype. Following 24 hours of serum starvation, neonatal cardiomyocytes from WT and zyxin-null mice were fixed and stained for alpha-actinin, a marker of cardiomyocytes. Zyxin-null mice consistently displayed loss of viability as depicted by alpha-actinin-positive cell debris as compared to characteristic z-line staining in WT cardiomyocytes (Figure 42A through C).

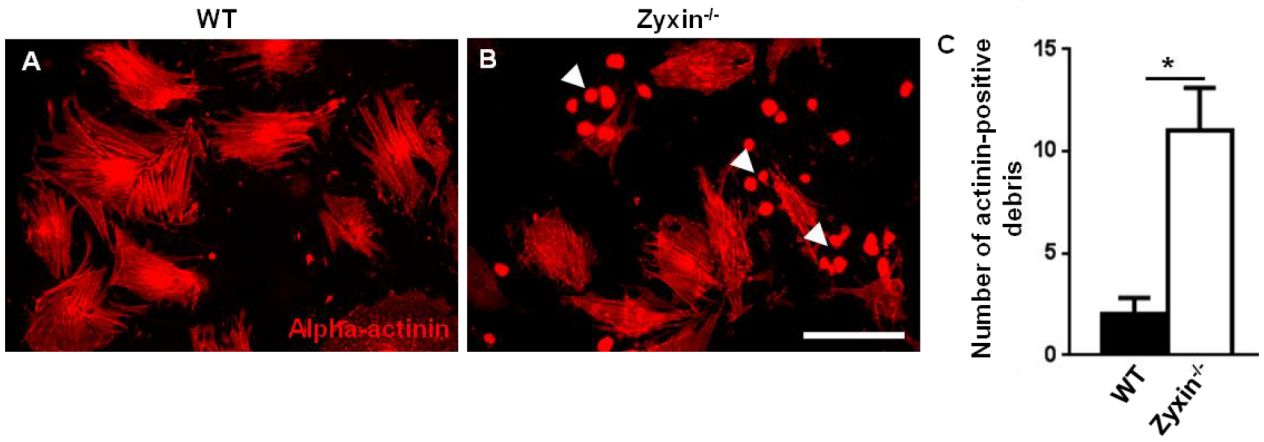

Figure 42: Cell viability of neonatal cardiomyocytes in culture. A, B, WT and zyxin-null neonatal cardiomyocytes fixed and stained with alpha-actinin (red) following serum starvation for 24 hours. Equal number of both WT and zyxin-null cardiomyocytes isolated during the same day were seeded on laminin-coated cover slips. Scale bar represents 100 µm. **C**, Statistical summary of actinin-positive cell clumps or debris per field of view indicative of loss of viability of cardiomyocytes. Alpha-actinin is a marker of cardiomyocytes and loss of its characteristic z-line staining is indicative for loss of cardiomyocyte integrity and viability, *$p<0.05$ as indicated and $n=3$ for each group.

4.3.9 *Pro-fibrotic gene expression in zyxin-null cardiac fibroblasts*

In order to identify the cell type responsible for the prominent cardiac fibrosis observed in DOCA-salt-treated zyxin-null mice, cardiomyocytes and cardiac fibroblasts isolated from neonatal WT and zyxin-null mice were stimulated with recombinant TGF-β_1 (10 ng/ml) for 24 hours following serum starvation overnight. TGF-β_1 induced an upregulation of pro-fibrotic CTGF and Itgb1 gene expression. These genes were upregulated in both WT and zyxin-null fibroblasts albeit much stronger in zyxin-null cardiac fibroblasts (Figure 43). On the contrary, CTGF expression but not Itgb1 expression was upregulated to the same extent in both WT and zyxin-null cardiomyocytes (Figure 44).

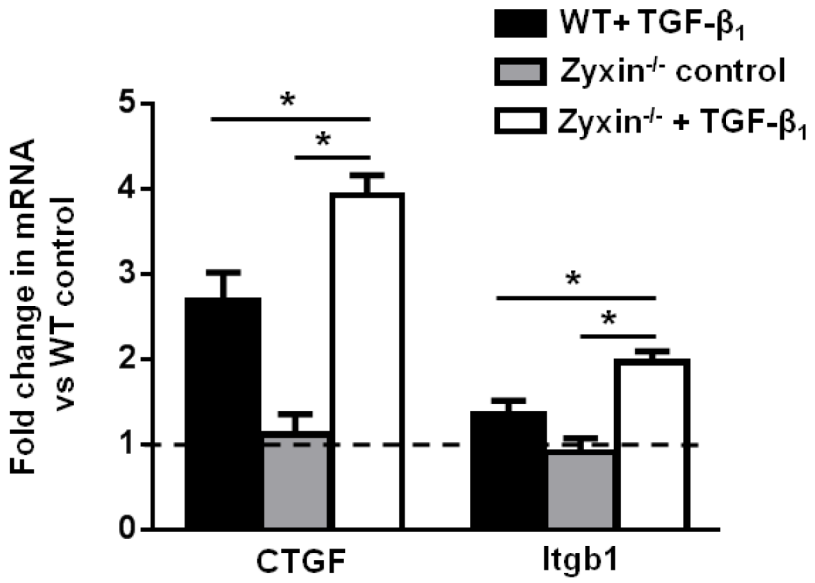

Figure 43: Pro-fibrotic gene expression in WT and zyxin-null fibroblasts. Cardiac fibroblasts from neonatal WT and zyxin-null mice were stimulated with mouse recombinant TGF-β_1 (10 ng/ml) for 24 hours. The cells were serum starved for 24 hours prior to stimulation with TGF- β_1. CTGF and Itgb1 gene expression were measured by real time PCR. Values were not significantly different between control (untreated) WT and zyxin-null cardiac fibroblasts as indicated by the fold change in gene expression in zyxin$^{-/-}$ control fibroblasts compared to WT control. The WT control was defined as a reference value of 1. *$p<0.05$ as indicated, n=3 for each group.

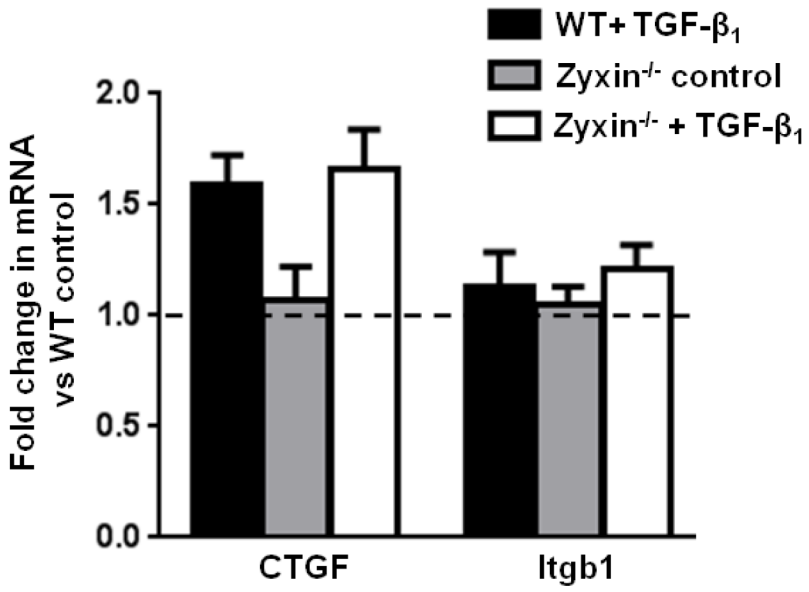

Figure 44: Pro-fibrotic gene expression in WT and zyxin-null cardiomyocytes. Cardiomyocytes isolated from neonatal WT and zyxin-null mice were stimulated with mouse recombinant TGF-β_1 (10 ng/ml) for 24 hours. CTGF and Itgb1 gene expression were measured by real time PCR. Values were not significantly different between WT and zyxin-null cardiomyocytes both under control and stimulated conditions. The WT control was defined as a reference value of 1, n=3 for each group.

5 DISCUSSION

Mechanical forces are crucial for a variety of important processes ranging from embryonic development to physiological functioning of the adult organism. Defects in this force sensing lead to various diseases such as hypertension, atherosclerosis, muscle dystrophy and cancer. However, current understanding of cellular mechanotransduction has not fully developed in comparison to biochemical signalling by growth factors and hormones. In the present study, efforts have been made to better understand one of the facets of cellular mechanotransduction, namely a component of the focal adhesions known as zyxin. Despite the existence of substantial evidence (Rauskolb et al. 201, Smith et al. 2010,Suresh Babu et al. 2012) pointing to its role as a pivotal component of the cellular response to biomechanical forces, there is lack of definitive proof based on animal studies. Using a combination of *in vitro* and *in vivo* tools, this work delineates for the first time, the consequences of the loss of zyxin in an animal model of pathophysiological stress, namely hypertension. The data support a bi-directional model of force-induced phenotype regulation. Thus, loss of zyxin disrupts an outside-in signalling affecting stretch-induced gene expression in vascular SMCs. Concurrently, absence of zyxin from focal adhesions promotes remodelling of the surrounding ECM (inside-out signalling). Additionally, this work clarifies some of the upstream mechanisms underlying force-induced activation of zyxin which is mediated in part by TRPC3 channels.

5.1 Mechanosensing by TRPC3 leading to zyxin activation in vascular cells

The role of TRPC3 in zyxin activation was originally elucidated using femoral arteries and vascular SMCs isolated from mice lacking a single or several different TRPC channels (Suresh Babu et al. 2012). In the present work, this concept was further confirmed using a combination of pharmacological tools and intracellular calcium measurements in an endothelial cell model (primary HUVECs). The DAG analogue, OAG, is a potent activator of TRPC channels, namely TRPC3, 6 and 7 (Hofmann et al. 1999). Activation of TRPC3 is specifically blocked by Pyr3 (Kiyonaka et al. 2009). The absolute inhibition of OAG-induced calcium transients by Pyr3 in the HUVECs (Figure 7) indicates that TRPC3 is the predominant OAG-sensitive TRPC channel in these cells.

Before testing the stretch-induced activation of TRPC3, functional activation of these channels in this cell culture model was confirmed. TRPC3 is negatively regulated in a PKC-dependent manner (Trebak et al. 2005). Thus, OAG-mediated induction of PKC might lead to a negative feedback loop inhibiting TRPC3 channel opening. Accordingly, a PKC inhibitor potentiated OAG-mediated TRPC3 activation and prolonged duration of the resultant calcium entry. The OAG-induced nuclear translocation of zyxin and subsequent up regulation of IL-8 gene expression confirmed TRPC3-mediated zyxin activation in the cultured ECs. Moreover, TRPC3 channel activation in this context was found to be independent of calcium release from intracellular stores but depended on and was associated with extracellular calcium entry into the cell. Nonetheless, stretch-induced activation of zyxinviaTRPC3 appears to be more complex.

The prospect of direct mechanosensing by TRPC channels is controversial. A direct activation of recombinant TRPC6 channels by stretch in isolated membrane patches (Spassova et al. 2006) has been reported. However, the threshold pressure level for such activation was even higher than that required for mechanosensitive ion channel activation in *Escherichia coli*. On the other hand, there is considerable data regarding the indirect activation of these ion channels. TRPC channels are activated following activation of PLC (Clapham et al. 2003) possibly through direct activation by DAG (Hofmann et al. 1999). Isolated cerebral arteries show increased expression of PLC and DAG under pressure (Osol et al. 1993).More recently, GPCRs have been reported to play a role in the activation of TRPC channels by stretch thereby offering an interesting mechanism upstream of TRPC channels for mechanosensing. Consistent with this mechanism, $G_{q/11}$-coupled GPCRs have been linked to myogenic vasoconstriction (Mederos y Schnitzler et al. 2008). In cardiomyocytes, ligand-independent activation of the AT_1 receptor (a GPCR) by mechanical stress has been reported (Zou et al. 2004). Thus, GPCRs can sense mechanical stress and signal via TRPC channels like TRPC6 leading to the entry of extracellular cations. This concept is complicated by reports of physical coupling of TRPC3 channels to IP_3 receptors in vascular SMCs (Adebiyi et al. 2011). Stretch-activated cation channels of unknown identity also apparently trigger the entry of ions. These channels are sensitive to the non-selective cation channel blocker gadolinium (Caldwell et al. 1998) and a peptide toxin from spider venom (Suchyna et al.

2000). The presence of a different set of these channels and their direct or indirect mechanism of activation indicate that the kinetics of mechanosensing is complex.

Data presented in this work reflect the biphasic kinetics of stretch-induced calcium transients in HUVECs. While the early peak response to stretch seems to be mediated by stretch-activated cation channels, the late or delayed response might be mediated by the TRPC channels, in this case TRPC3 in combination with PLCβ_1 activation via GPCRs (Figure 45).

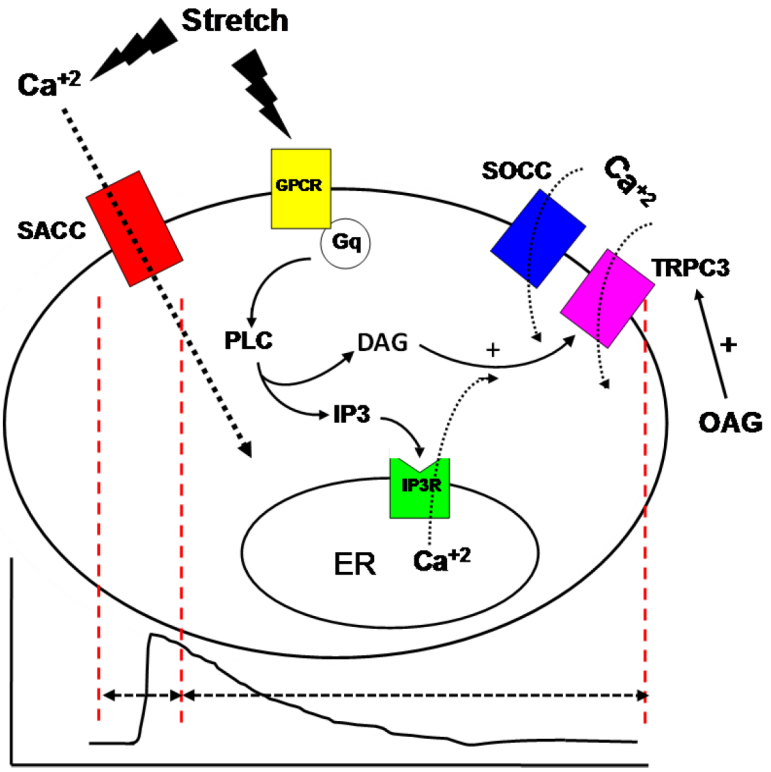

Figure 45: Hypothetical diagram of stretch-induced calcium transients in ECs.

While previous work with generic PLC inhibitors have failed to identify isoform-specific contribution of PLC, this study using siRNAs targeting selective PLC isoforms provides evidence of a role of PLCβ_1 but not β_3 or γ_1 in the endothelial cell response to stretch. Interestingly, inhibition of both PLCβ_1 and TRPC3 affect the slope of the delayed phase II of the calcium transient without any effect on the peak increase in calcium upon stretch. The inhibition of zyxin activation by the TRPC3 inhibitor Pyr3 clearly indicates that this process is independent of global calcium levels in the cell. Rather, it might be

explained by the spatial distribution of calcium ions most likely in the vicinity of the focal adhesion complex which influences the nuclear translocation of zyxin upon stretch. Thus, it is tempting to speculate that GPCRs and/or TRPC3 channels located close to these focal adhesion-ECM junctions might specifically regulate zyxin-mediated mechanotransduction. It is noteworthy that inhibition of the putative mechanosensitive $G_{q/11}$-coupled AT_1 receptor in the HUVECs by losartan had no effect on stretch-induced calcium transients. Thus, it is clear that vascular SMCs and ECs have a different set of mechanoreceptors and their relative sensitivity to stretch might be very different. While we failed to identify the real mechanosensor mediating zyxin activation, this work places the TRPC3 channel and PLC upstream of zyxin activation. Furthermore, by defining their phase-oriented activity in stretch and thereby zyxin activation, the present study explains why the process of zyxin activation itself is biphasic and complex, most likely depending on a spatial rather than global stimulus.

5.2 Zyxin-mediated gene expression and the resulting phenotype of SMCs

5.2.1 An *in vitro* model to mimic wall tension in cultured SMCs

According to Laplace's law, wall tension in a blood vessel is dependent on the transmural pressure, the radius of the vessel and the wall thickness. As it is difficult to expose cultured SMCs to a transmural pressure gradient, an easier, reproducible way of mimicking wall tension *in vitro* is to increase its radial component. This is accomplished by stretching vascular SMCs in a Flexercell unit. This is a well-established model (Cattaruzza et al. 2004,Demicheva et al. 2008, Wójtowicz et al. 2010, Arnold et al. 2014) and shows good correlation with *in situ* or *in vivo* models. However, cyclic stretch generated in this model is not a reflection of the pulsatile nature of blood flow in the body. This is used in order to prevent cultured cells from evading the stretch stimulus by their positional realignment. Accordingly, gene expression in cultured SMCs as well as their phenotypic characterization upon stretch was based upon this *in vitro* model of cyclic stretch.

5.2.2 Zyxin activation in endothelial cells versus SMCs

The translocation of zyxin to the nucleus in vascular SMCs follows a different threshold and kinetics as in ECs. While a 10% cyclic elongation is sufficient for this response in ECs, a much stronger intensity (15-18% cyclic elongation) is required in vascular SMCs for a similar response. Likewise, in experiments with isolated femoral arteries from mice, a much higher perfusion pressure (a gradient of 200 to 120 mmHg) is required for zyxin translocation to the nucleus in native SMCs compared to a pressure gradient of 150 to 90 mmHg in native ECs (Suresh Babu et al. 2012). The time course of this process also differs significantly between ECs and SMCs. As such, experiments with cultured SMCs were done predominantly using a slightly different stretch regimen compared to that previously used for ECs. Additionally, the time and intensity of stretch was optimized for each individual functional assay to suit their respective kinetics (e.g. high intensity and longer duration to induce apoptosis, short duration for measuring stretch-induced RhoA activation and nuclear translocation of MRTF-A).

5.2.3 Zyxin-regulated transcriptome in vascular SMCs

Previously, the influence of zyxin on stretch-induced gene expression in ECs has been reported (Wójtowicz et al. 2010). This report made use of a transient knock down of zyxin using target-specific siRNA to compare stretch-induced gene expression in ECs in the presence or relative absence of zyxin. In the present study, a more convenient method of comparison was used owing to the availability of vascular SMCs from WT and zyxin-null mice. This study reflects the consequences of a permanent loss of zyxin in SMCs thereby offering more robust results. Accordingly, using cDNA microarray analysis, 90% of stretch-sensitive genes were found to be zyxin-dependent in the mouse aortic SMCs compared to 68% reported in human ECs. Candidate genes from this microarray were validated by real time qPCR. More importantly, the differentially expressed gene products could be classified into a number of distinct pathways using gene set enrichment analysis (GSEA) together with Gene Ontology (GO) and Kyoto Encyclopedia of Genes and Genomes (KEGG). Important pathways such as proliferation, differentiation, migration, apoptosis and contractility of SMCs were found to be regulated by zyxin.

Whereas for endothelial cell genes, zyxin was shown to bind to a specific pyrimidine-purine (PyPu) rich sequence in their promoter regions and regulate stretch-dependent transcription of these genes, such a distinct binding domain is not prominent in the promoter regions of its target genes in vascular SMCs. *In silico* analysis of promoter regions of some candidate genes such as calponin, cyclin D1, cyclic E2, FasR for a consensus PyPu binding sequence did not yield any substantial zyxin-binding regions (Analyses were done by PD Dr. Andreas Wagner, Institute of Physiology and Pathophysiology). This together with the high threshold underlying zyxin translocation to the nucleus in vascular SMCs points to an altered mechanism of regulating gene expression in SMCs. At this point, there are two possibilities: a) Zyxin binds to an as yet unknown transcription factor in the nucleus of vascular SMCs driving gene expression; or b) the effect of zyxin on stretch-induced gene expression in vascular SMCs is mediated through the cytoskeleton. The latter option is not unprecedented. For example, changes in actin polymerization can control the nuclear localization of the myocardin-related transcription factor-A (MRTF-A) which is an important transcription factor driving SRF-mediated gene expression in vascular SMCs (Miralles et al. 2003). This interesting hypothesis will be further elaborated upon in the following section describing the phenotype of zyxin-null SMCs.

5.2.4 Loss of zyxin promotes a synthetic phenotype of vascular SMCs

Functional assays designed on the basis of zyxin-dependent stretch-induced pathways in vascular SMCs revealed a pro-migratory, growth promoting, poorly contractile phenotype of zyxin-null SMCs which were resistant to Fas ligand-induced apoptosis. The increased expression of cyclin E2 and MMP13 in zyxin-null SMCs is in line with the higher rate of proliferation in these cells. The consolidation of the difference in proliferation between WT and zyxin-null SMCs upon stretch might be due to an increased apoptosis of stretched WT SMCs. Zyxin-null SMCs appear to be primed for migration. There are conflicting reports in the literature about the role of zyxin in cell migration (Choi et al. 2013, Mise et al. 2012). This could be due to a cell-type specific role of zyxin in migration or the method used to induce zyxin knock down. While some studies using a siRNA approach to target zyxin have reported a positive effect of zyxin

on cell migration, a study by Hoffman *et al*. (Hoffman et al. 2006) and the present work both based on cells from the same zyxin-null mice reveal a negative regulation of migration by zyxin. There are also conflicting reports on the role of zyxin in apoptosis. Thus, zyxin has been reported to promote apoptosis (Hervy et al. 2010) as well as protecting cells against it (Kato et al. 2005). This predominantly appears to be a concentration-dependent effect whereby the net effect of zyxin depends on the strength of the stimulus used to induce apoptosis. In this context, zyxin protects cardiomyocytes from ANP-induced apoptosis within a narrow concentration range of ANP beyond which the protective effect is lost (Kato et al. 2005).

The contractile deficit in zyxin-null SMCs might be due to defects in actin cytoskeletal assembly. This deficit is further accentuated in the presence of vasoconstrictor agonists which might be a consequence of increased RGS5 expression in these cells. Notably, RGS5 is known to inhibit the contraction of SMCs by its inhibitory effect on $G_{q/11}$-mediated GPCR signalling (Arnold et al. 2014). The reduced expression of GPCRs such as α_1-adrenergic receptor and the endothelin A receptor (ET_A-R) in isolated femoral arteries from zyxin-null mice (doctoral dissertation of Agnieszka Wójtowicz) might be another reason for the same.

Zyxin is known to be involved in the assembly of actin stress fibres by interaction with α-actinin and Mena/VASP (Drees et al. 2000, Crawford et al. 1992). It is also critically important in mechanical stretch-induced stress fibre maintenance and repair (Smith et al. 2010). Most of these studies were done in mouse embryonic fibroblasts. Zyxin-null SMCs differ in some aspects. Interestingly, vascular SMCs under static conditions display a higher intensity of F-actin-specific phalloidin staining along the edges of the cells as compared to WT SMCs. Upon stretch, WT SMCs show a robust assembly of stress fibres which are oriented in a parallel, organized manner. However, zyxin-null cells show intense build-up of F-actin along the cell edges or as localized, condensed actin deposits. Apparently, in the absence of zyxin, vascular SMCs try to build stress fibres but fail to do so, instead resulting in accumulation of condensed actin likely resulting from stress fibre breakdown.

The subtle differences between the present study and that of Hoffman *et al*. (Hoffman et al. 2012)might be due to the differences in cell type. In the present work, we have used vascular SMCs from adult mice which might have had more time for build-up of dynamic stress fibres as compared to embryonic fibroblasts. Composition of stress fibres might also differ between these cell types as they depend on the inherent motility of cells (Pellegrin et al. 2007).

The high intensity of F-actin in zyxin-null cells led to the investigation of RhoA, a member of the Rho family of GTPases and its activation in zyxin-null SMCs. Interestingly, there was a stronger activation of RhoA already in static zyxin-null SMCs which was further consolidated by stretch. Since RhoA is associated with contractility (Wang et al. 2009,Chrzanowska-Wodnicka et al. 1996), the increase in RhoA activity in poorly contractile SMCs seems counterintuitive. However, in the absence of robust, well organized stress fibres, zyxin-null SMCs seemed unable to generate sufficient traction forces for contraction despite a high level of RhoA activity. These cells also have a pro-migratory phenotype despite the high RhoA activity. This is also not unprecedented. There is evidence that RhoA regulates membrane protrusion and cell migration(Ai et al. 2001),with high RhoA activity localized to cell protrusions and retracting tails of randomly migrating cells (Pertz et al. 2006). Our observation of strong F-actin staining along the boundaries of the zyxin-deficient SMCs might reflect this increased RhoA activity at sites promoting cell migration. In fact, RhoA-driven traction helps the cell to move forward following protrusion at the leading edge. Moreover, there are reports of RhoA supporting migration of vascular SMCs (B. Liu et al. 2002) and of Rho signalling being involved in vascular SMC proliferation, migration and in vascular remodelling processes such as neointima formation and arteriogenesis (Matsumoto et al. 2004, Arnold et al. 2014).

Rho GTPases determine the activity of important transcription factors MRTF-A and B in vascular SMCs by regulation of actin polymerization (Olson et al. 2010). These transcription factors can promote gene expression in vascular SMCs by interacting with SRF. Interestingly, expression of zyxin itself and several other focal adhesion proteins is regulated by SRF (Schratt et al. 2002). In zyxin-null SMCs, MRTF-A was found to be

strongly enriched in the nucleus already under static conditions and further accentuated by stretch. Although there is considerable evidence supporting the role of MRTF-A in maintaining a differentiated state of vascular SMCs (Parmacek et al. 2007), recent evidence suggests that MRTF-A drives an activated and synthetic SMC phenotype under conditions of reduced myocardin activity and promotes migration and proliferation of these cells (Minami et al. 2012). This is particularly true in various pathophysiological conditions where myocardin is down regulated. For example, myocardin is exported out of the nucleus of stretched SMCs under hypertensive conditions and thereby degraded (Pfisterer et al. 2012). On the contrary, the present work shows that MRTF-A accumulates in the nucleus of vascular SMCs following cyclic stretch.

Thus, loss of zyxin promotes a synthetic and activated state of vascular SMCs owing to the nuclear accumulation of MRTF-A. Constitutive MRTF-A activity in some cancer cell lines such as mDA-MB-231 breast carcinoma and B16F2 melanoma cells promotes their motility and invasiveness (Medjkane et al. 2009). In the same context, low levels of zyxin have been reported in some forms of cancer (Wu et al. 2011, Mise et al. 2012). Thus, it is likely that a reduced level of zyxin drives a migratory and proliferative phenotype by activation of RhoA-MRTF-A signalling. MRTF-A also seems to partly regulate zyxin-dependent gene expression since the expression of some of the zyxin-dependent genes could be reversed upon knock down of MRTF-A. Taken together, these data provide an interesting account of gene regulation by a mechanotransducer through modulation of the actin cytoskeleton. Zyxin thus seems to participate in outside-in signalling thereby affecting gene expression and hence the phenotype of vascular SMCs.

5.3 Vascular phenotype in zyxin-null mice: Role of zyxin in arterial remodelling

Zyxin is involved in stretch-induced gene expression in both ECs and SMCs. It also plays a pivotal role in determining the phenotype of SMCs *in vitro.* Considering these data, the lack of an overt cardiovascular phenotype in adult zyxin-null mice was surprising. However, some facts need to be considered in this context. We assume that one reason for the apparent lack of a (cardio)vascular phenotype in adult zyxin-deficient mice is functional redundancy of the closely related zyxin family members LPP and

TRIP6. Interestingly, LPP-deficient mice also do not seem to have a distinct phenotype apart from some embryonic lethality affecting the female offspring. TRIP6-deficient mice are not available at the moment. Our assumption of a compensatory mechanism is further strengthened by the more severe phenotype in flies and zebrafish lacking zyxin and LPP, respectively (Renfranz et al. 2010, Vervenne et al. 2008). In drosophila, zyxin is required for viability whereas LPP is important during gastrulation in zebrafish. Furthermore, in Caenorhabditis elegans, a zyxin orthologue is involved in dystrophin-dependent muscle degeneration (Lecroisey et al. 2013). Thus, in simpler organisms, the loss of such focal adhesion proteins has detrimental effects on vital functions. This effect seems to be lost with evolution with multiple redundant family members likely replacing a deleted gene product.

The zyxin-null mice used in this study are global knock-outs. The knock-out mice were generated in the laboratory of Prof. Mary Beckerle, Utah, USA (Hoffman et al. 2003). A neomycin resistance cassette was used to replace a 4.5-kb genomic region encompassing the translation initiation codon. This deletion removes a 5′-noncoding exon and the first four exons encoding zyxin (Figure 46).

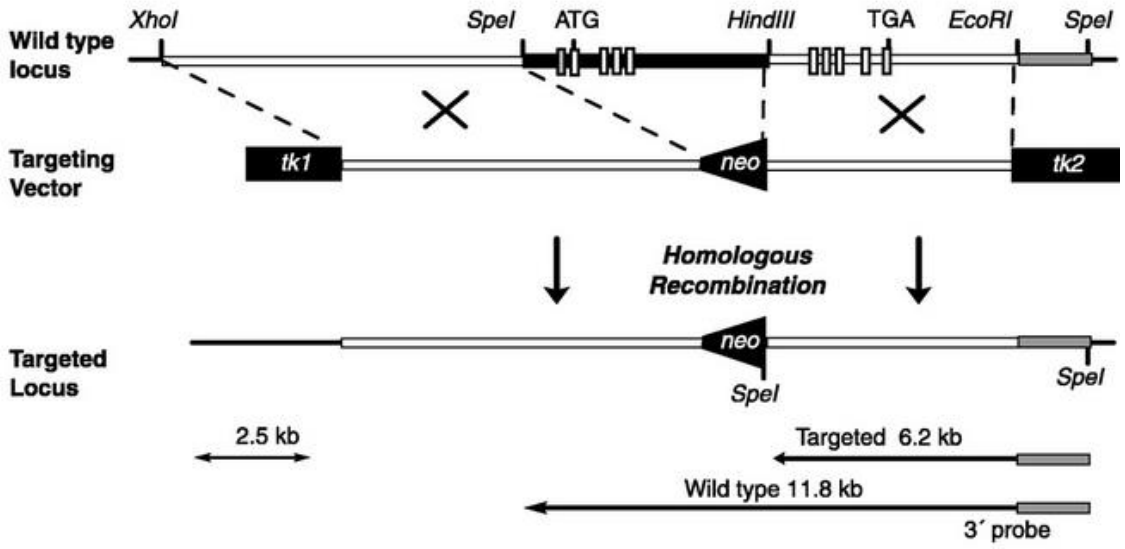

Figure 46: Generation of the construct for disruption of the murine zyxin gene (From Hoffman et al. 2003).

Although a global knock-out has some drawbacks due to loss of function in the whole organism, important information can still be derived from such mice using pathophysiological disease models. No overt phenotypes have been reported in previous studies using these mice. However, there are no published reports of studies using zyxin-null mice in combination with pathophysiological disease models. Furthermore, a detailed analysis of the cardiovascular system in these mice at different time points also has not been done before.

Interestingly, the changes in arterial structure in zyxin-null animals start appearing in mice aged approximately 52 weeks. In very old mice aged 78 weeks, the effect of loss of zyxin is well-defined with increased proliferation of medial SMCs and weakening of the ECM network with reduced cross-linking of collagen I fibres. The functional consequences of this weakened arterial wall are manifested as a decrease in active constriction and a failure to develop a robust increase in diastolic blood pressure upon DOCA-salt treatment. The consolidation of the vascular phenotype with age is reminiscent of the loss of arterial constriction in isolated femoral arteries from zyxin-null mice with increasing age (Figure 47). In line with the above observations regarding the age-dependent structural changes observed in the femoral arteries from zyxin-null mice, the response of isolated femoral arteries from these mice showed a diminished response to vasoconstrictors. Mounting of femoral arteries from older zyxin-null mice on the glass capillaries was also more challenging compared to WT mice due to higher fragility of these arteries. The normal vasodilation response to acetylcholine indicates the proper preparation of the femoral arteries with an intact endothelial cell layer. There were no significant differences in the agonist-induced constriction of femoral arteries from 3-6 month old zyxin-null mice (Figure 47). The deficit in constriction progressed with age and was subtle albeit insignificant in femoral arteries from 9 month old zyxin-null mice. These *in situ* observations thus support the observations made in this study regarding the age-dependent vascular phenotype observed in the very old zyxin-null mice.

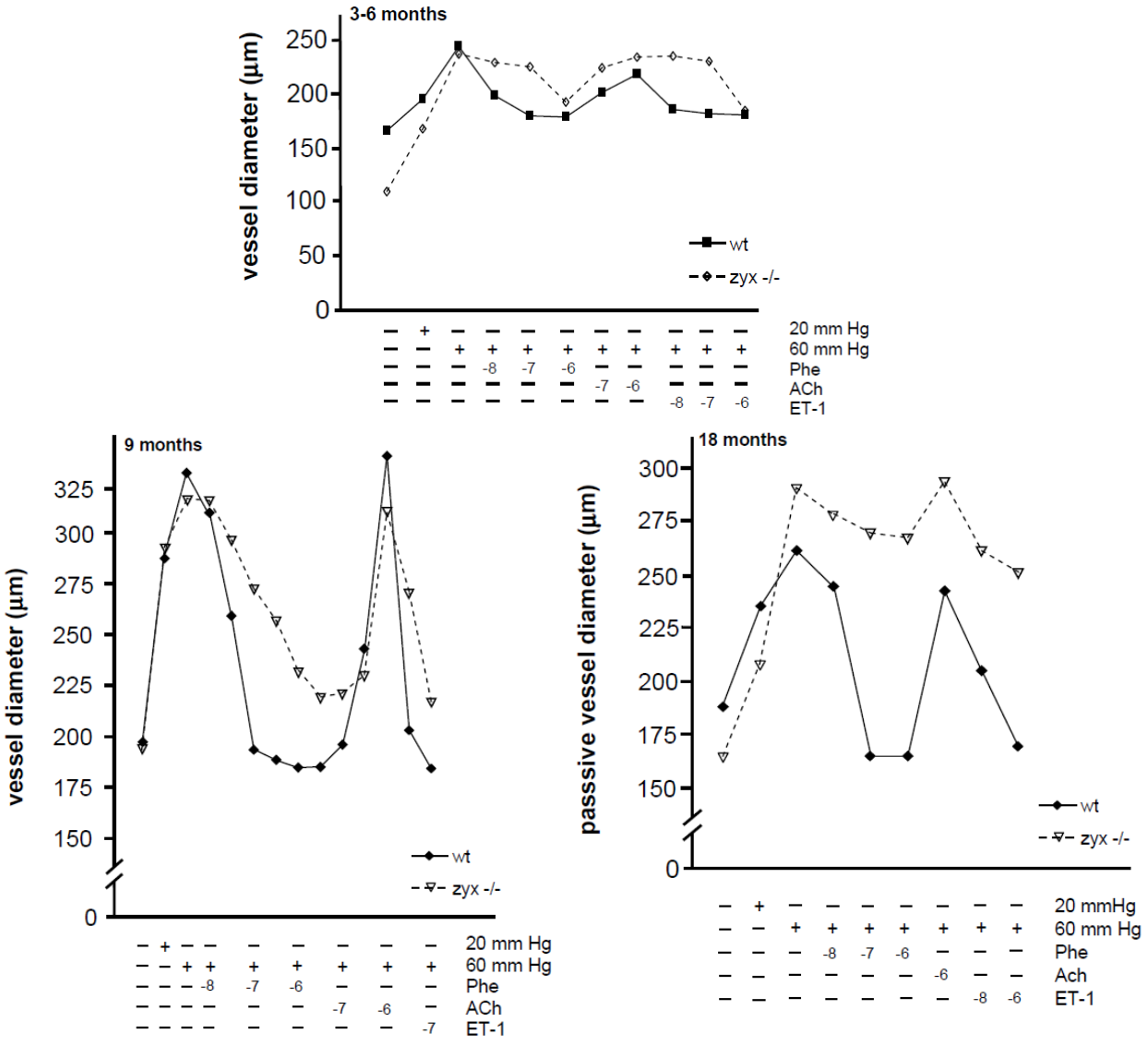

Figure 47: Loss of vasoconstriction response of isolated femoral arteries from zyxin-null mice with progressive age. Phenylephrine (Phe) and endothelin 1 (ET-1) were used to induce vasoconstriction while acetylcholine was used as a control for vessel integrity and responsiveness to vasodilatation (from doctoral dissertation of Agnieszka Wójtowicz, Heidelberg 2008).

The appearance of a distinct vascular phenotype only in older zyxin-null animals can be interpreted in two different ways: a) A compensation by other gene products of the zyxin family, e.g. LPP in younger mice. With increasing age, this compensation might be lost by a decline in expression of such redundant molecules and/or the inadequacy of such compensation in advanced stages of the phenotype in older animals. b) The other

possibility is that zyxin is indeed dispensable in younger mice. In older animals, a progressive stiffening of the arterial wall due to deposition of collagen would be sensed by normal SMCs leading to adaptive changes in their phenotype. However, in the absence of zyxin at the focal adhesions, the medial SMCs embedded in this stiff ECM fail to sense the mechanical forces identifying it as 'soft'. Thus, the SMCs respond to this virtual 'soft' matrix by a degradation of the ECM or changes in its cross-linking (Figure 48). This sequence of events ultimately leads to a weaker arterial wall with a defective constrictor response.

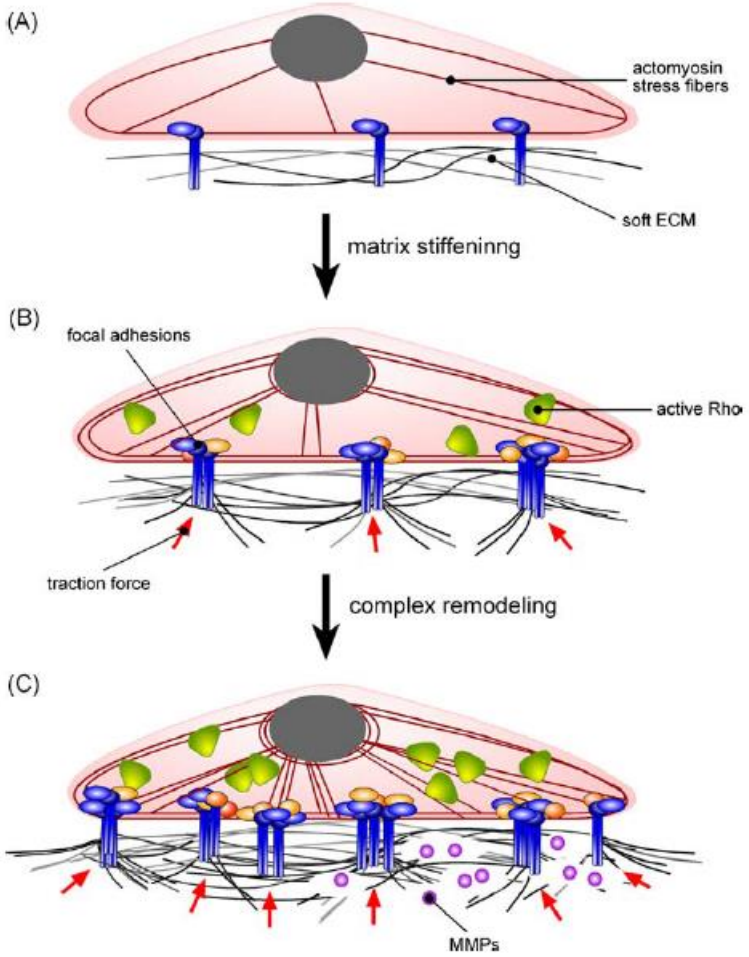

Figure 48: Bi-directional remodelling involving cell-ECM interactions induced by substrate stiffness (Adapted from Gjorevski et al. 2009). While proper force sensing from the surrounding matrix leads to a positive reinforcement of the cytoskeleton, a defect in this process can initiate degradation and loss of structural integrity.

The concept of modulation of ECM stiffness by vascular SMCs and vice versa is well supported by the literature. Vascular SMCs and fibroblasts can sense changes in the ECM through the cytoskeleton and integrins. These cells in turn can regulate the ECM by controlling the synthesis of ECM components and tune their cytoskeleton to respond to such mechanical forces (Lacolley et al. 2012, Forte et al. 2010). An increase in wall stress thus leads to SMC proliferation and synthesis of ECM components by humoral factors like TGF-β, thereby reinforcing the vessel wall (Humphrey et al. 2008). Likewise, a reduced wall stress triggers loss of vascular SMCs, up regulation of proteolytic enzymes and consequent reduction of wall thickness. Any defects in mechanosensing of the wall stress can thus lead to activation of degradation pathways instead of consolidation of the arterial wall.

Soft matrix has been reported to be a stimulator for cellular invasiveness (Gu et al. 2014). In this study, growing cells on a soft matrix led to up regulation of matrix metalloproteinase activity and induction of invadosome-like protrusion (ILP) formation. In this context, different cell types are capable of sensing stiffness including endothelial cells and vascular SMCs (Califano et al. 2010, Deroanne et al. 2001 and Isenberg et al. 2009). Stiffness of the matrix can influence focal adhesions, assembly of the cytoskeleton and the traction forces generated by the cell (Balaban et al. 2001, Beningo et al. 2001). The increased proliferation of the medial SMCs in femoral arteries from very old zyxin-null mice could in fact be a result of the altered ECM environment. Indeed there are several reports of ECM stiffness regulating cell migration, proliferation and differentiation (Fioretta et al. 2012, Peyton et al. 2008,Peyton et al. 2005). While the composition of the ECM might account for the changes in mechanical strength of femoral arteries in very old zyxin-null mice, there is also a distinct possibility of changes in the stiffness of the vascular SMCs (e.g., due to changes in stability of stress fibres) resulting in poor resistivity of the vasculature. Recently, the stiffness of vascular SMCs as a contributor of arterial stiffening in ageing has been studied (Qiu et al. 2010).However, at this point, it is difficult to specify the exact cause of the vascular phenotype initiated by the loss of zyxin. Whether it is driven by a defective mechanosensing at zyxin-deficient focal adhesions of vascular SMCs or a direct consequence of transcriptional activity of zyxin regulating the expression of proteins

such as MMPs remains to be elucidated. From the experimental evidence demonstrating a dramatic age-dependent weakening of the ECM cross-linking coinciding with the contractile deficit of the femoral arteries, it does seem to be an ECM-derived vascular phenotype in zyxin-null mice.

5.4 Cardiac phenotype in zyxin-null mice: A case of uncontrolled fibrosis?

Zyxin-null mice aged approximately 52 weeks display a failure to develop a robust increase in systolic but not diastolic blood pressure. At this time point, the changes in the vasculature are only subtle and cannot explain this phenotype. Since the kidney function of zyxin-null mice seems to be comparable to that of WT mice, the cardiac function of these animals was investigated in detail to address this question. This approach is also supported by the following: a) Zyxin has been reported to protect cardiomyocytes from apoptosis by virtue of its nuclear translocation and consolidating the protective effects of Akt in cardiomyocytes(Kato et al. 2005). This work reported the promotion of nuclear localization of zyxin by cardioprotective stimuli, association of zyxin with phospho-Akt triggered by such cardioprotective stimuli and consolidation of nuclear accumulation of phospho-Akt by zyxin and vice versa leading to cardiomyocyte survival. Thus, the absence of zyxin might trigger an apoptosis of cardiomyocytes in zyxin-null mice with experimentally elevated blood pressure. b) Zyxin is a putative mechanotransducer. As such, it might have an important role in the heart which is exposed to a pressure overload (enhanced biomechanical forces) in hypertension. Indeed, the zyxin-null mice displayed a systolic dysfunction upon DOCA-salt treatment. Histological investigation revealed significant apoptosis and advanced fibrosis in the heart of these mice. Two possibilities exist: a) Reduction of viable cardiomyocytes is itself sufficient to induce systolic dysfunction, and b) the loss of cardiomyocytes triggers the deposition of fibrotic tissue due to ECM remodelling, stiffening the heart and causing reduced systolic function.

Loss of cardiomyocytes due to apoptosis in hypertensive heart disease is well documented in the literature. In the hypertrophied left ventricle of spontaneously hypertensive rats (SHR) and in rats with renal hypertension, increase in cardiomyocyte apoptosis has been demonstrated (Diez et al. 1997,Liu et al. 2000, Fortuño et al. 2003).

Even in hypertrophied hearts of patients with essential hypertension, cardiomyocyte apoptosis has been shown despite the presence of normal cardiac function (González et al. 2002, Yamamoto et al. 2002).

There may be several possible reasons for such apoptosis. Pressure overload has been shown to induce cardiomyocyte apoptosis after aortic banding in rats (Teiger et al. 1996). By mimicking an increased diastolic stress *in vitro* by stretching of isolated papillary muscles, an increase in cardiomyocyte apoptosis was observed (Cheng et al. 1995). Besides the mechanical factors, altered humoral factors can also result in apoptosis in arterial hypertension. Angiotensin II may be a humoral factor responsible for induction of apoptosis. Cardiomyocyte apoptosis is induced in hypertensive Sprague-Dawley rats upon infusion of angiotensin II, which is prevented by the AT_1R blocker losartan (Diep et al. 2002). Notably, apoptosis of cardiomyocytes is inhibited by a variety of cardioprotective stimuli, an effect that is lost in response to cardiac stress due to down regulation of their expression. Cardioprotective stimuli such as IGF-1, adrenomedullin, estradiol and natriuretic peptides exert their protective effects via stimulation of cGMP production. Interestingly, this protection is dependent on the nuclear activation of Akt which offers resistance to apoptotic stimuli in cardiomyocytes (Shiraishi et al. 2004). In this context, zyxin was reported to promote cardiomyocyte survival mediated by ANP by its nuclear translocation and nuclear activation of Akt (Kato et al. 2005). Importantly, the protective effect of zyxin was maintained even after return of zyxin to the focal adhesions from the nucleus. This indicates that the long-term protection against apoptosis offered by zyxin is independent of its nuclear localization.

The possibility of a functional redundancy among the three zyxin family members was considered as a reason for the lack of apoptosis in zyxin-null cardiomyocytes. Indeed, the present study found comparable levels of apoptosis in the hearts from WT and zyxin-null mice. However, on exposure to DOCA-salt-induced hypertension, there was a significant increase in apoptosis in the hearts from zyxin-null mice. Thus, loss of functional cardiomyocytes offers a possible mechanism for the reduced systolic function in DOCA-salt-treated zyxin-null mice. This systolic dysfunction in zyxin-null mice could not be ascertained from measurements of cardiac contractile parameters in isolated

working heart experiments (Table 25 and 26). Although the systolic elastance (the slope of the end systolic pressure-volume relationship curve) was significantly lower in zyxin-null mice, no significant differences could be established among other parameters indicative of cardiac systolic and diastolic function. These experiments were performed using C57BL/6J mice (purchased from Charles River Laboratories, UK) to serve as controls for age-matched zyxin-null mice approximately 52 weeks old. This approach was used due to the lack of age-matched WT littermates from the same colony. Use of relatively older mice from two different animal housing facilities could be a source of potential variations in these measurements. It is also important to remember that the DOCA-salt-treated zyxin-null mice do not display enhanced cardiac hypertrophy compared to WT mice. Therefore, measurements using isolated working hearts might not detect modest changes in systolic function presumably resulting from an increased cardiac fibrosis in zyxin-null mice. Furthermore, an increased cardiac fibrosis leading to stiffening of the myocardium often results in diastolic dysfunction. In this context, it must be mentioned that the DOCA-salt model is not a prominent model for induction of cardiac fibrosis. Models such as infusion of angiotensin II or the transverse aortic constriction (TAC) might be better suited for induction of pronounced interstitial fibrosis and subsequent cardiac dysfunction detectable in isolated working heart measurements.

Enhanced cardiac fibrosis as a result of cardiac apoptosis is not unprecedented. Deposition of fibrillar collagen in the cardiac interstitium of SHR rats and hypertensive patients leads to an increase of left ventricular chamber stiffness (Brilla et al. 1991,Díez et al. 2002). The overarching question, however, is whether the increase in interstitial fibrosis is a result of the activation of fibroblasts by humoral and mechanical factors or is dependent upon stimulation of a fibrotic response initiated by cell death and insufficient wound healing. Indeed, failing hearts from SHR rats display a co-localized expression of collagen type I in areas of cardiomyocyte degeneration (Bing et al. 2002). Cardiac fibrosis in hypertension is complex and is a product of several factors. Collagen deposition is a predominant factor in this process. Collagen turnover is normally regulated by fibroblasts under normal physiological conditions. However, under pathological conditions, distinct fibroblast-like cells called myofibroblasts appear which

drive the ECM deposition. The resulting myocardial stiffness is mainly attributable to changes in composition of fibrillar collagens (type I and type III).

Collagen turnover is regulated by several growth factors such as angiotensin II, TGF-β1 and IGF-1 (Kagami et al. 1994). In the present study, analysis of gene expression in hearts from DOCA-salt-treated WT and zyxin-null mice using a PCR-profiler array showed a shift to a pro-fibrotic environment in zyxin-null mice. Notably, expression of collagen isoforms was increased along with higher expression of connective tissue growth factor (CTGF) and several integrin isoforms suggesting increased ECM synthesis. Increased expression of the TGF-β receptor-type I (TGFβRI) further explained the increased ECM deposition in the cardiac interstitium of zyxin-null mice. TGFβRI is the receptor for TGFβ1 which is capable of inducing the production of fibrillar collagen, fibronectin and proteoglycans by cardiac fibroblasts (Eghbali et al. 1991).

Moreover, ECM components can influence cardiac contractility by altering bidirectional signalling via integrins (Katsumi et al. 2005). For example, overexpression of integrin $\alpha_v\beta_1$ stimulates the expression of TGF-β_1 while TGF-β_1 can increase the expression of $\alpha_v\beta_1$ (Manso et al. 2006). In cardiac tissue lysates from zyxin-null mice, there was an up regulation of integrins α_5 and β_1. This might be a downstream effect of increased TGF-β_1 activity via TGFβRI. Additionally, there was an increased activation of focal adhesion kinase (FAK) which in turn reflects enhanced integrin activation. Thus, zyxin-null mice have exaggerated cardiac fibrosis which presumably leads to cardiac dysfunction in the presence of enhanced apoptosis in these mice. The quality of the ECM rather than its quantity is more important in determining its impact on cardiac function. Therefore, in addition to the synthesis of collagen fibrils, their cross-linking and the nature and extent of their degradation are important determinants of the consequences of fibrosis.

The enzyme lysyl oxidase (LOX) is a copper-dependent enzyme which catalyses the cross-linking of collagen and elastin. Thus, up regulation of LOX leads to an increase in cross-linking of collagen and stiffness of the ECM. Zyxin-null mice showed a robust increase in expression of LOX following DOCA-salt treatment. Therefore, increased LOX expression could underlie the increased cardiac fibrosis and dysfunction observed

in the zyxin-null mice. Indeed, induction of LOX is a common denominator in a variety of fibrotic processes in different organs (Mäki et al. 2009). Abnormal increase of LOX expression has been reported in the fibrotic myocardium of patients with hypertensive heart disease (López et al. 2010). Zyxin-null mice also displayed an up regulation of genes encoding matrix metalloproteinases (MMP2, 3 and 9) indicating a remodelling of the ECM in these mice. The role of MMPs in hypertensive remodelling of the heart has been demonstrated by using mice deficient in MMP2 which showed reduced cardiac interstitial fibrosis following aortic banding. Similarly, mice lacking MMP9 were also protected from cardiac fibrosis in response to pressure overload.

The enhanced apoptosis and fibrosis observed in the hearts from DOCA-treated zyxin-null mice might be derived from either the cardiomyocytes or the fibroblasts or both. However, experiments with neonatal cardiomyocytes isolated from WT and zyxin-null mice show enhanced apoptosis in the zyxin-null cardiomyocytes but not the fibroblasts. Furthermore, concurrently isolated zyxin-null fibroblasts showed an up regulation of integrin β_1 (Itgb1) and CTGF gene expression in response to TGF-$\beta_1$as compared to WT fibroblasts. This difference was not evident in cardiomyocytes further indicating that the pro-fibrotic response in zyxin-null mice is most likely of fibroblast origin.

5.5 Perspective

The present study offers insight into the role of the mechanotransducer protein zyxin in hypertensive arterial remodelling. Furthermore, in keeping with its potential as a mechanosensitive protein, it was found to be equally important in remodelling of the heart in response to cardiac pressure overload. This work provides a first detailed analysis of the phenotype of zyxin-null mice particularly when challenged with pathophysiological stress such as hypertension. It also elucidates a MRTF-A-dependent manner in which zyxin promotes a synthetic phenotype of vascular SMCs. A thorough characterization of the phenotype of these mice reveals a complex function of zyxin in the whole organism. Although not self-sufficient, the present study also confirms the role of TRPC3 channels in the stretch-induced zyxin activation and offers insight into the complexity of this process. Notably, it demonstrates the cumulative nature of the zyxin-dependent phenotype which is unmasked only in older mice. Thus, the presence of a

robust phenotype in isolated vascular SMCs from zyxin-null mice is not replicated *in vivo* in young mice. While adding to the existing knowledge regarding the importance of zyxin in transducing biomechanical forces from the ECM to the nucleus, this study raises several interesting questions which need to be answered in the future.

a) What is the reason behind the disparity between the *in vitro* and the *in vivo* phenotype? It is well known that vascular SMCs in the arterial wall are protected to some extent from the effects of changes in wall tension by a well-defined network of ECM fibrils. Exaggerated arterial remodelling in very old zyxin-null mice coincides with a loss of integrity of this ECM network further strengthening the argument. Whether the synthetic phenotype of zyxin-null SMCs can be rescued by seeding the cells on a three-dimensional compact matrix or using a different combination of ECM proteins is an interesting question that needs to be answered.

b) Can LPP or TRIP6 compensate for the loss of zyxin in zyxin-null mice? The changes in expression of these zyxin family members have to be analysed at different time points in zyxin-null mice. Furthermore, the DOCA-salt model can be used to test if a similar phenotype is present in LPP-null mice. Finally, using mice lacking both zyxin and LPP (double knock-outs), the possibility of a functional compensation can be verified. At present, both LPP-null mice and the double knock-out mice are being bred for such experiments.

c) What is the exact mechanism responsible for the cardiac dysfunction in zyxin-null mice? Further experiments need to be done to dissect the cell type and the precise molecular events initiating the cardiac phenotype. These experiments would include an assessment of contractility and calcium transients in isolated zyxin-null cardiomyocytes and comparing them to WT cardiomyocytes. Additionally, if cardiac fibroblasts are the source of this phenotype, the molecular mechanisms by which zyxin activates these fibroblasts need to be elucidated.

d) Finally, with technical improvements in the experimental set-up for measuring calcium transients in stretched cells (particularly vascular SMCs), the identity of the mechanosensor upstream of zyxin activation might be revealed.

6 REFERENCES

Adebiyi, Adebowale, Damodaran Narayanan, and Jonathan H. Jaggar. 2011. “Caveolin-1 Assembles Type 1 Inositol 1,4,5-Trisphosphate Receptors and Canonical Transient Receptor Potential 3 Channels into a Functional Signalling Complex in Arterial Smooth Muscle Cells.” *Journal of Biological Chemistry* 286: 4341–48.

Ai, S, M Kuzuya, T Koike, T Asai, S Kanda, K Maeda, T Shibata, and A Iguchi. 2001. “Rho-Rho Kinase Is Involved in Smooth Muscle Cell Migration through Myosin Light Chain Phosphorylation-Dependent and Independent Pathways.” *Atherosclerosis* 155: 321–27.

Althoff, Till F, Julián Albarrán Juárez, Kerstin Troidl, Cong Tang, Shengpeng Wang, Angela Wirth, Mikito Takefuji, Nina Wettschureck, and Stefan Offermanns. 2012. “Procontractile G Protein-Mediated Signalling Pathways Antagonistically Regulate Smooth Muscle Differentiation in Vascular Remodelling.” *The Journal of Experimental Medicine* 209: 2277–90.

Arnold, Caroline, Anja Feldner, Larissa Pfisterer, Maren Hödebeck, Kerstin Troidl, Guillem Genové, Thomas Wieland, Markus Hecker, and Thomas Korff. 2014. “RGS5 Promotes Arterial Growth during Arteriogenesis.” *EMBO Molecular Medicine*, June, 1–15.

Badier-Commander, Cécile, Tony Verbeuren, Christian Lebard, Jean Baptiste Michel, and Marie Paule Jacob. 2000. “Increased TIMP/MMP Ratio in Varicose Veins: A Possible Explanation for Extracellular Matrix Accumulation.” *Journal of Pathology* 192: 105–12.

Balaban, N Q, U S Schwarz, D Riveline, P Goichberg, G Tzur, I Sabanay, D Mahalu, et al. 2001. “Force and Focal Adhesion Assembly: A Close Relationship Studied Using Elastic Micropatterned Substrates.” *Nature Cell Biology* 3: 466–72.

Balasubramanian, Sundaravadivel, Lakeya Quinones, Harinath Kasiganesan, Yuhua Zhang, Dorea L. Pleasant, Kamala P. Sundararaj, Michael R. Zile, Amy D. Bradshaw, and Dhandapani Kuppuswamy. 2012. “β3 Integrin in Cardiac Fibroblast Is Critical for Extracellular Matrix Accumulation during Pressure Overload Hypertrophy in Mouse.” *PLoS ONE* 7(9):e45076.

Beamish, Jeffrey A, Ping He, Kandice Kottke-Marchant, and Roger E Marchant. 2010. “Molecular Regulation of Contractile Smooth Muscle Cell Phenotype: Implications for Vascular Tissue Engineering.” *Tissue Engineering. Part B, Reviews* 16: 467–91.

Beningo, Karen A., Micah Dembo, Irina Kaverina, J. Victor Small, and Yu Li Wang. 2001. “Nascent Focal Adhesions Are Responsible for the Generation of Strong Propulsive Forces in Migrating Fibroblasts.” *Journal of Cell Biology* 153: 881–87.

Bing, O. H L, Chester H. Conrad, Marvin O. Boluyt, Kathleen G. Robinson, and Wesley W. Brooks. 2002. “Studies of Prevention, Treatment and Mechanisms of Heart Failure in the Aging Spontaneously Hypertensive Rat.” *Heart Failure Reviews* 7(1):71-88.

Brilla, C G, J S Janicki, and K T Weber. 1991. “Cardioreparative Effects of Lisinopril in Rats with Genetic Hypertension and Left Ventricular Hypertrophy.” *Circulation* 83: 1771–79.

Caldwell, R A, H F Clemo, and C M Baumgarten. 1998. “Using Gadolinium to Identify Stretch-Activated Channels: Technical Considerations.” *The American Journal of Physiology* 275: C619–C621.

Califano, Joseph P., and Cynthia A. Reinhart-King. 2010. “Substrate Stiffness and Cell Area Predict Cellular Traction Stresses in Single Cells and Cells in Contact.” *Cellular and Molecular Bioengineering* 3: 68–75.

Cantley, Lewis C. 2002. “The Phosphoinositide 3-Kinase Pathway.” *Science (New York, N.Y.)* 296: 1655–57.

Cattaruzza, M, M M Berger, M Ochs, A Fayyazi, L Füzesi, J Richter, and M Hecker. 2002. “Deformation-Induced Endothelin B Receptor-Mediated Smooth Muscle Cell Apoptosis Is Matrix-Dependent.” *Cell Death and Differentiation* 9: 219–26.

Cattaruzza, M, I Eberhardt, and M Hecker. 2001. “Mechanosensitive Transcription Factors Involved in Endothelin B Receptor Expression.” *J Biol Chem* 276: 36999–3.

Cattaruzza, Marco, Claus Lattrich, and Markus Hecker. 2004. “Focal Adhesion Protein Zyxin Is a Mechanosensitive Modulator of Gene Expression in Vascular Smooth Muscle Cells.” *Hypertension* 43 (4): 726–30.

Chen, Kuang Den, Yi Shuan Li, Michael Kim, Song Li, Suli Yuan, Shu Chien, and John Y J Shyy. 1999. “Mechanotransduction in Response to Shear Stress. Roles of Receptor Tyrosine Kinases, Integrins, and Shc.” *Journal of Biological Chemistry* 274: 18393–400.

Chen, Xi Lin, Signe E. Varner, Anjali S. Rao, Janice Y. Grey, Suzanne Thomas, Christopher K. Cook, Martin A. Wasserman, Russell M. Medford, Anil K. Jaiswal, and Charles Kunsch. 2003. “Laminar Flow Induction of Antioxidant Response Element-Mediated Genes in Endothelial Cells: A Novel Anti-Inflammatory Mechanism.” *Journal of Biological Chemistry* 278: 703–11.

Cheng, W., B. Li, J. Kajstura, P. Li, M. S. Wolin, E. H. Sonnenblick, T. H. Hintze, G. Olivetti, and P. Anversa. 1995. “Stretch-Induced Programmed Myocyte Cell Death.” *Journal of Clinical Investigation* 96: 2247–59.

Chesley, A, M S Lundberg, T Asai, R P Xiao, S Ohtani, E G Lakatta, and M T Crow. 2000. “The beta(2)-Adrenergic Receptor Delivers an Antiapoptotic Signal to Cardiac

Myocytes through G(i)-Dependent Coupling to Phosphatidylinositol 3'-Kinase." *Circulation Research* 87: 1172–79.

Chien, Kenneth R. 1999. "Stress Pathways and Heart Failure." *Cell* 98(5):555-8.

Choi, Yun-Hee, Brian T McNally, and Peter Igarashi. 2013. "Zyxin Regulates Migration of Renal Epithelial Cells through Activation of Hepatocyte Nuclear Factor-1β." *American Journal of Physiology. Renal Physiology* 305: F100–10.

Chothia, C, and E Y Jones. 1997. "The Molecular Structure of Cell Adhesion Molecules." *Annual Review of Biochemistry* 66: 823–62.

Chrzanowska-Wodnicka, M, and K Burridge. 1996. "Rho-Stimulated Contractility Drives the Formation of Stress Fibres and Focal Adhesions." *The Journal of Cell Biology* 133: 1403–15.

Clapham, David E. 2003. "TRP Channels as Cellular Sensors." *Nature* 426: 517–24.

Coste, Bertrand, Bailong Xiao, Jose S. Santos, Ruhma Syeda, Jörg Grandl, Kathryn S. Spencer, Sung Eun Kim, et al. 2012. "Piezo Proteins Are Pore-Forming Subunits of Mechanically Activated Channels." *Nature* 483(7388):176-81.

Crawford, A W, J W Michelsen, and M C Beckerle. 1992. "An Interaction between Zyxin and Alpha-Actinin." *The Journal of Cell Biology* 116: 1381–93.

Crawford, Aaron W., and Mary C. Beckerle. 1991. "Purification and Characterization of Zyxin, an 82,000-Dalton Component of Adherens Junctions." *Journal of Biological Chemistry* 266: 5847–53.

Crone, Johanna, Carolina Glas, Kathrin Schultheiss, Jutta Moehlenbrink, Eva Krieghoff-Henning, and Thomas G. Hofmann. 2011. "Zyxin Is a Critical Regulator of the Apoptotic HIPK2-p53 Signalling Axis." *Cancer Research* 71: 2350–59.

Curry, F. E., and R. H. Adamson. 2012. "Endothelial Glycocalyx: Permeability Barrier and Mechanosensor." *Annals of Biomedical Engineering* 40(4):828-39.

Dekker, Rob J, Johannes V van Thienen, Jakub Rohlena, Saskia C de Jager, Yvonne W Elderkamp, Jurgen Seppen, Carlie J M de Vries, et al. 2005. "Endothelial KLF2 Links Local Arterial Shear Stress Levels to the Expression of Vascular Tone-Regulating Genes." *The American Journal of Pathology* 167: 609–18.

Demicheva, Elena, Markus Hecker, and Thomas Korff. 2008. "Stretch-Induced Activation of the Transcription Factor Activator Protein-1 Controls Monocyte Chemoattractant Protein-1 Expression during Arteriogenesis." *Circulation Research* 103: 477–84.

Deroanne, Christophe F., Charles M. Lapiere, and Betty V. Nusgens. 2001. “In Vitro Tubulogenesis of Endothelial Cells by Relaxation of the Coupling Extracellular Matrix-Cytoskeleton.” *Cardiovascular Research* 49: 647–58.

Diep, Quy N, Mohammed El Mabrouk, Ping Yue, and Ernesto L Schiffrin. 2002. “Effect of AT(1) Receptor Blockade on Cardiac Apoptosis in Angiotensin II-Induced Hypertension.” *American Journal of Physiology. Heart and Circulatory Physiology* 282: H1635–H1641.

Dietrich, A, Y.Schnitzler Mederos, M Gollasch, V Gross, U Storch, G Dubrovska, M Obst, et al. 2005. “Increased Vascular Smooth Muscle Contractility in TRPC6-/- Mice.” *Mol.Cell Biol.* 25: 6980–89.

Diez, J., A. Panizo, M. Hernandez, F. Vega, I. Sola, M. A. Fortuno, and J. Pardo. 1997. “Cardiomyocyte Apoptosis and Cardiac Angiotensin-Converting Enzyme in Spontaneously Hypertensive Rats.” *Hypertension* 30(5):1029-34.

Díez, Javier, Ramón Querejeta, Begoña López, Arantxa González, Mariano Larman, and José L. Martínez Ubago. 2002. “Losartan-Dependent Regression of Myocardial Fibrosis Is Associated with Reduction of Left Ventricular Chamber Stiffness in Hypertensive Patients.” *Circulation* 105: 2512–17.

Drees, Beth, Evelyne Friederich, Julie Fradelizi, Daniel Louvard, Mary C. Beckerle, and Roy M. Golsteyn. 2000. “Characterization of the Interaction between Zyxin and Members of the Ena/vasodilator-Stimulated Phosphoprotein Family of Proteins.” *Journal of Biological Chemistry* 275: 22503–11.

Durante, W, L Liao, I Iftikhar, K Cheng, and A I Schafer. 1996. “Platelet-Derived Growth Factor Regulates Vascular Smooth Muscle Cell Proliferation by Inducing Cationic Amino Acid Transporter Gene Expression.” *J Biol Chem* 271(20):11838-43.

Egan, Colin G., Cherry L. Wainwright, Roger M. Wadsworth, and Graeme F. Nixon. 2005. “PDGF-Induced Signalling in Proliferating and Differentiated Vascular Smooth Muscle: Effects of Altered Intracellular Ca2+ Regulation.” *Cardiovascular Research* 67: 308–16.

Eghbali, M, R Tomek, V P Sukhatme, C Woods, and B Bhambi. 1991. “Differential Effects of Transforming Growth Factor-Beta 1 and Phorbol Myristate Acetate on Cardiac Fibroblasts. Regulation of Fibrillar Collagen mRNAs and Expression of Early Transcription Factors.” *Circulation Research* 69: 483–90.

Feldman, L J, M Mazighi, A Scheuble, J F Deux, E De Benedetti, C Badier-Commander, E Brambilla, D Henin, P G Steg, and M P Jacob. 2001. “Differential Expression of Matrix Metalloproteinases after Stent Implantation and Balloon Angioplasty in the Hypercholesterolemic Rabbit.” *Circulation* 103: 3117–22.

Fioretta, Emanuela S., Joost O. Fledderus, Frank P T Baaijens, and Carlijn V C Bouten. 2012. “Influence of Substrate Stiffness on Circulating Progenitor Cell Fate.” *Journal of Biomechanics* 45: 736–44.

Forte, Amalia, Alessandro Della Corte, Marisa De Feo, Flavio Cerasuolo, and Marilena Cipollaro. 2010. “Role of Myofibroblasts in Vascular Remodelling: Focus on Restenosis and Aneurysm.” *Cardiovascular Research* 88(3):395-405.

Fortuño, María A, Natalia López, Arantxa González, and Javier Díez. 2003. “Involvement of Cardiomyocyte Survival-Apoptosis Balance in Hypertensive Cardiac Remodelling.” *Expert Review of Cardiovascular Therapy* 1: 293–307.

Fraley, Stephanie I., Yunfeng Feng, Anjil Giri, Gregory D. Longmore, and Denis Wirtz. 2012. “Dimensional and Temporal Controls of Three-Dimensional Cell Migration by Zyxin and Binding Partners.” *Nature Communications* 3:719.

Gevaert, Thomas, Joris Vriens, Andrei Segal, Wouter Everaerts, Tania Roskams, Karel Talavera, Grzegorz Owsianik, et al. 2007. “Deletion of the Transient Receptor Potential Cation Channel TRPV4 Impairs Murine Bladder Voiding.” *Journal of Clinical Investigation* 117: 3453–62.

Gjorevski, Nikolce, and Celeste M. Nelson. 2009. “Bidirectional Extracellular Matrix Signalling during Tissue Morphogenesis.” *Cytokine and Growth Factor Reviews* 20(5-6):459-65.

González, Arantxa, Begoña López, Susana Ravassa, Ramón Querejeta, Mariano Larman, Javier Díez, and María A. Fortuño. 2002. “Stimulation of Cardiac Apoptosis in Essential Hypertension Potential Role of Angiotensin II.” *Hypertension* 39: 75–80.

Grainger, D J, J C Metcalfe, A A Grace, and D E Mosedale. 1998. “Transforming Growth Factor-Beta Dynamically Regulates Vascular Smooth Muscle Differentiation in Vivo.” *J Cell Sci* 111 (Pt 1: 2977–88).

Grynkiewicz, G., M. Poenie, and R. Y. Tsien. 1985. “A New Generation of Ca2+ Indicators with Greatly Improved Fluorescence Properties.” *Journal of Biological Chemistry* 260(6):3440-50.

Gu, Zhizhan, Fei Liu, Elina a Tonkova, Soo Young Lee, Daniel J Tschumperlin, and Michael B Brenner. 2014. “Soft Matrix Is a Natural Stimulator for Cellular Invasiveness.” *Molecular Biology of the Cell* 25: 457–69.

Gudi, S, I Huvar, C R White, N L McKnight, N Dusserre, G R Boss, and J A Frangos. 2003. “Rapid Activation of Ras by Fluid Flow Is Mediated by G Alpha(q) and G Beta Gamma Subunits of Heterotrimeric G Proteins in Human Endothelial Cells.” *Arteriosclerosis Thrombosis and Vascular Biology* 23: 994–1000.

Hahn, Cornelia, and Martin A Schwartz. 2009. “Mechanotransduction in Vascular Physiology and Atherogenesis.” *Nature Reviews. Molecular Cell Biology* 10: 53–62.

Hervy, M., L. M. Hoffman, C. C. Jensen, M. Smith, and M. C. Beckerle. 2010. “The LIM Protein Zyxin Binds CARP-1 and Promotes Apoptosis.” *Genes & Cancer* 1(5):506-515.

Hirata, Hiroaki, Hitoshi Tatsumi, and Masahiro Sokabe. 2008. “Mechanical Forces Facilitate Actin Polymerization at Focal Adhesions in a Zyxin-Dependent Manner.” *Journal of Cell Science* 121: 2795–2804.

Hirota, Toru, Tetsuro Morisaki, Yasuyuki Nishiyama, Tomotoshi Marumoto, Kenji Tada, Toshihiro Hara, Norio Masuko, Masaki Inagaki, Katsuyoshi Hatakeyama, and Hideyuki Saya. 2000. “Zyxin, a Regulator of Actin Filament Assembly, Targets the Mitotic Apparatus by Interacting with H-warts/LATS1 Tumor Suppressor.” *Journal of Cell Biology* 149: 1073–86.

Hoffman, L. M., C. C. Jensen, A. Chaturvedi, M. Yoshigi, and M. C. Beckerle. 2012. “Stretch-Induced Actin Remodelling Requires Targeting of Zyxin to Stress Fibres and Recruitment of Actin Regulators.” *Molecular Biology of the Cell* 23(10):1846-59.

Hoffman, Laura M, Christopher C Jensen, Susanne Kloeker, C-L Albert Wang, Masaaki Yoshigi, and Mary C Beckerle. 2006. “Genetic Ablation of Zyxin Causes Mena/VASP Mislocalization, Increased Motility, and Deficits in Actin Remodelling.” *The Journal of Cell Biology* 172 (5): 771–82.

Hoffman, Laura M, David A Nix, Beverly Benson, Ray Boot-Hanford, Erika Gustafsson, Colin Jamora, A Sheila Menzies, et al. 2003. “Targeted Disruption of the Murine Zyxin Gene.” *Molecular and Cellular Biology* 23: 70–79.

Hofmann, T, A G Obukhov, M Schaefer, C Harteneck, T Gudermann, and G Schultz. 1999. “Direct Activation of Human TRPC6 and TRPC3 Channels by Diacylglycerol.” *Nature* 397: 259–63.

Humphrey, J. D. 2008. “Vascular Adaptation and Mechanical Homeostasis at Tissue, Cellular, and Sub-Cellular Levels.” *Cell Biochemistry and Biophysics* 50(2):53-78.

Ingber, Donald E, Van C Mow, David Butler, Laura Niklason, Johnny Huard, Jeremy Mao, Ioannis Yannas, David Kaplan, and Gordana Vunjak-Novakovic. 2006. “Tissue Engineering and Developmental Biology: Going Biomimetic.” *Tissue Engineering* 12: 3265–83.

Isenberg, Brett C., Paul A. DiMilla, Matthew Walker, Sooyoung Kim, and Joyce Y. Wong. 2009. “Vascular Smooth Muscle Cell Durotaxis Depends on Substrate Stiffness Gradient Strength.” *Biophysical Journal* 97: 1313–22.

Iwanaga, Yoshitaka, Takeshi Aoyama, Yasuki Kihara, Yoko Onozawa, Takeshi Yoneda, and Shigetake Sasayama. 2002. “Excessive Activation of Matrix Metalloproteinases Coincides with Left Ventricular Remodelling during Transition from Hypertrophy to Heart Failure in Hypertensive Rats.” *Journal of the American College of Cardiology* 39: 1384–91.

Iyer, Abishek, Vincent Chan, and Lindsay Brown. 2010. “The DOCA-Salt Hypertensive Rat as a Model of Cardiovascular Oxidative and Inflammatory Stress.” *Current Cardiology Reviews* 6(4):291-7.

Kagami, S, W A Border, D E Miller, and N A Noble. 1994. “Angiotensin II Stimulates Extracellular Matrix Protein Synthesis through Induction of Transforming Growth Factor-Beta Expression in Rat Glomerular Mesangial Cells.” *The Journal of Clinical Investigation* 93: 2431–37.

Kaïdi, S, F Brutel, F Van Deun, K Kramer, R Remie, W Dewé, P Remusat, A Delaunois, and O Depelchin. 2007. “Comparison of Two Methods (left Carotid Artery and Abdominal Aorta) for Surgical Implantation of Radiotelemetry Devices in CD-1 Mice.” *Laboratory Animals* 41: 388–402.

Kato, Takahiro, John Muraski, Yan Chen, Yasuyuki Tsujita, Jason Wall, Christopher C Glembotski, Erik Schaefer, Mary Beckerle, and Mark A Sussman. 2005. “Atrial Natriuretic Peptide Promotes Cardiomyocyte Survival by cGMP-Dependent Nuclear Accumulation of Zyxin and Akt.” *The Journal of Clinical Investigation* 115: 2716–30.

Katsumi, Akira, Tomoki Naoe, Tadashi Matsushita, Kozo Kaibuchi, and Martin Alexander Schwartz. 2005. “Integrin Activation and Matrix Binding Mediate Cellular Responses to Mechanical Stretch.” *Journal of Biological Chemistry* 280: 16546–49.

Khachigian, L M, K R Anderson, N J Halnon, M A Gimbrone, N Resnick, and T Collins. 1997. “Egr-1 Is Activated in Endothelial Cells Exposed to Fluid Shear Stress and Interacts with a Novel Shear-Stress-Response Element in the PDGF A-Chain Promoter.” *Arteriosclerosis, Thrombosis, and Vascular Biology* 17: 2280–86.

Kim, Sung Eun, Bertrand Coste, Abhishek Chadha, Boaz Cook, and Ardem Patapoutian. 2012. “The Role of Drosophila Piezo in Mechanical Nociception.” *Nature* 483(7388):209-12.

Kitazawa, Toshio, Masumi Eto, Terence P Woodsome, and Md Khalequzzaman. 2003. “Phosphorylation of the Myosin Phosphatase Targeting Subunit and CPI-17 during Ca2+ Sensitization in Rabbit Smooth Muscle.” *The Journal of Physiology* 546: 879–89.

Kiyonaka, Shigeki, Kenta Kato, Motohiro Nishida, Kazuhiro Mio, Takuro Numaga, Yuichi Sawaguchi, Takashi Yoshida, et al. 2009. “Selective and Direct Inhibition of TRPC3 Channels Underlies Biological Activities of a Pyrazole Compound.” *Proceedings of the National Academy of Sciences of the United States of America* 106: 5400–5405.

Koitabashi, Norimichi, Thomas Danner, Ari L. Zaiman, Yigal M. Pinto, Janelle Rowell, Joseph Mankowski, Dou Zhang, Taishi Nakamura, Eiki Takimoto, and David A. Kass. 2011. “Pivotal Role of Cardiomyocyte TGF-B Signalling in the Murine Pathological Response to Sustained Pressure Overload.” *Journal of Clinical Investigation* 121: 2301–12.

Lacolley, Patrick, Véronique Regnault, Antonino Nicoletti, Zhenlin Li, and Jean Baptiste Michel. 2012. “The Vascular Smooth Muscle Cell in Arterial Pathology: A Cell That Can Take on Multiple Roles.” *Cardiovascular Research* 95(2):194-204

Lagares, David, Oscar Busnadiego, Rosa Ana García-Fernández, Mohit Kapoor, Shangxi Liu, David E. Carter, David Abraham, et al. 2012. “Inhibition of Focal Adhesion Kinase Prevents Experimental Lung Fibrosis and Myofibroblast Formation.” *Arthritis and Rheumatism* 64: 1653–64.

Lan, Q, K O Mercurius, and P F Davies. 1994. “Stimulation of Transcription Factors NF Kappa B and AP1 in Endothelial Cells Subjected to Shear Stress.” *Biochemical and Biophysical Research Communications* 201: 950–56.

Lauth, M, A H Wagner, M Cattaruzza, H D Orzechowski, M Paul, and M Hecker. 2000. “Transcriptional Control of Deformation-Induced Preproendothelin-1 Gene Expression in Endothelial Cells.” *Journal of Molecular Medicine (Berlin, Germany)* 78: 441–50.

Lecroisey, Claire, Nicolas Brouilly, Hiroshi Qadota, Marie-Christine Mariol, Nicolas C Rochette, Edwige Martin, Guy M Benian, Laurent Ségalat, Nicole Mounier, and Kathrin Gieseler. 2013. “ZYX-1, the Unique Zyxin Protein of Caenorhabditis Elegans, Is Involved in Dystrophin-Dependent Muscle Degeneration.” *Molecular Biology of the Cell* 24: 1232–49.

Lee, John S., Qing Yu, Jordan T. Shin, Eric Sebzda, Cara Bertozzi, Mei Chen, Patti Mericko, et al. 2006. “Klf2 Is an Essential Regulator of Vascular Hemodynamic Forces In Vivo.” *Developmental Cell* 11: 845–57.

Lehoux, S, and A Tedgui. 1998. “Signal Transduction of Mechanical Stresses in the Vascular Wall.” *Hypertension* 32: 338–45.

Lehoux, S., Y. Castier, and A. Tedgui. 2006. “Molecular Mechanisms of the Vascular Responses to Haemodynamic Forces.” In *Journal of Internal Medicine*, 259:381–92.

Lehoux, Stéphanie, Catherine A. Lemarié, Bruno Esposito, H. Roger Lijnen, and Alain Tedgui. 2004. “Pressure-Induced Matrix Metalloproteinase-9 Contributes to Early Hypertensive Remodelling.” *Circulation* 109: 1041–47.

Li, Li, Donald K. Blumenthal, Christi M. Terry, Yuxia He, Mary L. Carlson, and Alfred K. Cheung. 2011. “PDGF-Induced Proliferation in Human Arterial and Venous Smooth

Muscle Cells: Molecular Basis for Differential Effects of PDGF Isoforms." *Journal of Cellular Biochemistry* 112: 289–98.

Li, Shijie, Shurong Chang, Xiaoxia Qi, James A Richardson, and Eric N Olson. 2006. "Requirement of a Myocardin-Related Transcription Factor for Development of Mammary Myoepithelial Cells." *Molecular and Cellular Biology* 26: 5797–5808.

Li, Shijie, Da-Zhi Wang, Zhigao Wang, James A Richardson, and Eric N Olson. 2003. "The Serum Response Factor Coactivator Myocardin Is Required for Vascular Smooth Muscle Development." *Proceedings of the National Academy of Sciences of the United States of America* 100: 9366–70.

Li, Song, James Jaehyun Moon, Hui Miao, Gang Jin, Benjamin P C Chen, Suli Yuan, Yingli Hu, Shunichi Usami, and Shu Chien. 2003. "Signal Transduction in Matrix Contraction and the Migration of Vascular Smooth Muscle Cells in Three-Dimensional Matrix." *Journal of Vascular Research* 40: 378–88.

Liu, Bo, Hiroyuki Itoh, Otway Louie, Kenji Kubota, and K. Craig Kent. 2002. "The Signalling Protein Rho Is Necessary for Vascular Smooth Muscle Migration and Survival but Not for Proliferation." *Surgery* 132: 317–25.

Liu, James J., Liming Peng, Christopher J. Bradley, Anthony Zulli, Jun Shen, and Brian F. Buxton. 2000. "Increased Apoptosis in the Heart of Genetic Hypertension, Associated with Increased Fibroblasts." *Cardiovascular Research* 45: 729–35.

Livak, Kenneth J, and Thomas D Schmittgen. 2001. "Analysis of Relative Gene Expression Data Using Real- Time Quantitative PCR and the 2 ⁻ΔΔ C T Method." *Gene Expression* 408: 402–8.

Long, Xiaochun, Robert D. Bell, William T. Gerthoffer, Berislav V. Zlokovic, and Joseph M. Miano. 2008. "Myocardin Is Sufficient for a Smooth Muscle-like Contractile Phenotype." *Arteriosclerosis, Thrombosis, and Vascular Biology* 28: 1505–10.

López, Begoña, Arantxa González, Nerea Hermida, Félix Valencia, Eduardo de Teresa, and Javier Díez. 2010. "Role of Lysyl Oxidase in Myocardial Fibrosis: From Basic Science to Clinical Aspects." *American Journal of Physiology. Heart and Circulatory Physiology* 299: H1–H9.

Mäki, Joni M. 2009. "Lysyl Oxidases in Mammalian Development and Certain Pathological Conditions." *Histology and Histopathology* 24(5):651-60

Manso, Ana Maria, Laila Elsherif, Seok Min Kang, and Robert S. Ross. 2006. "Integrins, Membrane-Type Matrix Metalloproteinases and ADAMs: Potential Implications for Cardiac Remodelling." *Cardiovascular Research* 69(3):574-84

Matsumoto, Yasuharu, Toyokazu Uwatoku, Keiji Oi, Kohtaro Abe, Tsuyoshi Hattori, Kunio Morishige, Yasuhiro Eto, et al. 2004. “Long-Term Inhibition of Rho-Kinase Suppresses Neointimal Formation after Stent Implantation in Porcine Coronary Arteries: Involvement of Multiple Mechanisms.” *Arteriosclerosis, Thrombosis, and Vascular Biology* 24: 181–86.

McKinsey, Timothy A., Chun Li Zhang, and Eric N. Olson. 2002. “MEF2: A Calcium-Dependent Regulator of Cell Division, Differentiation and Death.” *Trends in Biochemical Sciences* 27(1):40-7.

Mederos y Schnitzler, Michael, Ursula Storch, Simone Meibers, Pascal Nurwakagari, Andreas Breit, Kirill Essin, Maik Gollasch, and Thomas Gudermann. 2008. “Gq-Coupled Receptors as Mechanosensors Mediating Myogenic Vasoconstriction.” *The EMBO Journal* 27: 3092–3103.

Medjkane, Souhila, Cristina Perez-Sanchez, Cedric Gaggioli, Erik Sahai, and Richard Treisman. 2009. “Myocardin-Related Transcription Factors and SRF Are Required for Cytoskeletal Dynamics and Experimental Metastasis.” *Nature Cell Biology* 11 (3): 257–68.

Meininger, G A, and M J Davis. 1992. “Cellular Mechanisms Involved in the Vascular Myogenic Response.” *The American Journal of Physiology* 263: H647–H659.

Minami, Takeya, Koichiro Kuwahara, Yasuaki Nakagawa, Minoru Takaoka, Hideyuki Kinoshita, Kazuhiro Kazuwa Nakao, Yoshihiro Kuwabara, et al. 2012. “Reciprocal Expression of MRTF-A and Myocardin Is Crucial for Pathological Vascular Remodelling in Mice.” *The EMBO Journal* 31 (23). Nature Publishing Group: 4428–40.

Miralles, Francesc, Guido Posern, Alexia Ileana Zaromytidou, and Richard Treisman. 2003. “Actin Dynamics Control SRF Activity by Regulation of Its Coactivator MAL.” *Cell* 113: 329–42.

Miranti, Cindy K, and Joan S Brugge. 2002. “Sensing the Environment: A Historical Perspective on Integrin Signal Transduction.” *Nature Cell Biology* 4: E83–E90.

Mise, Nikica, Rajkumar Savai, Haiying Yu, Johannes Schwarz, Naftali Kaminski, and Oliver Eickelberg. 2012a. “Zyxin Is a Transforming Growth Factor-B (TGF-β)/Smad3 Target Gene That Regulates Lung Cancer Cell Motility via Integrin α5β1.” *The Journal of Biological Chemistry* 287: 31393–405.

Mujumdar, Vibhas S., Lane M. Smiley, and Suresh C. Tyagi. 2001. “Activation of Matrix Metalloproteinase Dilates and Decreases Cardiac Tensile Strength.” *International Journal of Cardiology* 79: 277–86.

Nix, D A, and M C Beckerle. 1997. “Nuclear-Cytoplasmic Shuttling of the Focal Contact Protein, Zyxin: A Potential Mechanism for Communication between Sites of Cell Adhesion and the Nucleus.” *The Journal of Cell Biology* 138: 1139–47.

Nix, David A., and Mary C. Beckerle. 1997. “Nuclear-Cytoplasmic Shuttling of the Focal Contact Protein, Zyxin: A Potential Mechanism for Communication between Sites of Cell Adhesion and the Nucleus.” *Journal of Cell Biology* 138: 1139–47.

Olson, E N, and R S Williams. 2000. “Remodelling Muscles with Calcineurin.” *BioEssays : News and Reviews in Molecular, Cellular and Developmental Biology* 22: 510–19.

Olson, Eric N, and Alfred Nordheim. 2010. “Linking Actin Dynamics and Gene Transcription to Drive Cellular Motile Functions.” *Nature Reviews. Molecular Cell Biology* 11 (5). Nature Publishing Group: 353–65.

Osawa, Masaki, Michitaka Masuda, Ken Ichi Kusano, and Keigi Fujiwara. 2002. “Evidence for a Role of Platelet Endothelial Cell Adhesion Molecule-1 in Endothelial Cell Mechanosignal Transduction: Is It a Mechanoresponsive Molecule?” *Journal of Cell Biology* 158: 773–85.

Osol, G. 1995. “Mechanotransduction by Vascular Smooth Muscle.” *Journal of Vascular Research* 32: 275–92.

Osol, G, I Laher, and M Kelley. 1993. “Myogenic Tone Is Coupled to Phospholipase C and G Protein Activation in Small Cerebral Arteries.” *The American Journal of Physiology* 265: H415–H420.

Owens, G K, P S Rabinovitch, and S M Schwartz. 1981. “Smooth Muscle Cell Hypertrophy versus Hyperplasia in Hypertension.” *Proceedings of the National Academy of Sciences of the United States of America* 78: 7759–63.

Parmacek, Michael S. 2007. “Myocardin-Related Transcription Factors: Critical Coactivators Regulating Cardiovascular Development and Adaptation.” *Circulation Research* 100(5):633-44.

Partridge, Jason, Harald Carlsen, Karine Enesa, Hera Chaudhury, Mustafa Zakkar, Le Luong, Anne Kinderlerer, et al. 2007. “Laminar Shear Stress Acts as a Switch to Regulate Divergent Functions of NF-kappaB in Endothelial Cells.” *The FASEB Journal : Official Publication of the Federation of American Societies for Experimental Biology* 21: 3553–61.

Pellegrin, Stéphanie, and Harry Mellor. 2007. “Actin Stress Fibres.” *Journal of Cell Science* 120: 3491–99.

Pertz, Olivier, Louis Hodgson, Richard L Klemke, and Klaus M Hahn. 2006. “Spatiotemporal Dynamics of RhoA Activity in Migrating Cells.” *Nature* 440: 1069–72.

Petit, M M, E F Schoenmakers, C Huysmans, J M Geurts, N Mandahl, and W J Van de Ven. 1999. “LHFP, a Novel Translocation Partner Gene of HMGIC in a Lipoma, Is a Member of a New Family of LHFP-like Genes.” *Genomics* 57: 438–41.

Peyton, Shelly R., Peter D. Kim, Cyrus M. Ghajar, Dror Seliktar, and Andrew J. Putnam. 2008. “The Effects of Matrix Stiffness and RhoA on the Phenotypic Plasticity of Smooth Muscle Cells in a 3-D Biosynthetic Hydrogel System.” *Biomaterials* 29: 2597–2607.

Peyton, Shelly R., and Andrew J. Putnam. 2005. “Extracellular Matrix Rigidity Governs Smooth Muscle Cell Motility in a Biphasic Fashion.” *Journal of Cellular Physiology* 204: 198–209.

Pfisterer, Larissa, Anja Feldner, Markus Hecker, and Thomas Korff. 2012. “Hypertension Impairs Myocardin Function: A Novel Mechanism Facilitating Arterial Remodelling.” *Cardiovascular Research* 96: 120–29.

Prewitt, Russell L, Darian C Rice, and Anca D Dobrian. 2002. “Adaptation of Resistance Arteries to Increases in Pressure.” *Microcirculation (New York, N.Y. : 1994)* 9: 295–304.

Prockop, D J, and K I Kivirikko. 1995. “Collagens: Molecular Biology, Diseases, and Potentials for Therapy.” *Annual Review of Biochemistry* 64: 403–34.

Qiu, Hongyu, Yi Zhu, Zhe Sun, Jerome P. Trzeciakowski, Meredith Gansner, Christophe Depre, Ranillo R G Resuello, et al. 2010. “Short Communication: Vascular Smooth Muscle Cell Stiffness as a Mechanism for Increased Aortic Stiffness with Aging.” *Circulation Research* 107: 615–19.

Rauskolb, Cordelia, Guohui Pan, B. V V G Reddy, Hyangyee Oh, and Kenneth D. Irvine. 2011. “Zyxin Links Fat Signalling to the Hippo Pathway.” *PLoS Biology* 9.

Regan, C P, P J Adam, C S Madsen, and G K Owens. 2000. “Molecular Mechanisms of Decreased Smooth Muscle Differentiation Marker Expression after Vascular Injury.” *The Journal of Clinical Investigation* 106: 1139–47.

Reiser, K, R J McCormick, and R B Rucker. 1992. “Enzymatic and Nonenzymatic Cross-Linking of Collagen and Elastin.” *The FASEB Journal : Official Publication of the Federation of American Societies for Experimental Biology* 6: 2439–49.

Renfranz, Patricia J., Elizabeth Blankman, and Mary C. Beckerle. 2010. “The Cytoskeletal Regulator Zyxin Is Required for Viability in Drosophila Melanogaster.” *Anatomical Record* 293: 1455–69.

Roos, Jack, Paul J. DiGregorio, Andriy V. Yeromin, Kari Ohlsen, Maria Lioudyno, Shenyuan Zhang, Olga Safrina, et al. 2005. “STIM1, an Essential and Conserved Component of Store-Operated Ca 2+ Channel Function.” *Journal of Cell Biology* 169: 435–45.

Rzucidlo, Eva M., Kathleen A. Martin, and Richard J. Powell. 2007. “Regulation of Vascular Smooth Muscle Cell Differentiation.” *Journal of Vascular Surgery* 45: 25–32.

Sachs, Frederick. 2010. “Stretch-Activated Ion Channels: What Are They?” *Physiology (Bethesda, Md.)* 25: 50–56.

Sadler, Ingrid, Aaron W. Crawford, James W. Michelsen, and Mary C. Beckerle. 1992. “Zyxin and cCRP: Two Interactive LIM Domain Proteins Associated with the Cytoskeleton.” *Journal of Cell Biology* 119: 1573–87.

Schratt, Gerhard, Ulrike Philippar, Jürgen Berger, Heinz Schwarz, Olaf Heidenreich, and Alfred Nordheim. 2002. “Serum Response Factor Is Crucial for Actin Cytoskeletal Organization and Focal Adhesion Assembly in Embryonic Stem Cells.” *The Journal of Cell Biology* 156: 737–50.

Shanahan, C M, P L Weissberg, and J C Metcalfe. 1993. “Isolation of Gene Markers of Differentiated and Proliferating Vascular Smooth Muscle Cells.” *Circulation Research* 73: 193–204.

Shiraishi, Isao, Jaime Melendez, Youngkeun Ahn, Maryanne Skavdahl, Elizabeth Murphy, Sara Welch, Erik Schaefer, et al. 2004. “Nuclear Targetin of Akt Enhances Kinase Activity and Survival of Cardiomyocytes.” *Circulation Research* 94: 884–91.

Smith, M.A., L.M. Hoffman, and M.C. Beckerle. 2014. “LIM Proteins in Actin Cytoskeleton Mechanoresponse.” *Trends in Cell Biology* 24(10):575-583.

Smith, Mark A., Elizabeth Blankman, Margaret L. Gardel, Laura Luettjohann, Clare M. Waterman, and Mary C. Beckerle. 2010. “A Zyxin-Mediated Mechanism for Actin Stress Fiber Maintenance and Repair.” *Developmental Cell* 19: 365–76.

Spassova, Maria A, Thamara Hewavitharana, Wen Xu, Jonathan Soboloff, and Donald L Gill. 2006. “A Common Mechanism Underlies Stretch Activation and Receptor Activation of TRPC6 Channels.” *Proceedings of the National Academy of Sciences of the United States of America* 103: 16586–91.

Sperry, Rebecca Bakkevig, Nicholas H. Bishop, Jeremy J. Bramwell, Michael N. Brodeur, Matthew J. Carter, Brent T. Fowler, Zachery B. Lewis, et al. 2010. “Zyxin Controls Migration in Epithelial-Mesenchymal Transition by Mediating Actin-Membrane Linkages at Cell-Cell Junctions.” *Journal of Cellular Physiology* 222: 612–24.

Storch, U., M. M. y. Schnitzler, and T. Gudermann. 2012. “G Protein-Mediated Stretch Reception.” *AJP: Heart and Circulatory Physiology*.

Subramanian, Aravind, Pablo Tamayo, Vamsi K Mootha, Sayan Mukherjee, Benjamin L Ebert, Michael a Gillette, Amanda Paulovich, et al. 2005. “Gene Set Enrichment Analysis: A Knowledge-Based Approach for Interpreting Genome-Wide Expression Profiles.” *Proceedings of the National Academy of Sciences of the United States of America* 102: 15545–50.

Suchyna, T M, J H Johnson, K Hamer, J F Leykam, D A Gage, H F Clemo, C M Baumgarten, and F Sachs. 2000. “Identification of a Peptide Toxin from Grammostola Spatulata Spider Venom That Blocks Cation-Selective Stretch-Activated Channels.” *The Journal of General Physiology* 115: 583–98.

Suresh Babu, Sahana, Agnieszka Wojtowicz, Marc Freichel, Lutz Birnbaumer, Markus Hecker, and Marco Cattaruzza. 2012. “Mechanism of Stretch-Induced Activation of the Mechanotransducer Zyxin in Vascular Cells.” *Science Signalling* 5: ra91.

Tang, Yuefeng, Xuehui Yang, Robert E. Friesel, Calvin P H Vary, and Lucy Liaw. 2011. “Mechanisms of TGF-β-Induced Differentiation in Human Vascular Smooth Muscle Cells.” *Journal of Vascular Research* 48: 485–94.

Teiger, Emmanuel, Than Vinh Dam, Lucie Richard, Claudine Wisnewsky, Bun Seng Tea, Louis Gaboury, Johanne Tremblay, Ketty Schwartz, and Pavel Hamet. 1996. “Apoptosis in Pressure Overload-Induced Heart Hypertrophy in the Rat.” *Journal of Clinical Investigation* 97: 2891–97.

Thannickal, Victor J, Daniel Y Lee, Eric S White, Zongbin Cui, Jose M Larios, Raquel Chacon, Jeffrey C Horowitz, Regina M Day, and Peedikayil E Thomas. 2003. “Myofibroblast Differentiation by Transforming Growth Factor-beta1 Is Dependent on Cell Adhesion and Integrin Signalling via Focal Adhesion Kinase.” *The Journal of Biological Chemistry* 278: 12384–89.

Thodeti, Charles K., Benjamin Matthews, Arvind Ravi, Akiko Mammoto, Kaustabh Ghosh, Abigail L. Bracha, and Donald E. Ingber. 2009. “TRPV4 Channels Mediate Cyclic Strain-Induced Endothelial Cell Reorientation through Integrin-to-Integrin Signalling.” *Circulation Research* 104: 1123–30.

Trebak, Mohamed. 2012. “STIM/Orai Signalling Complexes in Vascular Smooth Muscle.” *The Journal of Physiology* 590: 4201–8.

Trebak, Mohamed, Nadine Hempel, Barbara J Wedel, Jeremy T Smyth, Gary St J Bird, and James W Putney. 2005. “Negative Regulation of TRPC3 Channels by Protein Kinase C-Mediated Phosphorylation of Serine 712.” *Molecular Pharmacology* 67: 558–63.

Tsuda, Yuki, Masahiro Okazaki, Yasuhito Uezono, Akihiko Osajima, Hiroaki Kato, Haruhito Okuda, Yosuke Oishi, Akira Yashiro, and Yasuhide Nakashima. 2002. “Activation of Extracellular Signal-Regulated Kinases Is Essential for Pressure-Induced Proliferation of Vascular Smooth Muscle Cells.” *European Journal of Pharmacology* 446: 15–24.

Tzima, Eleni, Miguel Angel Del Pozo, Sanford J. Shattil, Shu Chien, and Martin Alexander Schwartz. 2001. “Activation of Integrins in Endothelial Cells by Fluid Shear Stress Mediates Rho-Dependent Cytoskeletal Alignment.” *EMBO Journal* 20: 4639–47.

Tzima, Eleni, Mohamed Irani-Tehrani, William B Kiosses, Elizabetta Dejana, David A Schultz, Britta Engelhardt, Gaoyuan Cao, Horace DeLisser, and Martin Alexander Schwartz. 2005. “A Mechanosensory Complex That Mediates the Endothelial Cell Response to Fluid Shear Stress.” *Nature* 437: 426–31.

Vartiainen, Maria K, Sebastian Guettler, Banafshe Larijani, and Richard Treisman. 2007. “Nuclear Actin Regulates Dynamic Subcellular Localization and Activity of the SRF Cofactor MAL.” *Science (New York, N.Y.)* 316: 1749–52.

Venkatachalam, Kartik, Damian B van Rossum, Randen L Patterson, Hong-Tao Ma, and Donald L Gill. 2002. “The Cellular and Molecular Basis of Store-Operated Calcium Entry.” *Nature Cell Biology* 4: E263–E272.

Vervenne, Hilke B V K, Koen R M O Crombez, Kathleen Lambaerts, Lara Carvalho, Mathias Köppen, Carl Philipp Heisenberg, Wim J M Van de Ven, and Marleen M R Petit. 2008. “Lpp Is Involved in Wnt/PCP Signalling and Acts Together with Scrib to Mediate Convergence and Extension Movements during Zebrafish Gastrulation.” *Developmental Biology* 320: 267–77.

Vig, M, C Peinelt, A Beck, D L Koomoa, D Rabah, M Koblan-Huberson, S Kraft, et al. 2006. “CRACM1 Is a Plasma Membrane Protein Essential for Store-Operated Ca2+ Entry.” *Science (New York, N.Y.)* 312: 1220–23.

Wagner, A H, R Krzesz, D Gao, C Schroeder, M Cattaruzza, and M Hecker. 2000. “Decoy Oligodeoxynucleotide Characterization of Transcription Factors Controlling Endothelin-B Receptor Expression in Vascular Smooth Muscle Cells.” *Mol Pharmacol* 58: 1333–40.

Wang, Yuepeng, Xiaoyu Rayne Zheng, Nadeene Riddick, Meredith Bryden, Wendy Baur, Xin Zhang, and Howard K. Surks. 2009. “ROCk Isoform Regulation of Myosin Phosphatase and Contractility in Vascular Smooth Muscle Cells.” *Circulation Research* 104: 531–40.

Wang, Z, D Z Wang, G C Pipes, and E N Olson. 2003. “Myocardin Is a Master Regulator of Smooth Muscle Gene Expression.” *Proc Natl Acad Sci U S A* 100: 7129–34.

Wang, Zhigao, Da-Zhi Wang, Dirk Hockemeyer, John McAnally, Alfred Nordheim, and Eric N Olson. 2004. “Myocardin and Ternary Complex Factors Compete for SRF to Control Smooth Muscle Gene Expression.” *Nature* 428: 185–89.

Weinbaum, Sheldon, Xiaobing Zhang, Yuefeng Han, Hans Vink, and Stephen C Cowin. 2003. “Mechanotransduction and Flow across the Endothelial Glycocalyx.” *Proceedings of the National Academy of Sciences of the United States of America* 100: 7988–95.

Welsh, Donald G., Anthony D. Morielli, Mark T. Nelson, and Joseph E. Brayden. 2002. “Transient Receptor Potential Channels Regulate Myogenic Tone of Resistance Arteries.” *Circulation Research* 90: 248–50.

Wier, W G, and K G Morgan. 2003. “Alpha1-Adrenergic Signalling Mechanisms in Contraction of Resistance Arteries.” *Reviews of Physiology, Biochemistry and Pharmacology* 150: 91–139.

Wilson, E, F Vives, T Collins, and H E Ives. 1998. “Strain-Responsive Regions in the Platelet-Derived Growth Factor-A Gene Promoter.” *Hypertension* 31: 170–75.

Wójtowicz, Agnieszka, Sahana Suresh Babu, Li Li, Norbert Gretz, Markus Hecker, and Marco Cattaruzza. 2010. “Zyxin Mediation of Stretch-Induced Gene Expression in Human Endothelial Cells.” *Circulation Research* 107 (7): 898–902.

Wu, Haidong, Tao Liu, Renjie Wang, Shuang Tian, Min Liu, Xin Li, and Hua Tang. 2011. “MicroRNA-16 Targets Zyxin and Promotes Cell Motility in Human Laryngeal Carcinoma Cell Line HEp-2.” *IUBMB Life* 63: 101–8.

Yamamoto, Shoji, Thomas N James, Keishiro Kawamura, and Masakiyo Nobuyoshi. 2002. “Cardiocytic Apoptosis and Capillary Endothelial Swelling as Morphological Evidence of Myocardial Ischemia in Ventricular Biopsies from Patients with Angina and Normal Coronary Arteriograms.” *Coronary Artery Disease* 13: 25–35.

Yamamura, Michiyo, Kazuma Noguchi, Yoshiro Nakano, Emi Segawa, Yusuke Zushi, Kazuki Takaoka, Hiromitsu Kishimoto, Tomoko Hashimoto-Tamaoki, and Masahiro Urade. 2013. “Functional Analysis of Zyxin in Cell Migration and Invasive Potential of Oral Squamous Cell Carcinoma Cells.” *International Journal of Oncology* 42: 873–80.

Yoshida, Tadashi, Sanjay Sinha, Frédéric Dandré, Brian R. Wamhoff, Mark H. Hoofnagle, Brandon E. Kremer, Da Zhi Wang, Eric N. Olson, and Gary K. Owens. 2003. “Myocardin Is a Key Regulator of CArG-Dependent Transcription of Multiple Smooth Muscle Marker Genes.” *Circulation Research* 92: 856–64.

Zou, Yunzeng, Hiroshi Akazawa, Yingjie Qin, Masanori Sano, Hiroyuki Takano, Tohru Minamino, Noriko Makita, et al. 2004. “Mechanical Stress Activates Angiotensin II Type 1 Receptor without the Involvement of Angiotensin II.” *Nature Cell Biology* 6: 499–506.

ACKNOWLEDGEMENTS

I would like to convey my deepest gratitude to Prof. Dr. Markus Hecker for providing me the opportunity to pursue my PhD training at the Institute of Physiology and Pathophysiology. As my principal supervisor, he has had a great influence on my approach to scientific research and my personal development. His leadership and problem solving skills have truly inspired me. I thank him for his incessant support and his willingness to allow independent scientific thinking. This thesis would not have been possible without his mentorship.

I would also like to thank Prof. Dr. Thomas Wieland and Prof. Dr. Stephan Herzig for their constructive criticism of my work and stimulating discussions during my annual thesis advisory committee (TAC) meetings. I have been fortunate to be a part of a vibrant scientific environment in Heidelberg. I would like to remember my interactions with PD Dr. Marco Cattaruzza as one my most cherished memories. He had a marked influence in shaping my interest in this project. I truly regret his untimely demise. My work has been greatly improved by inputs and advice from Prof. Dr. Thomas Korff, PD Dr. Andreas Wagner and Dr. Oliver Drews and Dr. Nina Ullrich during our team presentations. I would like to acknowledge the contributions of my collaborators, Prof. Dr. Rainer Nobiling and Dr. Jan Reil for their expert assistance with intracellular calcium measurements and isolated working heart experiments respectively.

My wonderful colleagues and friends have been part of this journey and I thank each one of them for their warmth and affection during my time in Heidelberg. My present and former colleagues, Maren, Cheryl, Taslima, Sibgha, Tanja, Franziska, Hanna, Felix, Synje, Hannes, Larissa, Caroline, Iva, Cordula, Eda, Sahana, Anja, Oliver, Jenny, Kerstin, Florian, Johannes, Max, Anca, Fan, Ralph, Ake, Phillip, Miruna, Sebastian, Branko, Hui, Andrea, Lidia, Victor, Svetlana, are all part of my fond memories. My special thanks to the technicians, Maria, Marie, Anita, Gudrun, Franziska, Nadine, Tilli, Ender, Manuela, Yvonne and Felicia, for their great technical assistance and for their smiling faces. I am deeply indebted to Renate for being more than a technical assistant, making me smile during hard times, for being like family and making me feel at home. My deep regards for Dr. Gerd Koenig, Barbara Richards, Jan Simon, Michaela Neidig and Stephanie Billeter for their great support and friendliness.

I have been privileged to have my brother, Sourav and my sister-in-law, Piu as my family in Heidelberg. They have kept me going during difficult times and enabled me to focus on my work. I cherish every moment I spent with them. Finally, my utmost gratitude is reserved for my parents, Sujit Kumar Ghosh and Sumitra Ghosh for making me what I am and for their unconditional love. I thank God for considering me worthy of this rich experience and showing me the way.